

REFINING SEA-BED PROCESS MODELS FOR AQUACULTURE

SAM/004/12



New DEPOMOD

Final Report

August 2016



 **SAMS**

Centre for
Aquaculture

Oban, Argyll, Scotland

UK, PA37 1QA

Acknowledgements

This report was prepared by:

Kenneth D Black, SAMS

Trevor Carpenter, SAMS

Andrew Berkeley, SEPA

Kevin Black, Partrac Ltd

Carl Amos, Tuscan Consulting

The project management team was:

Willie Cowan, Marine Scotland

Fiona Watt, Marine Scotland

Matt Gubbins, Marine Scotland Science

Alan Hills, SEPA

Andrew Berkeley, SEPA

Alex Adrian, The Crown Estate

Phil Crump, SAMS ran the multi-beam on the first cruise.

Saul Reynolds, Partrac Ltd. and Thom Nickell, SAMS participated on the benthic flume cruises.

We acknowledge the support of the masters and crews of the *Sir John Murray*, *Calanus* and *Seol mara*, and are grateful to the farmers for access to their sites.

Contents

0. Executive Summary.....	7
1. Introduction	9
1.1 Context.....	9
1.2. Compatibility issues	10
1.3 Future proofing and updating.....	10
1.4 Efficiency & Optimisation	10
1.5 Improving AutoDEPOMOD predictive performance: measuring and modelling	10
1.6 Resuspension	11
1.7 Goals.....	12
2. Recoding the model	13
2.1 Existing DEPOMOD and AutoDEPOMOD code base review.	13
2.2 Implementation of ported java application.....	13
2.3 Design of NewDEPOMOD	14
2.4 Datatypes and utility libraries.....	15
2.5 Numerical Engine and runtime frame work	16
2.6 Implementation of Physics from Partrack report	17
2.7 Support for SEPA model tuning	17
2.8 NewDEPOMOD user interface	17
2.9 User documentation	18
2.10 Implementation of product release and internal issue tracking support	18
2.11 Implementation of product updates	18
3. Research on Resuspension processes.....	19
3.1 research cruises	19
3.2 Results.....	20
3.2.1 Bathymetry data from Calanus Multi-beam Cruise.....	20
3.2.2 The resuspension cruises	24
4. Model validation	25
4.1 General hindcasting approach and test sites.....	25
4.2 Appraisal of original model.....	27
4.3 Calibration of new model	29
4.3.1 Hindcasting data for new model.....	29
4.3.2 Calibration approach	30
4.3.3 Indicative results.....	31
4.4 Consenting implications.....	40

4.5 Conclusions	44
5. Discussion.....	45
6. References	46
Annex 1. Benthic Flume and Flow Velocity Measurements	47
1. Introduction	56
1.1 Background to Project.....	56
2. instrumentation and theory	58
2.1 Partrac Voyager Series Benthic Flumes.....	58
2.1.1 Introduction to Benthic Flumes	58
2.1.2 The Partrac <i>Voyager II</i> Benthic Flume	58
2.1.3 <i>The Partrac Voyager I Benthic Flume</i>	62
2.2 <i>Introduction to Boundary Layer Flows</i>	65
2.2.1 Techniques for estimating bed stress (τ_0)	68
2.2.2 Technique for estimating roughness length (z_0).....	70
2.3 The Partrac-SAMS Boundary Layer Rig	71
3. SURVEY 1 – August 2013.....	73
3.1 Flume Deployment Programme.....	73
3.2 Rig Deployment Programme	76
3.3 Problems	81
4. Survey 2 – May 2014.....	82
4.1 Flume Deployment Programme.....	82
4.2 Problems	85
5. mini-flume pellet mobility studies	86
6. settling velocity analysis	87
7. data analysis.....	88
7.1 Grain Size, Dry Bulk Density Data and Organics.....	88
7.2 Benthic Flume Data	88
7.2.1 Bed Shear Stress Calculation for Voyager II.....	88
7.2.2 Bed Shear Stress Calculation for Voyager I.....	90
7.2.3 Turbidity Sensor Calibrations.....	92
7.2.4 Time Series Data Analysis	93
7.2.5 Derivation of Critical Entrainment Stress	94
7.3 Boundary Layer Flow Data	95
8. results.....	99
8.1 Sediment Bulk Density, Grain Size and Organics	99

8.2	Benthic Flume Data	102
8.2.1	QC Summary	102
8.2.2	Bed Stress Data	102
8.2.3	Results of Survey 1	105
8.2.4	Results of Survey 2	112
8.3	Boundary Layer Flow Data	115
8.3.1	QC Summary	115
8.3.2	Data	115
8.4	Pellet Mobility Studies	124
8.5	Settling Velocity.....	125
9.	references	127
10.	Appendix i Sediment photographs	129
	Annex 2. Recommendations from field and desk studies	140
	LIST OF FIGURES & TABLES	143
1.	introduction	150
1.1	A summary of the recommended upgrades to DEPOMOD	150
2.	Fundamental variables.....	153
2.1	Grain Density (ρ_s)	153
2.2	Water Temperature, Salinity, Density and Viscosity.....	154
2.3	Settling of Particles from the Fish Pen to the Seabed.....	155
2.3.1	Modification of Settling Velocity for Moving Flow Situations.....	158
2.4	Settling Velocity of Resuspended Faeces/Pellets	161
3.	Sediment transport regime.....	163
3.1	Cohesive or Non-Cohesive Bed?	163
3.2	Critical Entrainment Stress of Impacted Faeces-Rich Sediments	164
3.2.1	Relationship with Dry Bulk Density Parameter (ρ_d).....	166
3.3	Comparison with Far-Field Sediment Critical Entrainment Stresses	167
3.4	Resuspension Rates of Impacted (Cohesive) Bed Material & Erosion Through Eroded Depth 168	
3.4.1	Erosion With Eroded Depth (Friction Coefficient).....	168
3.4.2	Resuspension Rates of Impacted (Cohesive) Bed Material	169
3.5	Onset of Motion of Intact Pellets on the Seabed.....	173
3.5.1	Theoretical Approach.....	173
3.5.2	Project Data on Pellet Mobility.....	178
3.5.3	Direct Measurements of ϕ	180

4.	Flow (hydraulic) regime	182
4.1	Specification of Hydraulic Regime.....	182
4.2	Benthic Boundary Layer Parameterisation and Bed Roughness.....	184
4.2.1	Bed Roughness Parameterisation.....	186
4.2.2	Revision of z_0 during model testing	189
5.	eXTernal concerns for the revised model.....	191
6.	Recommendations for further upgrades in the future.....	193
7.	References	194
8.	Appendix BEd stress – erosion rate formulations	198

0. Executive Summary

DEPOMOD was funded by a NERC-MAFF Link programme and was a collaboration between SAMS (NERC DML then), Marine Harvest and SEPA from 1997 to 1999. Its purpose is to predict the benthic impacts on sediment dwelling animals from marine cage farms given farm (configuration, feeding rate) and environmental information (bathymetry, water currents). The purpose of AutoDEPOMOD (2005) was to iteratively run the DEPOMOD from an initial biomass, automatically assessing the result then re-running the model as many times as required, until a compliant solution was obtained. AutoDEPOMOD was adapted to determine medicine residues in sediments. Rather than duplicating functions available in 3rd party software, AutoDEPOMOD incorporated processes which called on these functions in an automated way.

Windows and the other 3rd party applications utilised have been updated many times causing functional problems. These have been worked around by running AutoDEPOMOD on virtual machines (e.g. XP in a VirtualBox or VMware VM), but these older systems and applications are not being supported and may soon not even be available to future users. The coding language used in AutoDEPOMOD is obsolete and the software design was determined by the computing constraints of the 1990s. Moreover, while giving good results at the majority of Scottish sites, it has been increasingly obvious that it underestimates the impacts at dispersive sites. This is important as the salmon farming industry is increasingly looking for larger sites in more dispersive environments.

The goals of the present project were:

1. To completely rewrite the model code in a modern language (Java) in a modular form that will facilitate future maintenance and development. Hereafter, this model will be referred to as NewDEPOMOD to distinguish it from its successors.
2. To remove dependencies on third party software (e.g. excel, MS Excel) as far as possible
3. To carry out field and laboratory studies to improve our understanding of resuspension processes around fish farms and to use these to refine the modelling of resuspension processes and hence improve the predictive ability of the model.

Recoding the model was done in 2 phases. The first aimed to reproduce the AutoDEPOMOD model coded in Borland Delphi and in Java code retaining the existing structure. The second aimed to refactoring¹ the code in order for it to be much better able to be adapted in future developments. In addition the refactored model was designed to take advantage of modern computing engineering (e.g. multiple processors) and to include insights from fieldwork on resuspension process (annexes 1 and 2). All third party dependencies have been removed (except Java, which is likely to be a long-lived platform). This has demanded the development of a new User Interface to complement the new model engine.

Three research cruises were implemented at fish farm sites chosen by the project management team. The first cruise obtained detailed multi-beam bathymetry at 8 salmon farms on the west Coast of Scotland. The second 2 cruises engaged Partrac Ltd who deployed state of the art benthic flumes which were used to determine erosion/resuspension properties of the seabed around these same farms. In addition, the frictional effect of the

¹ https://en.wikipedia.org/wiki/Code_refactoring

seabed on water movements was measured by using a custom built hydrodynamic lander containing an acoustic Doppler current meter (ADCM) set at a known distance above the bed, a downward looking ADC profiler (ADCP) set at ca. 1 m above the bed and an upward looking ADCP set at ca. 2m above the bed. This lander was deployed for a tidal cycle at each of the sites in order to estimate bed roughness.

Analysis of the data generated during this field work (annex 1) resulted in a series of recommendations and considerations for advancing the modelling of resuspension processes (annex 2).

The revised model, NewDEPOMOD, has been tested by SEPA in order to establish its suitability for environmental risk assessment and determination of consent limits on licences for aquaculture-related discharges. This test was undertaken with 3 goals in mind:

to produce a model which:

1. Is more accurate
2. Is more flexible, configurable
3. That supports industry expansion

Given the greatly increased range of features, representing new or enhanced physical concepts, and the increased flexibility with respect to input data, the new model offers a much greater variety of scenarios which can be simulated. Consequently, the model can produce a vastly greater range of outcomes than the old model. The challenge for validating the model is, therefore, not so much *whether* the model can produce accurate predictions, but rather *how* can it be set up and configured to produce the most accurate predictions. With this in mind, the validation of the model was approached in three main ways:

1. **Appraisal of original model:** this used *hindcasting* approach to compare the output of the original model with observed seabed impacts
2. **Calibration of the new model:** this tested configuration options for the new model using a similar hindcasting approach in Approach 1.
3. **Testing consenting implications:** this used the model configuration options identified in Approach 2 to test the implications of the new model for SEPA's consenting purposes.

The advantage of the hindcasting approach, used to appraise the old model and calibrate the new model, is that it measures the absolute accuracy of the model against empirical data. However, sufficient coverage of seabed data was only available for 6 sites, and in these cases with some important limitations. The testing of consenting implications therefore answers important practical questions about future policy implications for SEPA but it also adds many more sites to the test suite (~50) and therefore provides a greater breadth of tested scenarios in terms of environmental (flow regime, bathymetry, etc.) and operational (cage layout, biomass, etc.) conditions. SEPA continue to experiment with model settings to achieve optimum performance.

As with AutoDEPOMOD, NewDEPOMOD will be distributed by SAMS. Unlike AutoDEPOMOD, the NewDEPOMOD code will be made available to researchers on an open source basis to encourage future developments and to establish a Global User and Researcher Platform which we hope will ensure that the model will remain fit for purpose across a range of environmental and regulatory settings for the foreseeable future as well as helping to ensure the sustainable growth of the Scottish finfish sector.

1. Introduction

1.1 Context

The original DEPOMOD project was funded by a NERC-MAFF Link programme and was a collaboration between SAMS (NERC DML then), Marine Harvest and SEPA from 1997 to 1999. There were 2 publications which came from this: the first Cromeey *et al.* (2002a) described the model and its application at 2 Scottish fish farms with contrasting dispersiveness and the second (2002b) described an experiment which followed the dispersion over time of plastic particles with similar density to fish faeces that were placed on the sea bed in Loch Linnhe, Scotland. These dispersion data were used to parameterise the resuspension component of the model (resus module).

DEPOMOD was programmatically implemented as a set of executable modules that had to be run in sequence to complete one model run. Initial parameters were provided through a set of configuration files, and then through a set of intermediate files that were generated by each module and then read by the subsequent following module in the process. This was a very manual process: each module having to be manually run after the completion of the previous one: grid generation defining the cage geometry and bathymetry, followed by initial particle tracking then finally the resuspension. In addition the initial text-based configuration files needed to run the model, such as those defining cage geometry and bathymetry, had to be created first and initially SEPA developed tools to make this process easier; such as the excel workbook that allowed users to more easily define cage location and geometry. In addition, output from the model was always in a raw gridded format and additional tools were also then required to provide analysis of this raw data: again SEPA used both Excel and a third party piece of software, Surfer, to provide these functions (e.g. gridding of data, analysis of defined contoured areas, etc.). This process was required for every model run: when trying to determine a compliant stocking solution for a particular site this had to be repeated several times before a solution was found (by iteratively changing the stocking levels in the configuration files and then by analysing the result of the run using these files). This was a very laborious process, requiring anything from 5 to 25 (or more) runs: so AutoDEPOMOD was conceived.

Again developed at SAMS, the purpose of AutoDEPOMOD was to automate the iterative process by iteratively running the DEPOMOD modules in sequence (from an initial predefined stocking level), automatically assessing the result, then re-running the model, as many times as required, until a compliant solution was obtained. This was successful, but due to time and money constraints at the time, the dependency on the tools in the 3rd party applications (Excel and Surfer) was left, although the interaction between the DEPOMOD modules and these tools was automated, e.g. AutoDEPOMOD generated the required configuration files from the Excel sheet and the Surfer functions were automatically run by AutoDEPOMOD on the output files through Surfer's ActiveX API. Later versions included a basic GIS module that allowed users to directly view model results and extract point and transect profiles.

However in the years since these applications were developed, computing technology, both software and hardware, has moved on and this has created several problems with the current versions of DEPOMOD and AutoDEPOMOD

1.2. Compatibility issues

1. AutoDEPOMOD was developed on Windows XP, Windows 7/10 is now the norm. This has created installation problems.
2. The original Excel spreadsheets were Office XP, current version is now Office 365/ Excel 2016. Although this has proved surprising robust, there are no guarantees it will work in future.
3. AutoDEPOMOD was developed with Surfer version 7 then 8: v13 is the latest. Program had to be recompiled to support version 8 – no guarantee of function beyond Surfer 8..

These issues have been solved by running on virtual machines (e.g. XP in a VirtualBox or VMware VM), but eventually these older systems and applications will not be supported and may not even be available to future users.

1.3 Future proofing and updating

1. DEPOMOD was written in Borland Delphi (pascal) which is no longer seen as a mainstream language
2. AutoDEPOMOD written in VB6 – now superseded by VB.NET. Support for VB6 will end in 2013.
3. Currently restrict application to Microsoft Windows platform.

1.4 Efficiency & Optimisation

1. Applications written in days of limited memory resources
2. Single threaded – most PCs have multiple cored processors
3. Reliance on multiple files –the application could be better coded to take advantage of new computer hardware, potentially making it faster and capable of running larger and more complex models. In addition, the current versions are not easily extended without major programming of the original code

1.5 Improving AutoDEPOMOD predictive performance: measuring and modelling

DEPOMOD and AutoDEPOMOD were created over several projects with a variety of objectives. Initially designed as a rational method of matching farm biomass with site characteristics to ensure the ability of the environment to assimilate wastes while leaving an infaunal biomass sufficient to allow bioturbation and bio-irrigation of sediments, it was first used by SEPA to regulate the consent of in-feed medicines. AutoDEPOMOD was designed to allow an iterative modelling approach based on sediment quality standards within the AZE and later developments on the thinking of site specific Allowable Zone of Effect were incorporated which were intended to facilitate a more rational use of seabed assimilative capacity in more dispersive environments.

The original DEPOMOD work was calibrated at only 2 sites (Cromey *et al.*, 2002a) which may not be representative of the large variety of sites that are currently in use or proposed in Scotland. An analysis of the relationship between modelled organic solid loading and predicted benthic response (using ITI) has shown that there is in general a tendency for DEPOMOD to over predict impact at quiescent sites and under predict impact at more dispersive sites. In addition there is a considerable degree of variation between predicted and actual values of ITI over a range of sites (Figure 1.1).

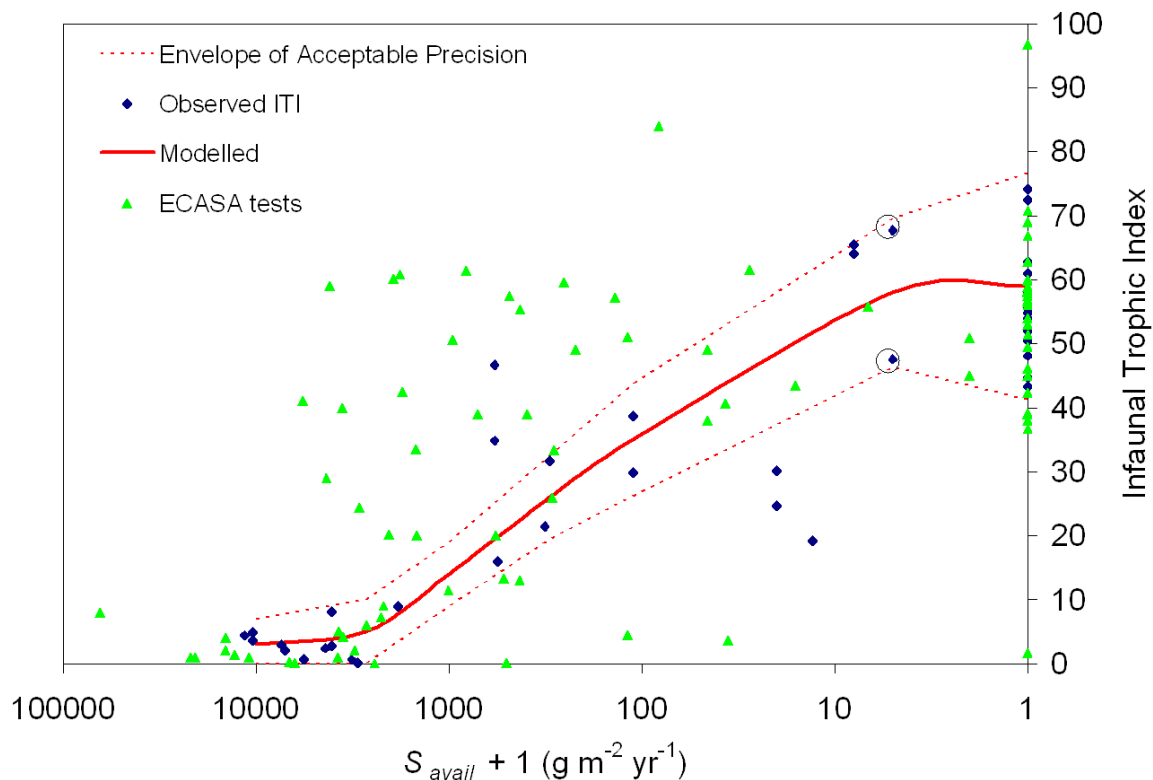


Figure 1.1. The relationship between prediction and observation: blue diamonds represent the original DEPOMOD calibration stations whereas the green triangles represent data from a range of test sites taken from the SEPA database and analysed under the ECASA project (www.ecasatoolbox.org.uk)

The SEPA fish farm monitoring and audit datasets are a rich source of information, for example in terms of comparing model predictions with subsequent observations (Fig 1.1), and it is likely that a lot more could be learned from these. They also present a cost-effective opportunity for validation of any proposal to allow more flexibility on the parameterisation of the model as may result from the work proposed here. Mayor *et al.* (2010) published a statistical analysis of SEPA's fish farm monitoring benthic data and concluded that "in isolation, current speed, water depth, and farm size are not necessarily good predictors of benthic impact" which supports the concept of using a modelling framework to rationalise large amounts of fish farm derived benthic data.

Wells (2007) used a subset of the SEPA database to consider: emamectin benzoate measurements, noting that the model typically over-predicted sediment concentrations; the response of the benthos at a range of fish farms, concluding inter alia that the majority of failures to meet SEPA sediment quality criteria (SQC) occurred at 25 m stations rather than at the cage edge (a result worthy of further attention in terms of modelling) and; concentrations of metals in fish farm sediments, particularly copper and zinc, concluding that there was no evidence that these were causing a negative effect on the macro-benthos at these farms.

1.6 Resuspension

Resuspension is a key process in DEPOMOD and, as it is the result of a complex set of interacting processes that may vary in magnitude between farming environments, the majority of the research effort will be focussed on this area. At present, in the model,

resuspension occurs when currents reach a critical threshold for erosion and generate sufficient bed shear stress to resuspend particles from the seabed. The extent of erosion is controlled by an estimate of erodibility and waste particles are considered as being consolidated 4 days after deposition and hence un-erodible. Bed shear stress is not only a function of current speed but also of hydraulic roughness length which may vary spatially at a fish farm site but may also be altered by deposition from the farm.

As an illustration of this, consider a generally eroding rough bottom on which sediments from a fish farm may accumulate faster than they are eroded thus changing the sediment surface and therefore sediment roughness. Reduced roughness will tend to lower the bed shear stress and, therefore, reduce resuspension. Further from the farm, supply of particles from the farm may become lower than the rate at which they are eroded and so roughness (and therefore erosion rate) is maintained. This does not, however, mean that there will be no impacts further from the farm, as it is likely that fine organic material will occupy the interstices between larger sediment particles even though the sediment surface is relatively clear. This is likely to be responsible for at least some of the results found by Chamberlain and Stucci (2007) at a coarse-bottomed site in British Columbia and was also observed in the Sound of Mull (2010).

1.7 Goals

The goals of the work reported here were:

1. To completely rewrite the model code in a modern language (Java) in a modular form that will facilitate future maintenance and development. Hereafter, this model will be referred to as NewDEPOMOD to distinguish it from its successors.
2. To remove dependencies on third party software (e.g. excel, MS Excel) as far as possible
3. To carry out field and laboratory studies to improve our understanding of resuspension processes around fish farms and to use these to refine the modelling of resuspension processes and hence improve the predictive ability of the model.

2. Recoding the model

2.1 Existing DEPOMOD and AutoDEPOMOD code base review.

The existing DEPOMOD product was written in Delphi as two completely separate and self-contained units of code, the partrack unit and the resus unit. The partrack unit was used to model the transport of waste feed and faeces from the fish farm cages to the sea bed. Then the resus unit would 'replay' the arrival of the particles and then either add them permanently to the sea bed if they had not moved for four days or resuspend particles which could then be transported around the modelled domain. Both were executable programs with two separate and distinct libraries of supporting functions². Analysis of the code bases showed that much of the functionality between the partrack and resus units was replicated; however it also revealed discrepancies between the implementations of apparently similar functions. To carry out an analysis, text files describing the various inputs to the model and its configuration were grouped together into a collection of folders (often referred to as a project). The outputs from the partrack and resus programs could then be analysed in external programs. Such analysis was mainly carried out in a contouring product called surfer (*Surfer*® 7 Golden Software, LLC).

AutoDEPOMOD was an ancillary program that was written to facilitate the use of DEPOMOD. Apart from the main executable (which provided a user interface) it relied upon MS excel 2003 and Surfer. AutoDEPOMOD coordinated the actions of the user updating the required entries in the excel spreadsheet which was stored as part of the project, launching the DEPOMOD programs and carrying out analysis of the model output.

The Excel spreadsheets were used to implement functions, written in Visual Basic for Application (VBA) which calculated the feed and chemical inputs to a fish farm based upon the Biomass and other factors as well as carrying out calculations required for testing the environmental quality standards. The excel spreadsheets were also used to layout the fish farm cages. When the DEPOMOD model was being run, AutoDEPOMOD injected the output files into Surfer to carry out complicated calculations associated with measuring the projected area and volumes of contours on the calculated discharge surfaces (mass of Carbon on sea floor etc.).

After the layout of cages and definition of inputs AutoDEPOMOD repeatedly called the partrack and resus programs to calculate new depositions of mass on the sea floor, altering the biomass between iterations. This process continued until the model had found the maximum biomass that passed the environmental quality standard set by SEPA. Three separate types of model configuration were available modelling benthic impact of carbon in feed and faeces, and the distribution of two different types of in feed treatment Teflubenzuron (TfBZ) and Emamectin Benzoate (EmBZ).

2.2 Implementation of ported java application

After the initial analysis of the existing code base, the decision was taken to port the application without any major alteration to its structure. This decision was taken in part due to the complexity of the code base and also many limiting factors such as the visibility of variables between units and the proprietary and non-atomic nature of its input files. It is

² Functions are small self-contained segments of code which can be called from the main body of a program to perform a defined task and return a result.

important to note however, that many of the design choices made were required to address the limitations of computer hardware available at the time.

Replicating the structure of the applications in Java was not straightforward since the language structures assume object orientated programming. The ported application therefore uses programming practices which are generally considered to be anti-patterns³ (see references to design patterns in subsequent sections). For example the non-atomic nature of the inputs meant that data structures returned from one unit of code would not contain all the required information in order for them to fulfil their purpose, meaning they would then be passed to other code sections in order to have the missing entries completed. Consequently, they represented an amalgam of data that in the real world we would think of as distinct. Due to the structure of the original DEPOMOD code base testing and debugging the application required 'single stepping'⁴ the applications in unison, checking the values of individual variables after executing each line.

Another complexity was that licensing issues of the code base had not been resolved and therefore it was decided not to use third party software libraries since the redistribution of such code and binaries might contravene the eventual NewDEPOMOD licensing. Consequently java based libraries for topology, numerical algorithms and geographical information were implemented. Much project design, coding and testing time was devoted to contouring of sea floor deposition and calculations of the projected area and volumes using numerical quadrature. Comparison of the results showed that the methods applied by Surfer resulted in different results compared to the methods implemented in Java. As part of the testing of the ported application a library of routines was written in C++ to provide java with an interface to call the Surfer algorithms and consume the results, allowing changes in the numerical algorithms to be isolated from examinations of divergent behaviour between the original and ported applications.

2.3 Design of NewDEPOMOD

The two guiding principles of the design of the NewDEPOMOD datatypes were:

- 1) That they should naturally extend from the parameters of the problem that were considered to be important e.g. flows, bathymetry, feed inputs, distinct physical processes, etc.
- 2) That the individual entities (objects in an object orientated programming context) should be atomic being provided with all the information and functionality required to carry out their role at creation time.

However, in order to avoid the code base becoming rigid and to achieve the open-closed paradigm⁵ two more important principles were rigorously applied:

³ An anti-pattern is an informal term referring to a reinvented bad solution to a problem which has an established solution. See <https://en.wikipedia.org/wiki/Anti-pattern>

⁴ In 'single stepping' the program is executed inside an application that allows execution to be stopped at predefined points and then individual instructions to be executed and their effects on the data held in memory to be seen.

⁵ The open-closed paradigm simply states that a computer program or library of objects should be open to extension but closed to changes. By extension is meant addition of separate units of code or code that changes the behaviour without affecting the original code behaviour, changes refer to modifications to the previously written code itself. See https://en.wikipedia.org/wiki/Open/closed_principle

- 1) The relationships between the units of code were defined via Java interfaces (supported by generics)⁶
- 2) Extensive use of constructor dependency injection was made⁷

Several iterations of analysis, design, implementation and testing were gone through as the coding progressed, but the existing interfaces and implementations have remained stable during the final stages of the project.

2.4 Datatypes and utility libraries

To isolate code dealing solely with the representation and manipulation of data from the main body of the application, separate datatypes and utility libraries were introduced. Datatypes can be loosely thought of as separate physical entities e.g. bathymetry, flow, particles, etc. that carry out some defined purpose e.g. provide the depth of the sea floor at a specific x,y coordinate. The external storage of the inputs to the numerical model and user interface was rationalised; with specific data being stored in a single dedicated file and extension of existing xml and java properties formats. To achieve backward compatibility, an importer application has been designed that reads the original DEPOMOD data and saves it in the new formats.

The datatypes libraries also provide the interfaces referred to earlier which provide the opportunity for future contributions to NewDEPOMOD to be provided by other groups and users interested in extending its capabilities. In addition, using standard design patterns⁸ makes the code-base easier to understand, with the existing implementations serving as a template to guide future contributions. For example, using the observer pattern to inform other objects when a value inside another object has changed helps to decouple the classes and allows future and unknown relationships to be accommodated.

One of the largest and most complicated of the datatype structures was the sediment bed model. This was based upon an adaptation of work originally produced by Sanford (2006) and represents a major change from the previous version of the DEPOMOD resus unit. In the new bed model, discharge from fish farms is not sequestered (consolidated) after four days. Instead the discharge from the farm is built up in layers, as each layer is filled a new layer is created on top of it. As a layer of sediment is buried deeper in the bed so a property known as the critical erosion stress is increased. When the erosion begins and the layers above are emptied so the deeper layers are exposed, however the reduction in the critical erosion stress is not instantaneous and therefore erosion may cease despite the bed shear stress being maintained at the same level. This relaxation time constant introduces a property to the bed

⁶ Interfaces are a method of defining what functions (referred to as methods in Java) a particular object implementing it exposes to other objects. This allows any two (or more) Objects that fulfil that interface to be used interchangeably.

⁷ Dependency injection is a programming technique that means that the internal functionality of an object can be modified by externally providing different implementations when the object is brought into existence (constructed). As an example: think about interpolation - there are lots of different methods of interpolating data, an object could implement each one internally but if a new one is required this would immediately violate the open-closed principle. A better alternative would be to define an interface for interpolators and then produce implementations that provide specific interpolation methods. These are then injected into objects that need interpolation functionality. See: https://en.wikipedia.org/wiki/Dependency_injection

⁸ Design patterns are strategies for dealing with commonly encountered requirements of software, they are not a library implemented in a particular language but rather show the relationship between objects that solves a problem without introducing undesirable effects. See: https://en.wikipedia.org/wiki/Software_design_pattern

called hysteresis and represents a significant modification in the behaviour of the bed and erosion.

Two other areas of change were the bathymetry and the flow datatypes. The Bathymetry data has been designed and implemented so that the consumers of the interface methods it exposes are unaware of the representation of the underlying data. For example Bathymetry data could be represented on a regular grid of sample points or, as is commonly the case for numerical hydrodynamic models, on an irregular grid of triangles (triangulated irregular networks or TIN). To achieve this the bathymetry is now represented as polygons (squares, rectangles, triangles) with the depth at a particular point in space being found using interpolation. The polygons also provide for estimation of the gradient of the plane as well as accurate location of a particle's intercept with the sea floor. The ability of the model to run using a TIN has been tested using Mike DHI formatted bathymetry data. Such data formats commonly represent data in an arbitrary order. To support this format a counter rotating edge rule was used to identify boundary vertices and edges.

The flow data interface also provides support for flow data represented as spatially varying currents again either defined on a regular grid or a TIN. It also allows for spatiotemporal variation in other flow related parameters such as salinity, temperature or diffusivity, used to simulate turbulence.

The utility libraries provide implementations of numerical algorithms that are required mainly by the environmental quality standards and estimation of biomass when the model is optimising stocking levels. Again standard software engineering practices have been applied here where interfaces in combination with the façade pattern would allow alternative numerical libraries to be used in the future.

2.5 Numerical Engine and runtime frame work

The numerical engine was designed by analysing the different phases of the transport of waste feed and faeces, and is broadly similar to the previous DEPOMOD except that all phases of transport are now included in a single framework and time runs forwards only. Four separate transports are defined: suspension transport (cage to sea floor), bed transport (motion of intact particles on the sea floor), the bed model (storage of discharge (mass) within the sediment) and the resuspension transport (distribution of discharge eroded from the sea floor). The transports are designed so that they can be run in parallel on separate threads of a modern multi-processor computer. To achieve this, an interleaved iterator was designed and implemented so that access to a single unified list of particles in a particular phase of transport could be split between separate processors. Structural modifications to the list are then carried out on a single thread. This removes the need to externally synchronise the collections (an example of a structural modification would be transferring particles that entered a new phase of transport from one list to another). Another advantage of the interleaved iterator is that since the processing time for the movement of a particle is similar, the required page of memory is more likely to be found in the cache within the CPU. Once the number of particles becomes large enough this dramatically reduces the amount of cache turnover when compared to the alternative of splitting the list into contiguous segments.

Because of the use of interfaces and dependency injection, the numerical engine is quite complicated to configure. In order to manage the creation of the numerical engine, handle storage of the outputs and prepare subsequent iterations, a runtime framework has been introduced. Its role is in fact similar to parts of the original AutoDEPOMOD except that it does

not have a graphical user interface. This allows large numbers of projects to be run either sequentially or simultaneously if a batch queuing system is used. This may be used to provide a mechanism to verify the model results submitted when fish farmers are applying to SEPA for discharge consent.

2.6 Implementation of Physics from Partrack report

The Partrack Ltd. were contracted to carry out the erosion experimental work and their recommendations report came out in its final form in 31st of March 2015 and is presented in Annex 2. The report detailed additions to the physics determining the transport of waste feed and faeces from the farm cages as well as the erosion processes from the sea floor. The recommendations specified the equations that should be used in the transports (although the transports are not completely specified by the recommendations in the report) as well as default parameter values obtained from extensive measurements of fish farm impacted sediments (see next chapter).

The recommended transports equations were implemented in individual objects abstracted by interfaces as they may represent possible points of extension and change in the future. The default parameters have a major impact upon the model results and these are stored internally so will not be user alterable in the final release.

2.7 Support for SEPA model tuning

After the numerical engine and runtime framework were developed to the stage of reasonable stability, they were released to SEPA for them to tune the parameter set against field data. This was done by taking the reported feed and treatment usage data for a group of fish farms extending over several years and using it as the input time series to NewDEPOMOD. NewDEPOMOD was then used to simulate the discharge using the extended inputs data and the predict impact on the sediment was compared to the samples taken from fish farms over the simulated period. NewDEPOMOD successfully handled the extended inputs data as well as changes in the sampling period of the flow data from 1hr to 2 min. This demonstrated that NewDEPOMOD was able to handle both extended data and that there was no interdependency between the temporal resolutions or lengths of the input datasets. NewDEPOMOD has also been successfully run using bathymetry data that represents spatial extents other than the commonly used 1 km domains with 25 m square grid cells.

2.8 NewDEPOMOD user interface

The AutoDEPOMOD user interface was extremely simple and aligned to the task of planning fish farms; in fact the original motivation for the AutoDEPOMOD project was to accelerate the planning of fish farms for SEPA. Guided by annex H of the SEPA Fish Farm Manual and the original AutoDEPOMOD interface, the task of planning a fish farm was broken down into a series of distinct tasks, each of which was then analysed to obtain a series of actions. Together these tasks and actions along with the data can be viewed as the plot and props for a play. When a user is planning out a fish farm they are effectively following this script and acting out the play, this strong narrative form helps to direct the user within their role. It also influences the design of the interface since it indicates what actions must be supported and helps to remove extraneous features from the interface.

The NewDEPOMOD user interface was implemented using the NetBeans platform, this avoided writing large amounts of user interface code since the NewDEPOMOD interface could be written as plugins to the existing platform. Although, as described above, the created

plugins are very much directed towards streamlining the task of planning fish farms, any plugins can consume the same inputs and outputs of the model. Therefore if other groups of users require certain functionality, for example simulating benthic chemistry processes, they can easily be added for that group to both the model and the user interface without them affecting all users of the product.

2.9 User documentation

The NetBeans platform provides support for contextualised user documentation i.e. pressing the help button within a sub window provides help pages specific to that user interface element. Additional pages will also be added to cover system requirements, installation and post installation configuration. The documentation used by the NetBeans help system is written in HTML. This means that it can also be easily provided in parallel from a webserver with both copies remaining synchronised as well as distributed in a static offline version with the download folder of the product.

2.10 Implementation of product release and internal issue tracking support

Version control has been routinely used throughout the development of the product and has been used to track releases to SEPA for testing. However, once the NewDEPOMOD enters distribution a more traceable system of issue tracking and update issuing needs to be implemented. SAMS is currently in the process of migrating NewDEPOMOD so that it is controlled by Atlassian. This provides not only source control separating development from production source code but also internal issue tracking for identified bugs as well as mechanisms to build the software and run it against unit tests.

2.11 Implementation of product updates

The NetBeans platform provides a mechanism for automatically receiving updates from a secure webserver (they can also be downloaded and installed manually). This provides a convenient mechanism that allows updates to be pushed to users. Version information within the individual units of the data and the outputs of the model help to ensure that data submitted in the fish farm license have been run using the most up to date version of the software.

When the application is in production potential errors and bugs that are identified by users can be reported. By requesting the users to transfer the application's log files, along with the data and a sequence of events required to reproduce the error, the issue can then be examined. If the issue lies with the input data, support can be provided to produce data that is correctly formatted. Otherwise the bug can be added to the internal issue tracking described above.

3. Research on Resuspension processes

3.1 research cruises

Six fish farms were selected in consultation with SEPA (Figure 2.1)



Figure 31 Sites used for field work

On an initial research cruise on *Calanus*, high resolution multibeam bathymetry data were collected from *Calanus* from each of these sites (Table 3.1). This was followed by 2 cruises which focussed on seabed erosion and determining seabed frictional forces. These cruises are presented in detail in the report by Partrac Ltd. as Annex 1.

Table 3.1. Research cruises

Dates	Vessel	Purpose
24 th /26 th Jun 2013	<i>Calanus</i>	To map fish farms using multibeam and use occasional grabs for qualitative assessment of bottom types.
19 th /30 th Aug 2013	<i>Sir John Murray</i>	Deployment of Voyager flume to determine erosional properties of seabed around fish farms and current meter rig to determine seabed friction
20 th /30 th May 2014	<i>Seol Mara</i>	Deployment of the mini-flume at cages edge stations to examine the erosion properties of fish farm derived sediments

3.2 Results

3.2.1 Bathymetry data from Calanus Multi-beam Cruise

Bathymetry data were collected at each of the sites, processed and archived at SAMS. Figures 2.2-2.6 show an image of these data superimposed on a chart from Google Earth. Figure 2.7 shows the bathymetry in the Sound of Shuna which includes the Shuna Castle Bay and BDNC sites as an image overlaid on an Admiralty chart. This is a composite of data collected during this project together with other data collected on other projects using the same technique.

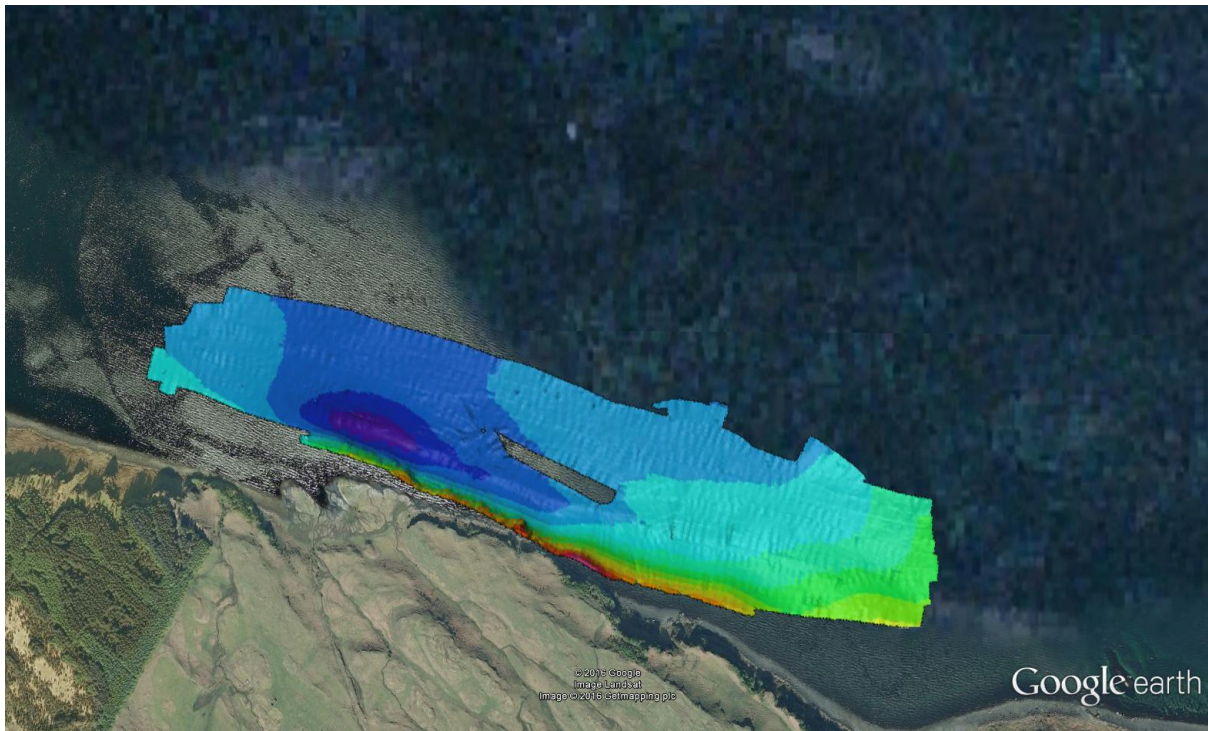


Figure 3.2 Bloody Bay

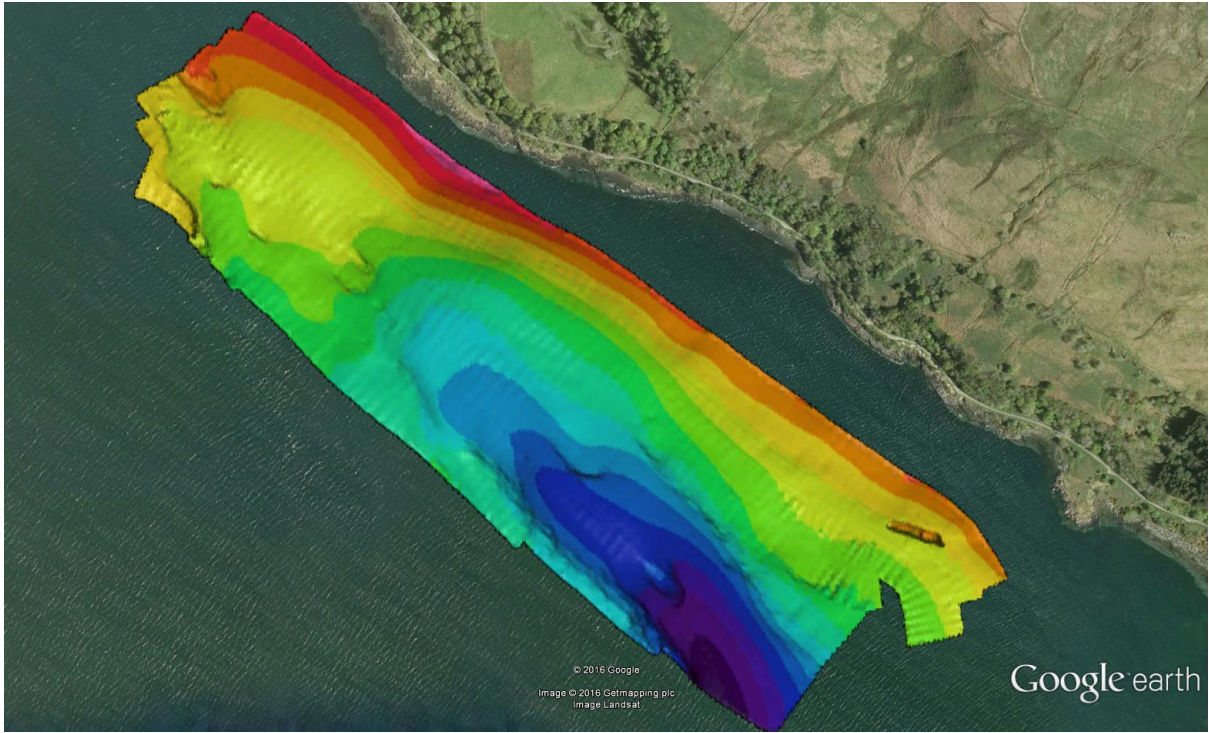


Figure 3.3 Fuinary

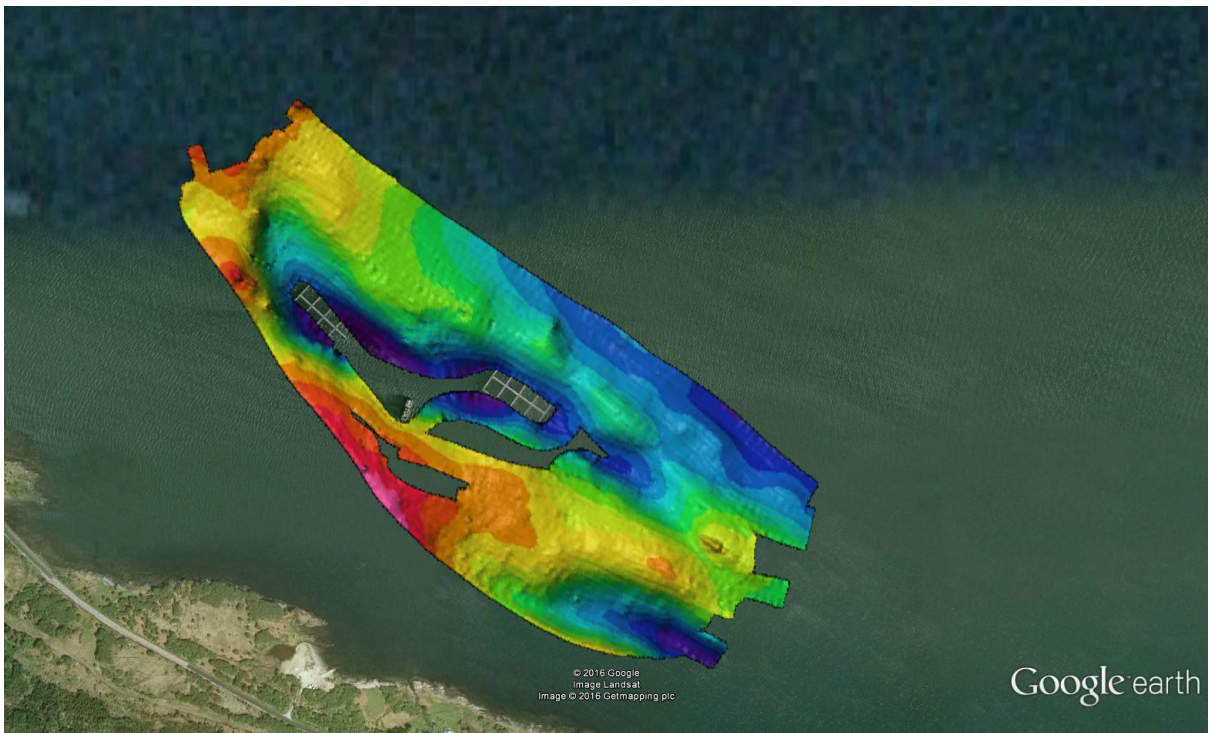


Figure 3.4 Scallastle Bay

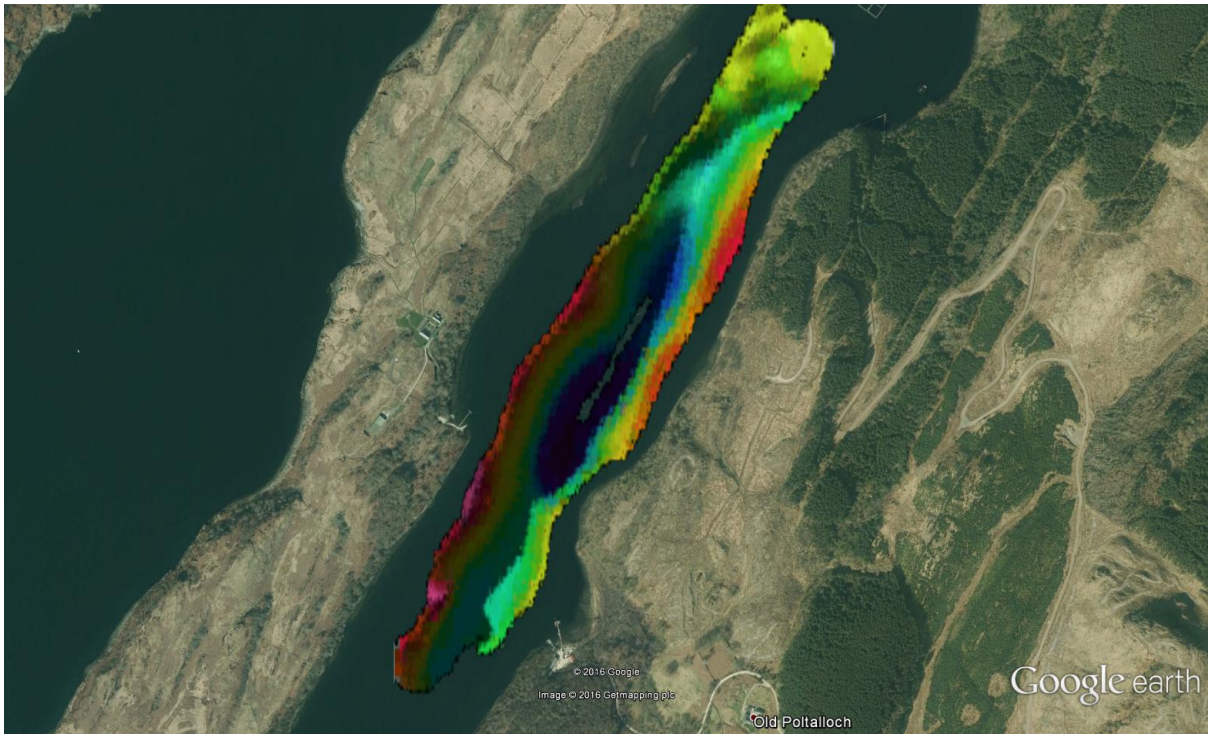


Figure 3.5 Port na Moine

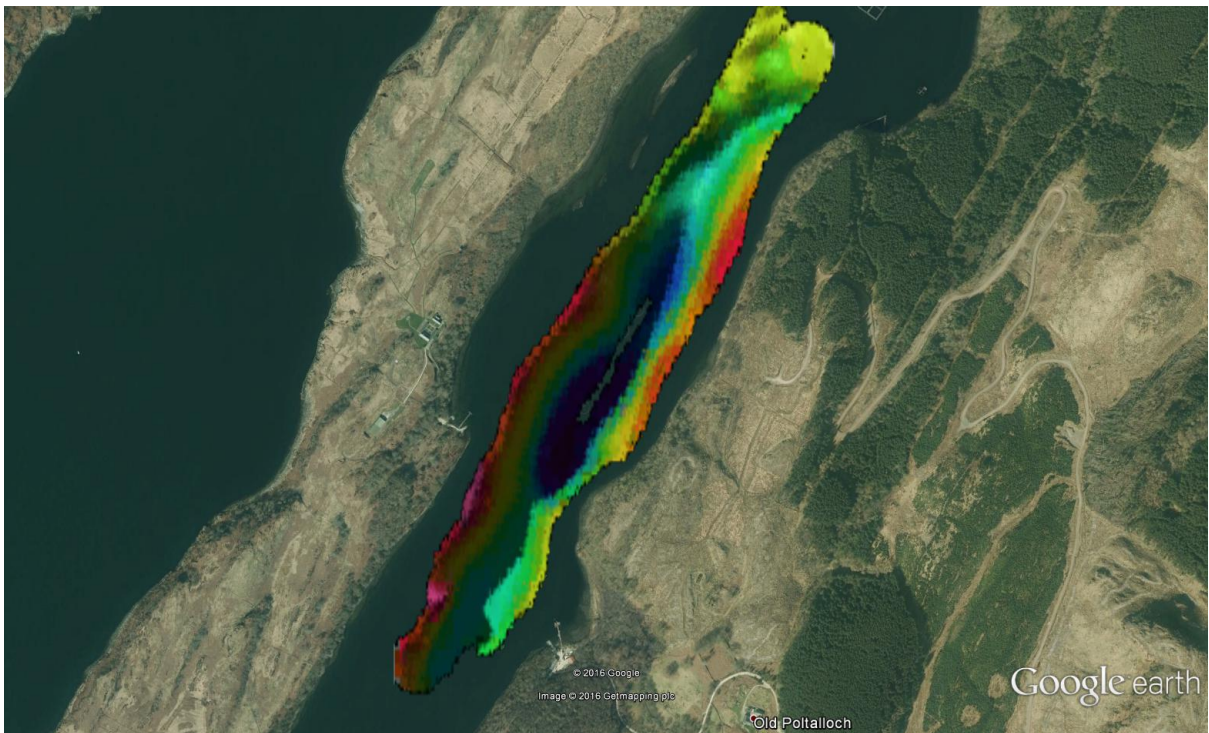


Figure 3.6 Ardifuir

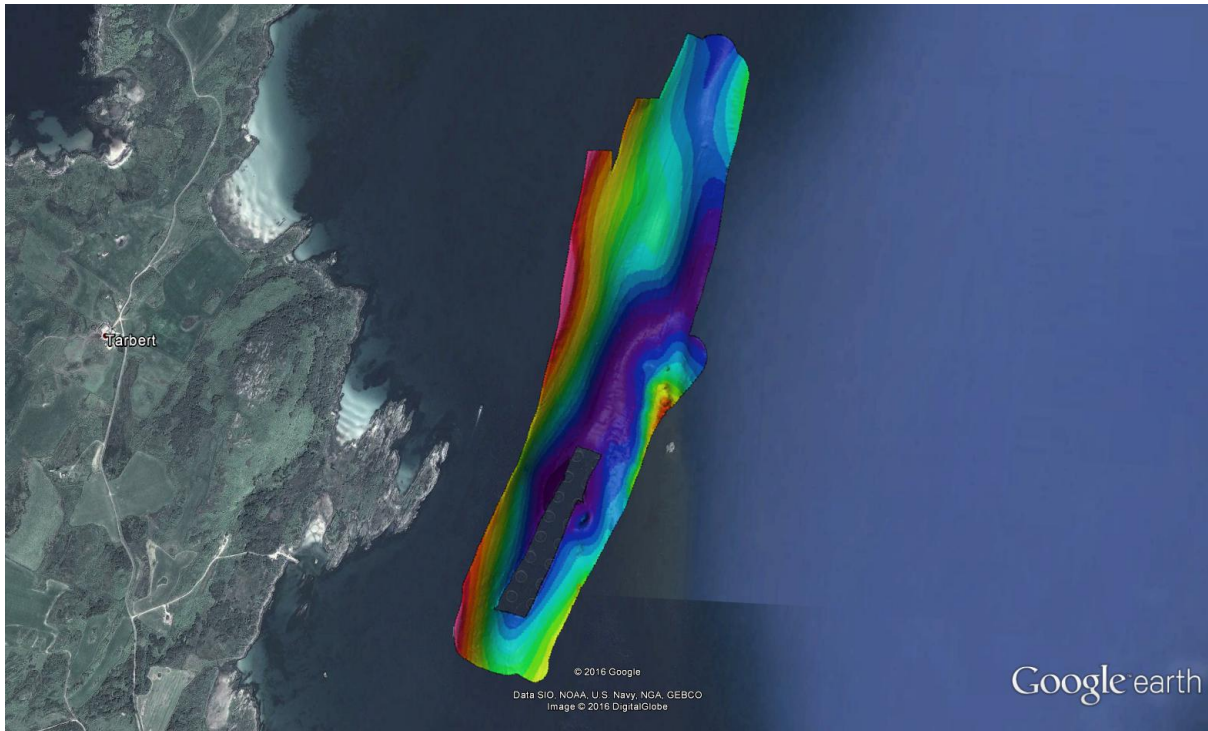


Figure 3.6 Druimyeon Bay

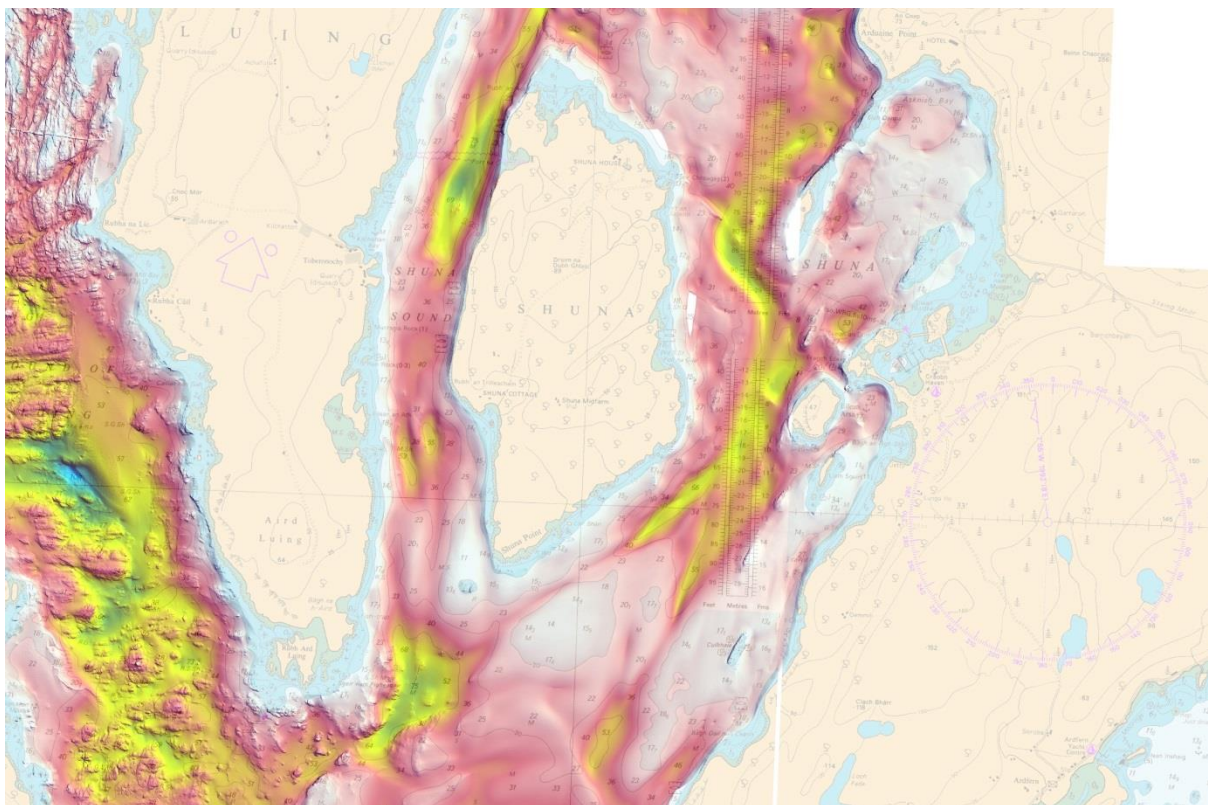


Figure 3.7 Sound of Shuna

The bathymetry data were used to inform site selection for subsequent cruises. They were intended to be used in comparative model runs to determine *inter alia* the value of using

high resolution as opposed to low resolution data during validation. This work was deprioritised but will be done some time after the model is released.

3.2.2 The resuspension cruises

The work of the cruises on Sir John Murray and Seol Mara was written up as a stand-alone document which is attached as Annex 1. The discussion of these results and recommendations for modelling were also written up in a separate report which is attached as Annex 2.

4. Model validation

The new model has been tested by SEPA in order to establish its suitability for environmental risk assessment and determination of consent limits on licences for aquaculture-related discharges. This test was undertaken with 3 goals in mind. To produce a model which:

1. Is more accurate
2. Is more flexible, configurable
3. That supports industry expansion

Given the greatly increased range of features, representing new or enhanced physical concepts, and the increased flexibility with respect to input data, the new model offers a much greater variety of scenarios which can be simulated. Consequently, NewDEPOMOD can produce a vastly greater range of outcomes than the old model. The challenge for validating the model is, therefore, not so much *whether* the model can produce accurate predictions, but rather *how* can it be set up and configured to produce the most accurate predictions. With this in mind, the validation of the model was approached in three main ways:

1. **Appraisal of original model:** this used *hindcasting* approach to compare the output of the original model with observed seabed impacts
2. **Calibration of the new model:** this tested configuration options for the new model using a similar *hindcasting* approach in Approach 1.
3. **Consenting implications of the new model:** this tested configuration options for the new model using a different approach – comparing the “sustainable” biomass quantities predicted by the new model with known, historical site performance..

An advantage of the hindcasting approach, used to appraise the old model and test the new model, is that it measures the absolute accuracy of the model against empirical data. However, sufficient coverage of seabed data was only available for 6 sites, and in these cases with some important limitations. The testing of consenting implications therefore answers important practical questions about future policy implications for SEPA but it also adds many more sites to the test suite (~50) and therefore provides a greater breadth of tested scenarios in terms of environmental (flow regime, bathymetry, etc.) and operational (cage layout, biomass, etc.) conditions.

4.1 General hindcasting approach and test sites

Hindcasting refers to the use of a model to “predict” an event that has already been observed, using input data that corresponds to the known conditions under which the event occurred. The logic behind the approach is that if a model can translate an observed set of inputs or “forcings” into the correct – i.e. observed - response, then the model can be considered to represent the functioning of that system adequately. In the case of AutoDEPOMOD this means using, for example, accurate data on bathymetry, flow conditions and historical feed and treatment quantities to produce a model estimate which can be directly compared with accurate, historical seabed impact data.

AutoDEPOMOD predicts two types of seabed impact: (1) a measure of the ecological impact on benthic invertebrates arising from the flux of organic solids; and (2) the concentrations of the active ingredient of an in-feed sea lice medicine, Emamectin Benzoate (EmBZ), following a simulated treatment. In principle, empirical observations of either of these types of impact could form the basis of a hindcasting exercise. However, the response of benthic invertebrates to an organic flux is associated with a high degree of uncertainty and therefore

when comparing such data to model output it is difficult to differentiate between the accuracy of the physical dispersion processes encoded in the model and the uncertainty with which any modelled physical impact (i.e. solids flux) is translated into an ecological impact. Therefore, the use of EmbZ as a reactive hindcasting “tracer” was preferred (the theoretical decay rate of EmbZ is known). Since EmbZ is bound to organic solids, the settling, dispersion, erosion and transport of EmbZ is considered to be entirely representative of the dynamics of organic solids generally. Therefore, validating and/or calibrating AutoDEPOMOD on the basis of EmbZ residue hindcasting implicitly tests the (identical) mechanics behind the dispersion modelling of organic solids.

Seabed EmbZ residue data from routine monitoring undertaken in association with all treatments is held by SEPA. However, this data only comprises two sampling locations per site. Such a sparse coverage of impact data is insufficient for adequately characterising the spatial extent and intensity of a seabed impact. Therefore this routinely collected data was considered inadequate for the purpose of assessing model performance.

For several sites, however, SEPA has a greater coverage of residue data as a consequence of SEPA’s own surveys in 2013 as well as some additional data collected by farm operators. In these cases, between 10-12 residue measurements per site, collected concurrently from 4 transects radiating out from around the farm cages, were available and provided a detailed spatial coverage of residue data against which the modelled, spatial impacts could be assessed. In two cases, the Noster and Seaforth sites, 3 flow data sets were available respectively, and this therefore presented an opportunity to test the sensitivity of the new model to differing samples of flow conditions.

Table 4.1 The 6 test sites with characteristic hydrographic information.

site	Water body	flow data start date	mean speed (m/s)		mean tidal range (m)
			surface	bottom	
Ardintoul	L. Alsh	10-Jun-12	0.07	0.07	3.34
Gorsten	Up. L. Linnhe	30-Dec-12	0.17	0.07	2.51
Ardgour	Up. L. Linnhe	18-Apr-13	0.11	0.08	2.75
Noster	L. Seaforth	10-Mar-05	0.06	0.04	3.0
Noster	L. Seaforth	25-Oct-10	0.06	0.06	3.0
Noster	L. Seaforth	23-Jul-15	0.04	0.08	3.0
Portnalong	L. Harport	16-May-06	0.05	0.04	3.08
Seaforth	L. Seaforth	02-May-05	0.05	0.04	3.0
Seaforth	L. Seaforth	24-Sep-10	0.12	0.05	3.0
Seaforth	L. Seaforth	25-Jul-15	0.07	0.06	3.0

For each of these sites (and flow datasets) hindcasting model runs were undertaken. The precise details of these runs differed (for technical reasons) in the case of appraising the old model and calibrating NewDEPOMOD, and these are described below. In all cases, however, hindcasting involved simulating up to 4.5 years of real, historical treatments. The 4.5 year limit reflects the fact that the theoretical decay rate of EmbZ indicates that discharged quantities reduce to <1% of their original mass during a period of 4.5 years. It follows that all treatments over this time period prior to seabed sampling could, in principle, have contributed to the observed seabed impact.

4.2 Appraisal of original model

Since multiple treatments cannot be simulated in the original model, hindcasting was approached in the following way:

1. Single treatments were simulated using actual historical treatment quantities for all treatment occurring within 4.5 years of the sampling date at each site.
2. Each treatment was modelled over 223 days, the maximum possible in the original model.
3. For each site, the predicted seabed impacts – i.e. the spatial concentrations of EmBZ – of each successive treatment were added together to form a “cumulative” impact arising out of all treatments.
4. When adding impacts, concentrations of EmBZ were artificially “decayed” to an extent which depended on the time in between the historical treatment date and the sampling date. This was intended to represent the decay which would occur between treatments but was not captured in the individual 223 day runs
5. The cumulative, artificially decayed impacts were compared with the observed seabed residue concentrations

Since the original model could only accept a single, constant feed rate, this was determined using the 8-month average, historical feed rate which corresponded to the period subsequent to each treatment at each site, derived from SEPA’s database of monthly operation data which is provided as a requirement of discharge licences. The original model could also only accept 1 hour flow data resolution (in contrast to the new model) and therefore this was used in all hindcasting tests of the original model.

The results across all sites are summarised in Fig. 4.1. Each plot shows modelled and actual concentrations for samples situated at similar distances relative to farm cages. The upper plot shows sample locations at the “cage edge”, that is immediately adjacent to cages (usually in north, east, south and west directions). The lower plot represents the samples taken furthest from cages in 4 directions at each farm, with the distance notionally equating to the position where concentrations were expected to meet SEPA’s Environmental Quality Standard (EQS). The middle plot shows sample taken in between these two extremes.

The general pattern indicated by the residue samples are for concentrations to be much lower at cage edge locations in comparison with model predictions (upper plot, Fig. 4.1) but generally higher than predicted by the model further out. This is especially at the farthest, “EQS”, locations where the model under-estimates actual concentrations in many cases, including some which exceed the EQS.

This indicates a general tendency for the model to under-predict dispersion - essentially concentrating the impact underneath the farm cages to a greater extent than appears in reality. This may arise from a number of reasons:

- General model configuration that produces low dispersion (e.g. mass erosion rate, roughness height, dispersion coefficients)
- Averaging of peaks in flow data
- 4 day (permanent) lock down of particles

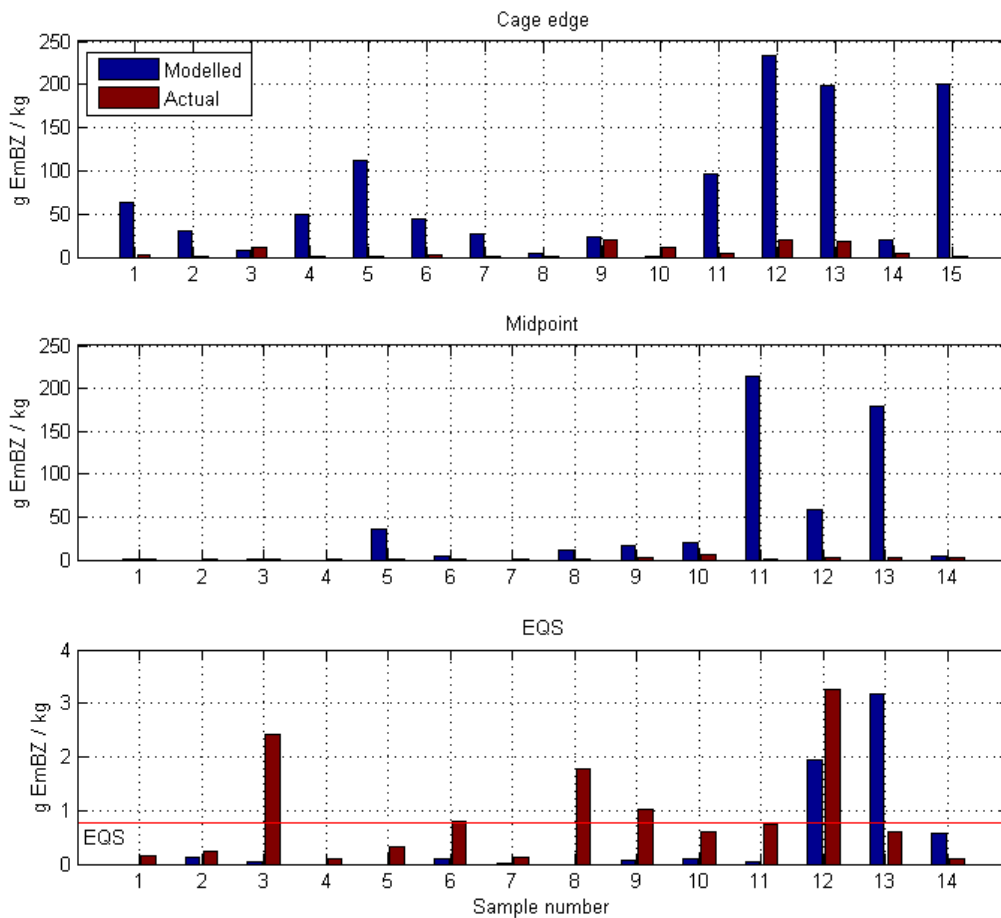


Figure 4.1 Comparisons of AutoDEPOMOD (old model) predictions vs observations at 14 stations near the cages (top plot), at the notional EQS limit (bottom plot) and at an intermediate distance (middle plot)

Another possibility is that this result reflects representativeness of hydrographic data (i.e. astronomical, meteorological variations) in the sense that the model has used a hydrographic data sample describing much slower conditions than were seen in reality. This seems unlikely since some of the sites were modelled with data collected during large spring tide conditions and it is unlikely that all datasets represent unusually calm meteorological conditions.

The occurrence of cage edge concentrations which fall considerably short of modelled predictions (often by an order of magnitude) is consistent with routine (but patchy) monitoring data seen by SEPA. This suggests that there is an inherent tendency in the original model to accumulate mass beneath the cages that does not correspond with reality.

Other anecdotal evidence suggests that in some cases – typically with very fast flow - footprints are observed despite none being predicted by the original AutoDEPOMOD. Together with the above conclusions, this implies that the original model can, in some (or perhaps most) cases, be too depositional, but in other cases too dispersive. This may reflect highly non-representative hydrographic data in some cases. It may also reflect the sensitivity of the original model to flow speeds (perhaps in relation to grid resolution), the fact that the original model ignores bathymetry when resuspending and transporting particles, or other issues related to the implementation of sediment transport process. In any case, a

requirement of the new model is to disperse material sufficiently to approximate the comparatively small concentrations observed in reality - particularly close to farm cages - but to also produce realistic impacts in cases with high flow speeds.

4.3 Calibration of new model

The hindcasting assessment of the new model took a slightly different approach to the assessment of the old model. Although the old model was configurable to some extent, the use of the model as a consenting tool involved an invariant set of parameters. Therefore, the old model was assessed in terms of the result provided using the standard configuration. It is possible that the old model would give different (possibly better) results using a different configuration, but exploring and understanding that was not considered to be worthwhile at this stage. Instead it was important to understand how the old model *has* performed in practice, and how the new model *could* be used in principle. Therefore, the validation of the new model *would* include the exploration of configuration options with a view to identifying a configuration and method of using the new model that could be considered acceptable and an improvement over previous practices. The assessment of the new model was technically more of a *calibration* than a validation - each site would be tested against a range of parameter and other options in order to understand the model response and identify preferred options.

The second significant difference in hindcasting with the new model is that the new model is much more flexible in terms the range of input data that can be used and the types of scenarios that can be represented. Therefore an additional effort was made to use more detailed input data where possible. This included:

1. Monthly resolution feed data
2. Multiple treatments applied over single, continuous model run
3. Longer time series of flow data, either empirical or artificially extended
4. More detailed bathymetry data over a larger domain

These are described in more detail below.

4.3.1 Hindcasting data for new model

4.3.1.1 Feed and treatment data

The new model enables arbitrary time series data for faecal and medicine discharges to be used (i.e. any length and resolution). This presented two advantages over hindcast modelling in the original model:

1. Monthly feed data could be used (rather than a constant, average feed rate, as used in the original)
2. The entire period of 2-4 years preceding the residue surveys could be modelled in one run. This meant multiple treatments could be simulated in succession and that the interim periods in-between treatments were fully represented in terms of continual discharge, decay and transport

Feed data was collated from the monthly data returns held by SEPA and converted into hourly faecal discharges using water content and wastage assumptions (as used in model). The excretion time series for each successive treatment was also compiled into a single time series, incorporating the overlapping discharges of treatments where appropriate (i.e.

treatments within ~220 days of each other), and reducing to zero at times with no onsite biomass.

4.3.1.2 Flow data

Although SEPA have good EmbZ residue data available for 6 sites, contemporaneous flow data is not available for the periods relating to those impacts. Therefore hindcast modelling has been performed using relatively small samples of flow data which may be non-representative of the actual flow conditions experienced when the impact was being created. This, naturally, leads to some, unavoidable, level of discrepancy between modelled and observed concentrations. A more robust test of the model, and more accurate approach to model-site calibration would be to use flow data collected through the time period over which a measured impact has formed.

Some of the sites used for hindcasting/calibration have several flow datasets available and therefore each of these has been used for separate hindcasting analyses. This provides some indication of the variability of flow conditions at individual sites and the sensitivity of the model to different flow datasets.

As a partial workaround to the possible non-representativeness of the flow data, each flow dataset was artificially extended and scaled in order to more accurately represent astronomical variations in flow. Extending the datasets was done by sampling a full spring-neap period from the data and repeating until a dataset 1600 days long was obtained. Spring-neap period length samples of the original data were taken alternately from different starting positions in order to minimize discontinuities in the water level and flow records at the boundaries between repeated sections. The extended (repeated) dataset was then scaled according to reference to water level variations for the hindcasting period obtained using Admiralty TotalTide®. For each spring-neap period, the tidal component of flow magnitude was scaled by a factor representing the ratio of the maximum astronomical tidal range in the Total Tide dataset to the maximum astronomical tidal range in the sampled dataset. A modification was also applied to treat spring and neap phases differently - neap tides were scaled *down* in cases where spring tides were scaled *up*. The random component of flow was not scaled but it was randomized in time through the extended and repeated dataset. This approach accounts (to some extent) for differences in the magnitude of the astronomical forcing of flow which occur in reality but are not captured in the short, sampled dataset. It does not account for variations in the non-tidal component, such as those driven by episodic wind, buoyancy driven flow or loch overturning which occurred during the collection of data and may or may not be representative of longer-term conditions. Nor does this approach rectify any directional biases present in the sampled data.

4.3.1.3 Bathymetry data

Four of the sites used have been surveyed by the SEPA vessel, Sir John Murray, using multi-beam sonar technology (WASSP) to measure bathymetry. These sites are Ardgour, Gorsten, Noster and Seaforth. In these cases new bathymetry data was developed for use in the model based on a 2 km domain.

4.3.2 Calibration approach

Calibrating AutoDEPOMOD to produce good results basically means (in most cases) getting the correct scale of dispersion - not too depositional, not too dispersive. There are a large number of parameters that have an effect on dispersion in the model. These include:

1. **domain configuration:** size and resolution
2. **dispersion:** settling and resuspension phase dispersion coefficients
3. **settling:** use of shear modified settling velocity (settling and/or resuspension phase)
4. **erosion function:** mass erodibility coefficient and exponent, critical shear stress for resuspension
5. **bed model parameters:** consolidation and relaxation times, etc.
6. **bed roughness**

These represent a large model space to explore with a vast range of potential outcomes depending on combinations of configuration options. In principle, many combinations of these options could produce a reasonable model fit and therefore every possible combination could be tested, although this would be impractical for computational reasons. In any case, some judgement has been exercised, based on experimentation or other considerations, in order to identify suitable values for each of these options without resorting to an exhaustive and time-consuming exploration of the many-dimensional model space.

4.3.3 Indicative results

Hindcasting scenarios were run for the 6 test sites using a range of parameter configurations. No single model configuration was seen to demonstrably provide close agreement with empirical residue concentrations across all of the sites. Rather, the hindcasting exercise provided several general outcomes:

1. The model is able to simulate more complex scenarios than previously (e.g. larger domain, longer flow datasets, arbitrary feed and medicine time series)
2. The model is highly configurable in terms of the range parameter choices available
3. Empirically observed seabed impacts can be reasonably approximated on the basis of a 14 day sample of flow data in some cases but requires a tuned configuration of parameters
4. The model output is highly sensitive to the flow dataset used, with 14 day samples proving inadequate for representing the longer-term conditions under which impacts were formed.
5. Calibration/validation of the model using long-term (e.g >6 months) flow data collected concurrently with residue impact data would be highly valuable

Some indicative model outputs are shown below. In each of figures 4.2 – 4.15 :

- cages are shown as black circles
- sampling locations as red stars, along with concentrations in ug/kg
- contours represent modelled concentrations
 - **yellow** = 0.1 ug/kg
 - **green** = 0.763 ug/kg (EQS)
 - **red** = 7.63 ug/kg
 - **black** = 25.0 ug/kg

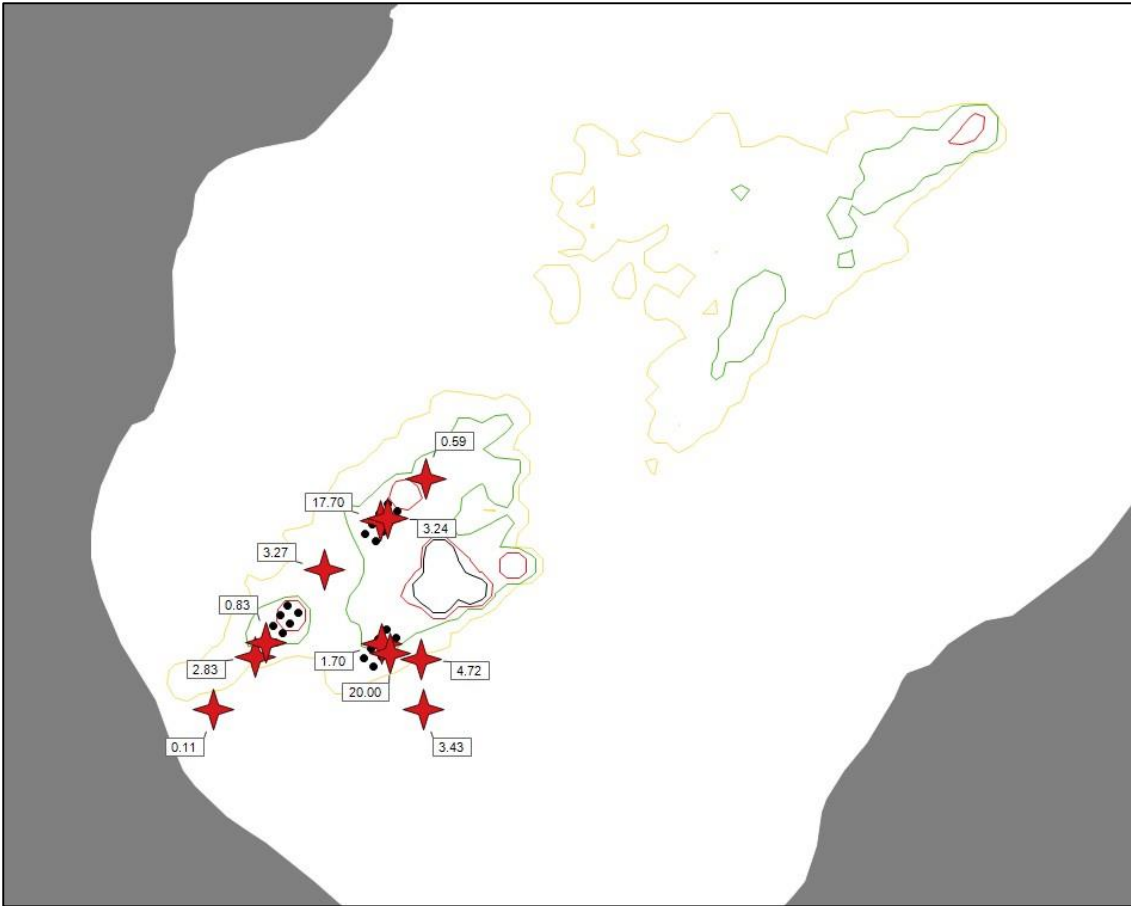


Figure 4.1: Ardgour, $z_0 = 1^{-10}$

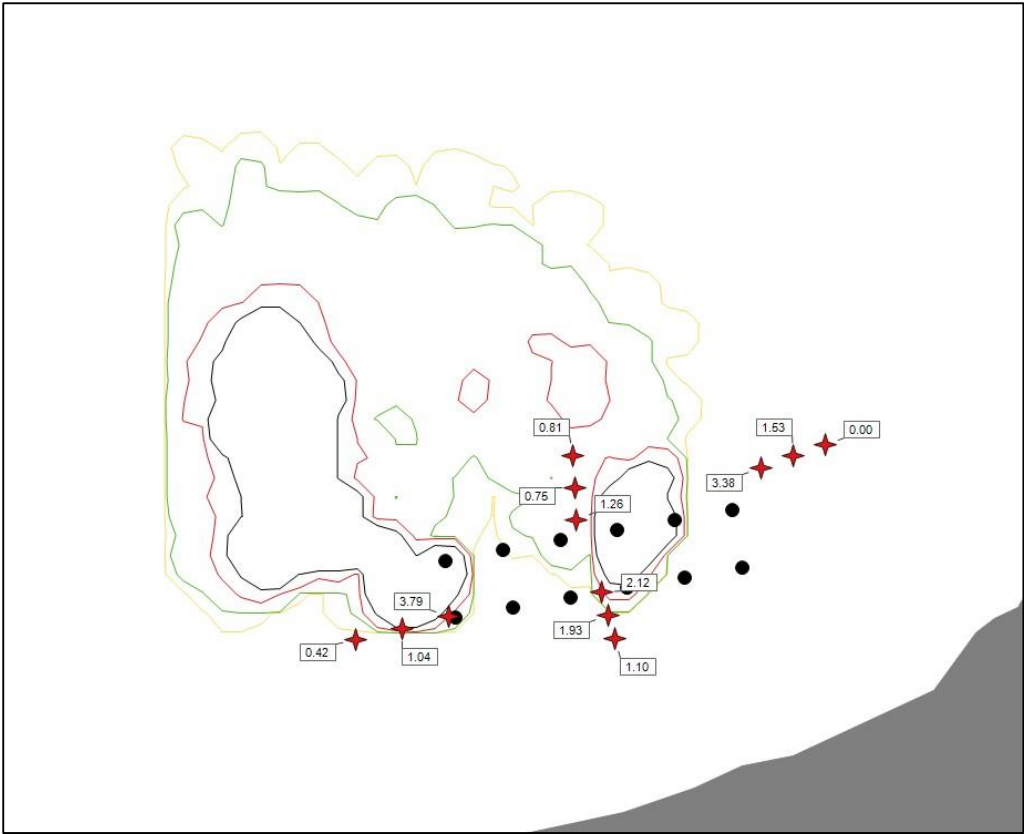


Figure 4.2: Ardintoul, $z_0 = 5^{-6}$

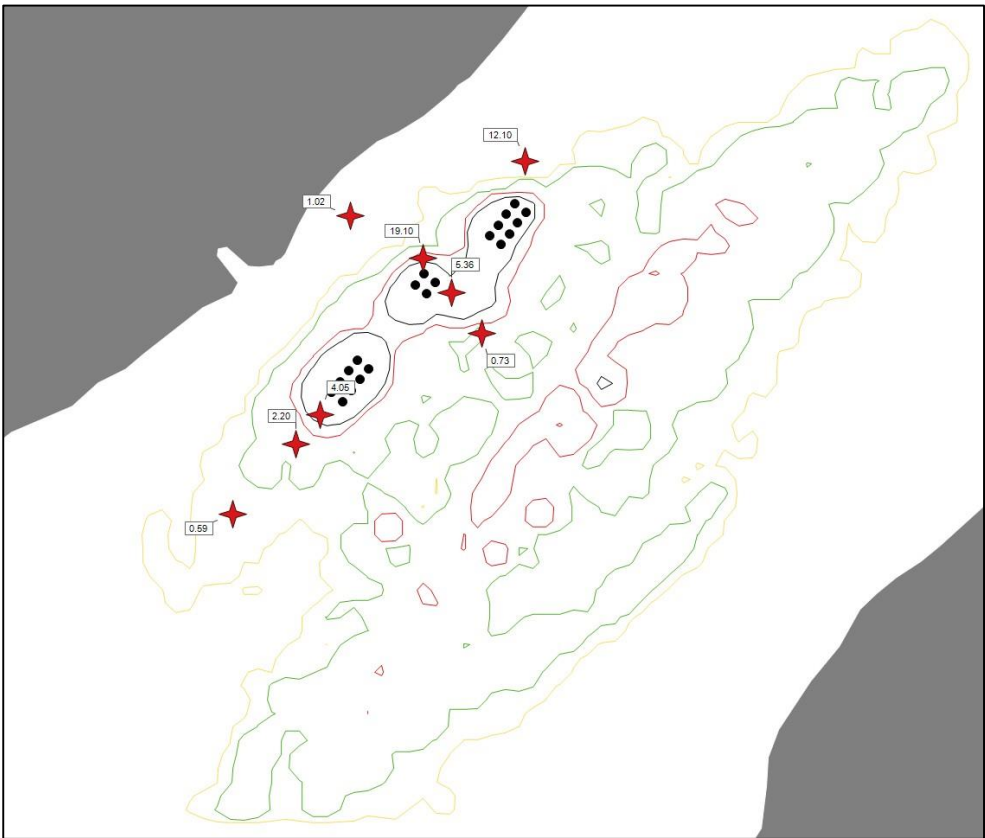


Figure 4.3: Gorsten, $z_0 = 1^{-6}$

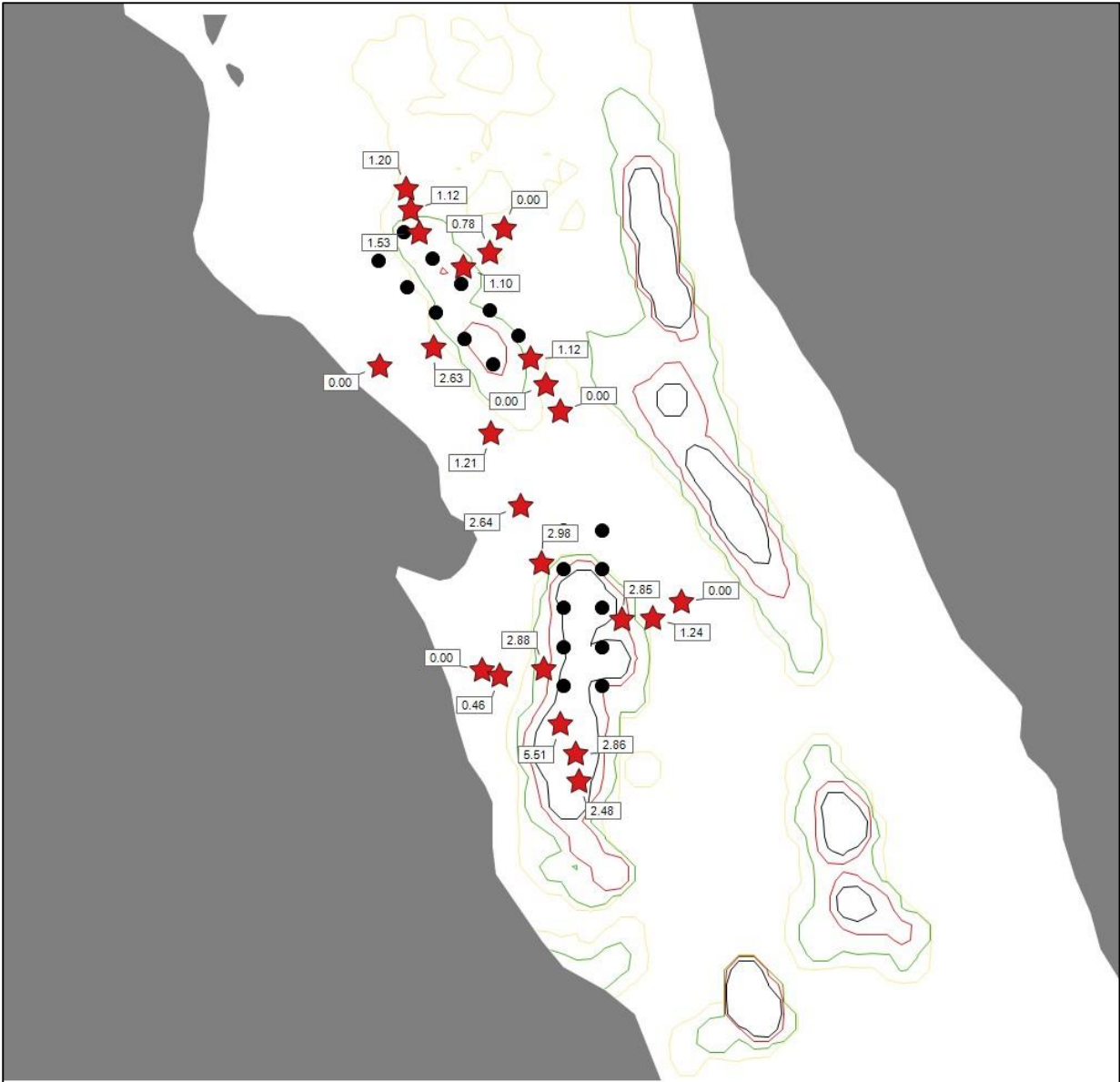


Figure 4.4:Noster/Seaforth (2005 flow data), $z_{0,N} = 0.003$, $z_{0,S} = 0.008$

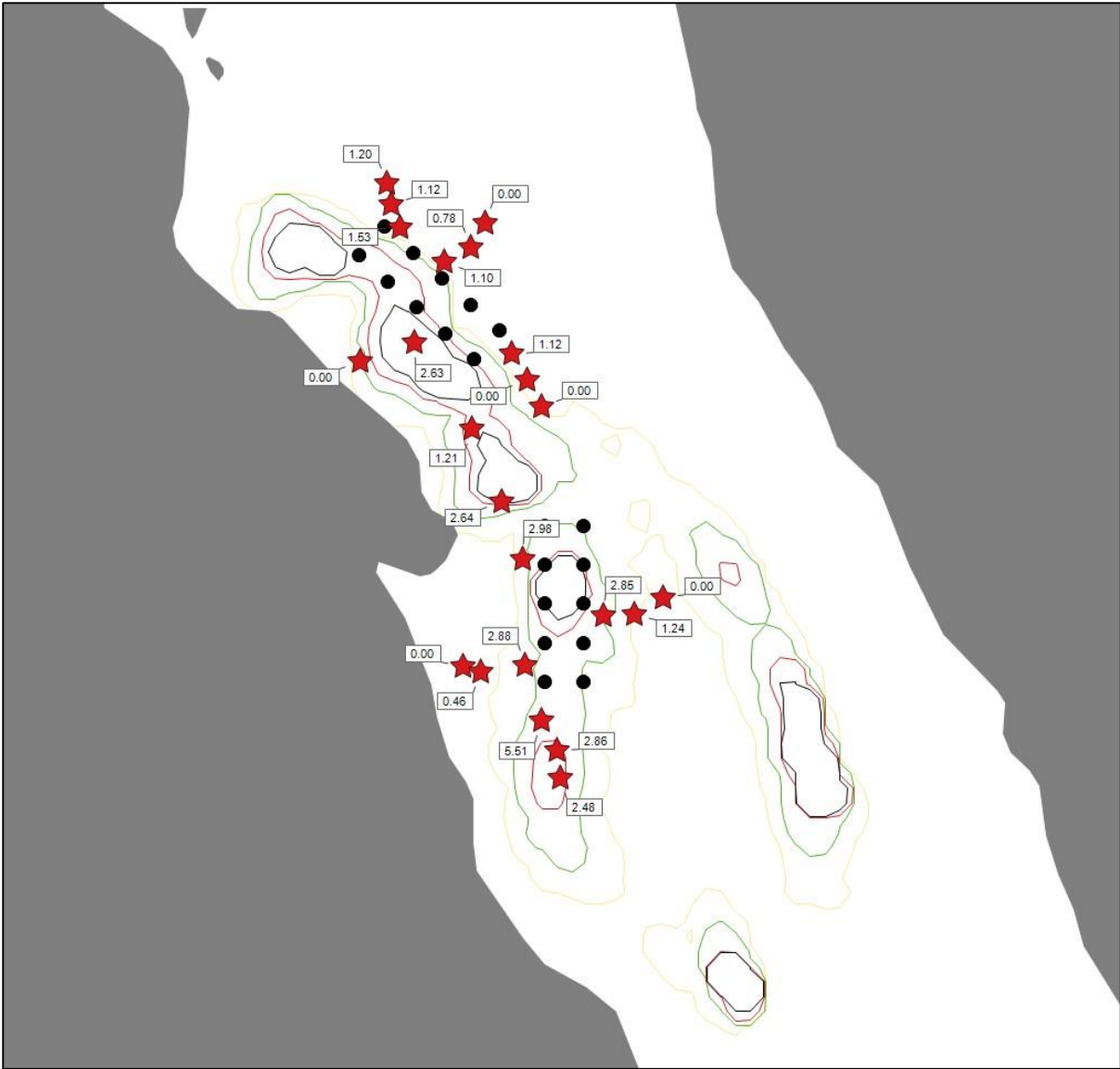


Figure 4.5: Noster/Seaforth (2010 flow data), $z_{0,N} = 0.00003$, $z_{0,S} = 0.02$

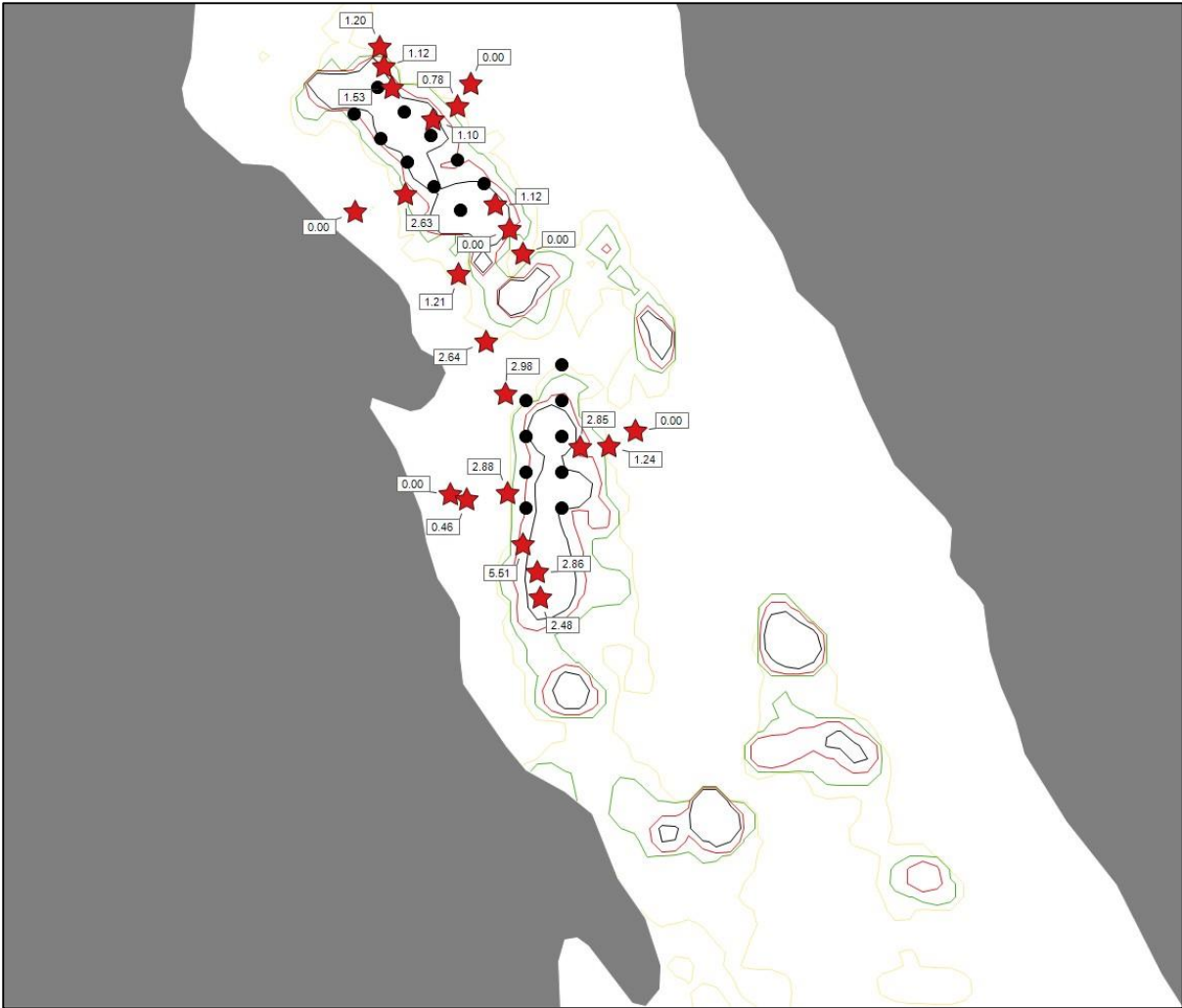


Figure 4.6: Noster/Seaforth (2015 flow data), $z_{0,N} = 8^{-8}$, $z_{0,S} = 0.00003$

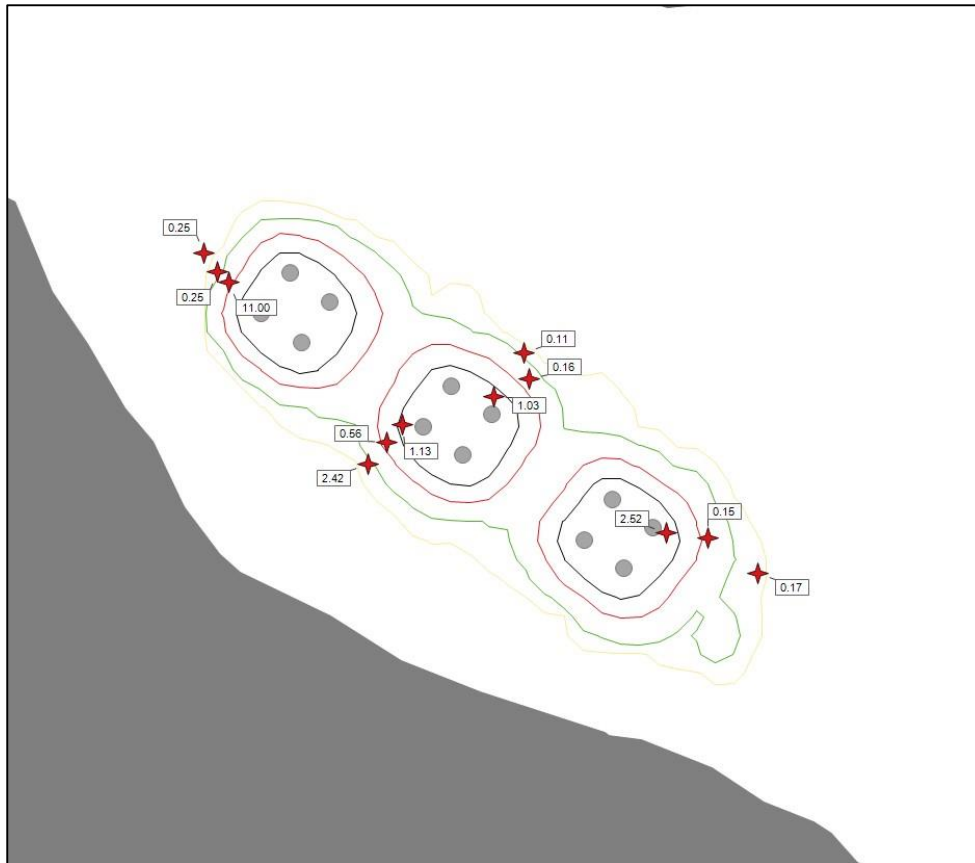


Figure 4.7: Portnalong, $z_0 = 0.0002$

These plots illustrate the best fits to the empirical residue data achieved for each site, and were ostensibly based on tuning the model specifically via the bed roughness (z_0) parameter. The bed roughness parameter scales the magnitude of shear stresses which are imparted on the model sediments relative to the forcing flow dataset. This parameter was found to have the most profound effect on the scale of dispersion in the model and needed to take a large range of values across all of the test sites in order to achieve reasonable fits to the data.

In many cases extended or secondary footprints were predicted. This is considered to reflect both the greater dispersion (on average) in the new model as well as the larger model domains used in most cases. Two sites, Ardintoul and Portnalong, used a 1 km domain whereas the other sites used a 2 km domain. In the case of Ardintoul an impact can be observed against the western boundary of the domain, which indicates that the domain is too small relative to the dispersion that occurs at that site. This is not observed at Portnalong, a site which has much less energetic flow conditions. Isolated experiments with domain size showed that the use of a 1 km domain caused, in some cases, an *export bias*. This was established by measuring the size of an EQS level impact using different sized domains. The use of larger domains caused not only the overall mass balance to be larger, but also the EQS footprint to be larger. This was interpreted to reflect the fact that less material was vanishing over the domain boundary in the larger domain cases and was therefore available for reworking around the domain including the potential for transport back towards the farms as current direction varied during the simulation. At all sites an impact was observed, even in those cases with sufficiently fast flow (e.g. Ardgour, Noster (2015)) that no impact would have been produced in the original version of the model.

Bathymetry plays an important role in determining the extent and locations of impacts. Footprints not elliptical – as they typically, approximately were in the original version - but have shapes which follow bathymetry and in some cases are patchy reflecting bathymetric changes. Ardintoul and Gorsten, for example, have steep gradients and deep areas (not shown) close to the cages which skews the footprints – material is less likely to settle on the steep gradients and most likely to accumulate in the deep flat areas adjacent to the steep gradients. This causes the footprints to become extended in one or more directions and considerably larger than in the original model. Loch Seaforth has a deep trough on east side of loch where material from the Noster and Seaforth farms concentrates in the model. There is also a sill at the mouth of the loch (south) which prohibits transport and is therefore conducive to accumulation. Such areas of preferential accumulation are consistent with an intuitive understanding of the effects of bathymetry on sediment transport and therefore represent a significant improvement over the bathymetry-agnostic original version.

These experiments also show the sensitivity of the model to flow data. In particular, the Noster/Seaforth cases, in which hindcasting was performed using 6 (3 x 2) flow datasets, shows the effect of flow conditions sampled at different times. Firstly, the flow datasets from different years (2005, 2010, 2015) show different levels of flow speed, and therefore energy for sediment transport, and this is reflected in the z_0 values which are required to calibrate each flow dataset to the observed impact. In addition though, the scenarios using different flow datasets show quite different impact zones, with the 2005 datasets producing impacts to the north and east, and the 2010/2015 datasets producing impacts more to the south, southwest and east of the farms. This highlights the significant directional artefacts that are present in the 2-week flow data samples and that cannot be accounted for by either astronomical scaling of the flow dataset or tuning of the bed roughness (z_0) parameter.

There was no single configuration of parameters that could be considered to decisively provide good, spatially accurate fits, to the empirical data across all sites. These experiments did show that the model can produce approximately “correct” (relative to the empirical data) *magnitudes* of impact, however, if not the precise seabed *positions* of these impacts. Furthermore, these experiments showed that the model responds to configuration changes in physically intuitive ways. Discrepancies between observed impacts and those produced by the model must, however, be considered in the context of the highly limited flow data which does not closely represent the conditions under which the observed impacts arose both in terms of long term flow magnitudes and the predominance of flow directions. The development of a more comprehensive calibration dataset(s), including long-term (>6 months) current meter data together with concurrent seabed impact data would be a significant improvement on this exercise and invaluable for validating the model.

Previous use of AutoDEPOMOD in Scotland has generally followed a highly prescriptive approach, developed by SEPA, in which a default model configuration together with 14 days of flow data are used to define modelling scenarios which are taken as a more or less definitive expectation of how the site will function. Experience of the new model, together with reflections over the historical usage of the previous version, suggest that a shift in modelling philosophy to incorporate some or all of the following would be beneficial:

1. The use of significantly longer flow datasets, incorporating a greater range of astronomical and meteorological conditions, including episodic events

2. A probabilistic approach using the outputs of multiple modelling scenarios which emphasises patterns of relative risk over absolute spatial predictions
3. Site-specific calibration of the model using long-term flow, feed, medicine data with concurrent seabed impact data

4.3.4 Technical observations

4.3.4.1 Shear modified settling velocity

The first release of the new model engine caused an amount of erosion and export of particles which, judged against empirical EmBZ residues, was highly excessive. Some consideration was given as to which parameters might be changed in order to reduce some of this erosive behaviour and *shear-modified settling velocity* was hypothesised to be a candidate. Shear-modified settling represents an adjustment to the settling velocity of particles on the basis of shear (that is, vertical variation in velocity) in the water column: the settling velocity is reduced depending on the magnitude of shear in the water column. This adjustment is applied to particles in the initial phase of settling from cages, as well as those eroded during resuspension events. The impact of shear modification, however, is significantly greater for eroded particles due to their much smaller densities. This feature can be turned off for the settling and/or resuspension phases respectively in which case particles fall at their (faster) still water settling velocity.

A particular reason for concern was the fact that particles can achieve *negative* settling velocities on the basis of this shear-modification, that is, they can become *buoyant*. That suspended particles can rise through the water column, even to the water surface, due to the effects of turbulence is not disputed. However, it was felt that turbulence would act to *diffusively* transport *some* particles to the surface as concentration gradients are reduced and the water column is mixed. The implication of the model implementation of shear-modified settling velocity, however, is that eroded particles may become buoyant *en masse* and the entirety of the suspended load could - depending on flow conditions in successive time steps - rise together as an *organised* layer, potentially reaching the surface together. The latter scenario was not considered realistic and, as a consequence, a switch was built into the model configuration options for disabling this potential, positively buoyant state. The use of shear-modified settling can therefore be configured to be enabled or disabled in both the settling and resuspension phases, and in both cases the option to allow positive buoyancy can be additionally and separately configured.

4.3.4.2 Vertical dispersion coefficient

A consequence of turning off shear-modified settling in the resuspension phase is that the particles move much less during resuspension events (because they settle faster). In the context of the "out of the box" model configuration, this caused the model to be *under*-dispersive. Related to this change, and a partial cause of the reduced dispersion, is that, without shear-modified settling, particles respond very sensitively to bathymetry. This occurs because, in cases where the bathymetry shallows in the direction of transport, the interception of the seabed occurs sooner than otherwise. This can cause particles to become stuck behind even small bathymetric artefacts, possibly to an unrealistic extent. To be clear, this response to bathymetry is considered to be a *good* thing, and represents one of the significant improvements on this new model over the original one. But the extent to which particles are sensitive to the bathymetry needs to be appropriate if magnitudes of dispersion and transport are to be predicted adequately.

One way around this "problem" is to use the vertical dispersion parameter to "tune" this sensitivity to bathymetry. This parameter represents a random component to the vertical position of particles intended to account for turbulent diffusion. The parameter determines the length of a random walk which is applied to the particle motion in either the upwards or downwards directions on each time step. This parameter therefore controls, to some degree, the extent to which eroded particles are lifted into the water column, and therefore how quickly they settle. A number of experiments were made using an artificial bathymetric bowl with several values for the z-direction dispersion coefficient (as well as with shear-modified settling velocity enabled/disabled) to test the sensitivity to bathymetry and effects on erosion and export more generally. It was tentatively concluded that, in a configuration with shear-modified settling velocity disabled for the resuspension phase, a z-dispersion value of $0.005 \text{ m}^2 \text{ s}^{-1}$ used in the resuspension phase (as opposed to the assumed default 0.001) provides a reasonable compromise between transport and dispersion on the one hand, and response to bathymetry on the other.

4.3.4.3 Erosion function

Two alternative erosion functions are recommended in the Partrac report: a linear function of the critical shear stress exceedance, and a power law function. In basic terms, the linear function causes the mass of eroded material to increase at a constant rate relative to the shear stress exceedance over the critical value. So, as shear stresses increase over the critical value, so the eroded mass increases, linearly. The power law function is more complicated. At lower shear stress levels an increase in shear stress delivers a larger increase in the mass eroded than does a similar increase at higher shear stress levels. The implication of this is that the power law function is very sensitive to differences in flow speed at relatively low energy levels compared with higher energy level. This would mean that large differences could be expressed, in terms of levels of erosion, between fairly low energy sites, whereas high energy sites may be treated a lot more similarly despite differences in their flow speeds.

An absolute comparison between the effects of the two functions depends on the bed roughness chosen and so they are not easily comparable in a like-for-like way. Using the bed roughness values recommended by Partrac, the power law function causes significantly greater erosion at the range of flow speeds exhibited by the test case sites. At much higher flow speeds, the power law function would eventually cause less erosion than the linear function (at some bed roughnesses). But in any case, the power law function caused too much erosion when used in comparison against residue data in the test cases and so the linear function was tentatively favoured. In principle, the power law function, used in conjunction with other configuration settings and appropriate values for bed roughness could deliver a reasonable model response, but this has not been exhaustively explored.

4.3.4.4 Bed model

The "bed model" in NewDEPOMOD describes the consolidation and relaxation of buried and exhumed sediments which alters the critical shear stress required for erosion. In experiments, varying the parameters of the bed model showed no observable effect. Therefore, this feature has been tentatively ignored, with a view to further exploratory testing at a later date.

4.4 Consenting implications

While the hindcasting tests were designed to assess the absolute accuracy of the model, additional tests were made on the "consenting outcomes" (i.e. estimates of sustainable

biomass) of different model configurations. These can be judged against patterns of known site performance on the basis that “good model performance” would predict a lower sustainable biomass than the previous model for sites that have historically failed under cage intensity standards. On the other hand, sites which have not failed these under cage standards should be predicted to have a similar or larger predicted sustainable biomass.

Given concerns about the representativeness of 14 day current meter flow datasets, two modelling scenarios were tested: (1) standard scenario using the full 14 day flow data; and (2) a “tidal-only” scenario, which involved using only the flow that is attributable to astronomical effects, i.e. the tide. Two benefits arise from using tidal-only flow. Firstly, the tidal-only flow creates a scenario which represents the flow that can be “guaranteed”, that is, not subject to the episodicity of meteorological effects such as wind- or freshwater-driven currents. This presents a worst-case scenario for dispersion and accumulation under the farm cages, and therefore a modelling scenario which is conservative and can be treated with additional confidence from an environmental risk perspective. Secondly the omission of the non-tidal component of the flow removes the most significant source of variability between the sampled 14-day flow dataset and longer term conditions. This, to some extent, minimises sampling and representativeness issues with sampled flow data.

4.4.1 Results

A test suite of >50 sites was established and biomass optimisation runs made using a variety of model configurations and the two types of flow data: full and tidal only. Results using the default parameter configurations recommended by Partrac are plotted below, against the biomass values that were estimated from the original version and used to license the operations of the farms.

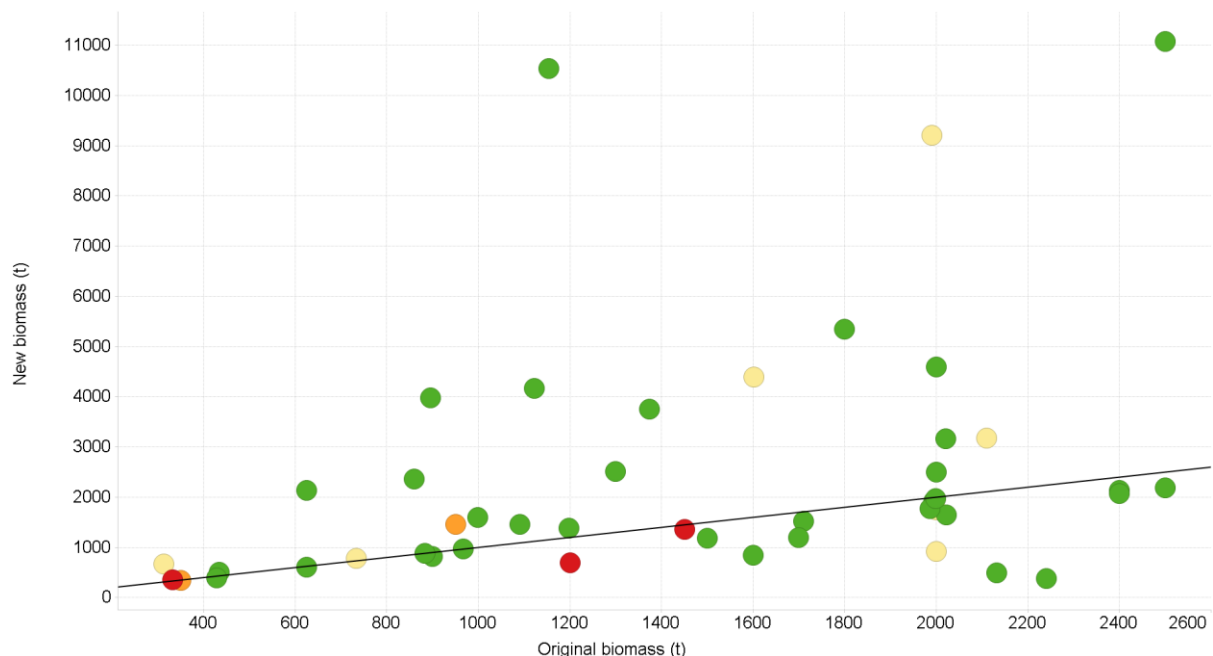


Figure 4.8: Original versus revised biomass estimates using full flow data

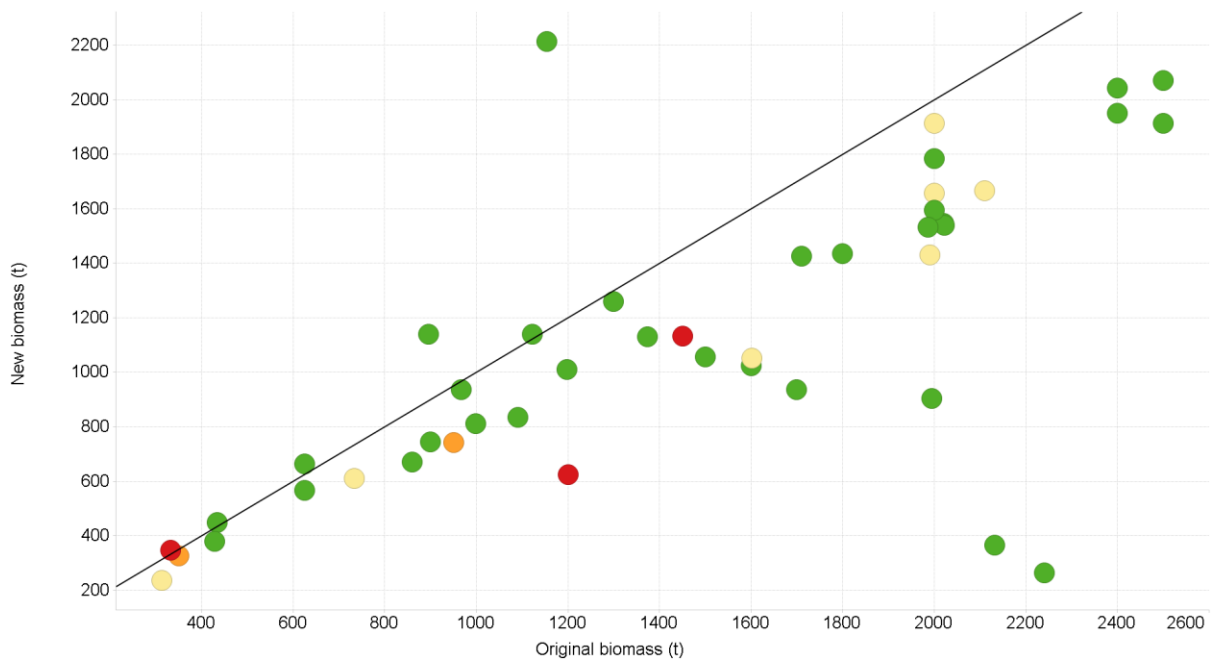


Figure 4.9: Original versus revised biomass estimates using tidal-only flow data

The black line in each plot is the line of equality between originally estimated biomass and the estimated biomass in the revised model. Points falling below the line are estimated to have a lower sustainable biomass in the new model compared with the old model. Points falling above the line are estimated to be able to accommodate more biomass according to the new model. The colour of the points indicates the number of cage edge intensity failures which have occurred historically at each site, as follows:

- green = 0
- yellow = 1
- orange = 2
- red = 3

Figure 4.8 shows the comparison between original and revised model biomass estimates in the case of using *full flow* data. The revised model runs use entirely Partrac recommended parameters, including shear-modified settling velocities although positive particle buoyancy was disabled. Most farms are seen to model at a higher biomass than in the original version (points above the line), with the average increase being ~20% plus ~600 t. This demonstrates that the new model is more dispersive, on average, when using default parameter values and similar flow forcing. Figure 4.9 shows the same sites and model configuration but executed using tidal-only flow. In this case most sites are considered to have lower sustainable biomass than in the original model. Together these two scenarios constitute an envelope of potential sustainable biomass for each: the lower, tidal-only estimate representing a minimal biomass for which confidence in achieving a sustainable seabed impact is high; the higher, full flow estimate representing what *may* be sustainable given the meteorological conditions at the site, but which is subject to more uncertainty. The actual sustainable biomass on site is likely to be somewhere in between these values.

Several sites which have failed their cage edge intensity standards in the past are awarded more biomass in the new model *under conditions of full flow*. This can be interpreted to mean that the actual conditions on site are less dispersive than those implied by the sampled dataset and under which the site was originally modelled and licensed. No failing sites,

however, are awarded more biomass in the new model *under tidal-only conditions*. This suggests that the model, under default parameter configurations, is capable of protecting against under-cage intensity failures when modelling using the “worst-case” tidal-only scenario.

Some of the sites that are predicted to have a lower sustainable biomass using the new model have not previously failed their under cage standards which implies their existing larger biomasses are indeed sustainable. In two of these cases, the sites sit above bathymetric depressions which are likely to concentrate material in both reality and in the new version of the model but which is a feature that would have been ignored in the original model. This is encouraging from a mechanistic point of view as it shows how the new model is reflecting the complex bathymetry and explains why the new model predicts a lower biomass than the original. But the overall outcome, for practical purposes, is not correct in these cases and therefore this approach needs to be augmented with longer flow datasets or potentially site-specific calibration or other modelling approaches.

4.4.2 Technical observations

The test made above used a 365 day model run time to simulate the discharge and dispersion of farm waste. Historically, AutoDEPOMOD has been run using 30 day run times with output units scaled up to represent per annum quantities. Isolated experiments were performed in order to establish whether this run time was significant and it was concluded that 30 day run times are prohibitively short for two reasons.

Firstly, at sites with appreciable quantities of exported material there can be an initial “transitional” period in the model run where no material has yet reached the domain boundary and therefore the model domain is seen to be accumulating mass as it is discharged from the farm cages. Eventually this material reaches the domain boundary and is “exported” resulting a loss of mass from the domain. Subsequently the model achieves an approximate balance between discharge from the farm and export at the domain boundary. The result is that estimates of *net* mass accumulation within the domain on the basis of the first 30 days can be a significant over-estimate of the quantities accumulated over an explicit 365 day run.

Secondly, the response of the new model to bathymetry causes complex effects on particle transport which compounds over time. Depending on local bathymetric conditions, particles may experience a bias towards specific transport directions: they can move in some directions when the flow data and seabed slope permit, but may be blocked in other directions by the seabed relief. This enables particles to achieve a *net* transport position in a particular direction which was absent from the bathymetry-agnostic earlier model. This net transport position imparted by the bathymetry can accumulate over successive time steps, whereas in the original model it would be cancelled out by transport in the opposite direction, uninhibited by the implied flat bathymetry. The extent of this bathymetry-forced cumulative transport depends on the number of time steps under consideration and therefore the total model run time. It follows that 365 day runs can produce very different seabed impacts to 30 day simulations, although the difference depends on the characteristics of the domain bathymetry in question.

4.5 Conclusions

1. The original model had a tendency to significantly over-estimate the amount of material accumulating underneath farm cages in most cases.
2. A large range of features in the new model have been experimented with showing that the model produces stable, coherent and physically sensible responses
3. The new model is able to produce impacts of a similar magnitude to those observed empirically
4. Bed roughness, or z_0 , is a parameter highly suited to tuning the model – with reference to a particular flow dataset – to produce reasonable prediction of impacts
5. The new model is sensitive to idiosyncrasies in sampled flow data. Anomalies associated with the magnitude of sampled flow data can be mitigated to some extent using a combination of astronomical scaling and z_0 tuning. Directional anomalies cannot be accounted for and require longer datasets.
6. By virtue of the use of z_0 as a tuning parameter, the model is able to produce footprints at both low and high flow sites.
7. The new model is able to offer good protection against prohibitively high under cage impacts when run using a “worst-case” tidal-only scenario.

5. Discussion

NewDEPOMOD is the result of a major investment by Scottish Government. This has produced a significant research output involving 3 research cruises, considerable data analysis and the employment of a very wide range of theoretical concepts particularly relating to post-depositional particle behaviour. The work is encapsulated in a completely redesigned model of some >90k lines of computer code.

As proposed, NewDEPOMOD is free of dependencies on 3rd party software. Although reproduction of some of the features of such software, especially Surfer, has involved considerable effort and cost, the resulting software is much more resilient to obsolescence. However, given the rapid advances in computation technology, no software is likely to have a very long useful life unless it is maintained. Our decision to licence the code to other researchers as open source allows for the development of a NewDEPOMOD Researchers Forum whereby advances and improvements can be tested and propagated rapidly to users.

NewDEPOMOD has many “levers” to pull to calibrate against real world data. The model remains highly sensitive to the hydrodynamic data inputs. In Scotland, at present, these are generally restricted to 15 days at multiple depths and this constitutes a major source of error in model predictions. Given this context, we have chosen to fix most of the levers and adjust model predictions against empirical data using the seabed roughness parameter Z_0 .

It is highly likely that for most sites new and longer current records will become available in the near future. This is in part caused by the new Scottish containment standard⁹. Use of these records may allow future calibration work which will mean that it is more appropriate to tune the model with some of the other “levers”.

⁹ <http://www.gov.scot/Publications/2015/06/5747>

6. References

- Black, K.D., Cromey, C.J., Dale, A. and Nickell, T.D., 2010 Modelling benthic effects of salmon cage farms in Scotland: driving autoDEPOMOD with hydrodynamical model outputs. 143 pp.
- Chamberlain, J. and Stucchi, D. 2007. Simulating the effects of parameter uncertainty on waste model predictions of marine finfish aquaculture. *Aquaculture*. 272. 296-311.
- Cromey, C.J., Nickell, T.D. and Black, K.D. 2002a. DEPOMOD - modelling the deposition and biological effects of waste solids from marine cage farms. *Aquaculture*. 214. 211-239.
- Cromey, C.J., Nickell, T.D., Black, K.D., Provost, P.G. and Griffiths, C.R. 2002b. Validation of a fish farm waste resuspension model by use of a particulate tracer discharged from a point source in a coastal environment. *Estuaries*. 25. 916-929.
- Mayor, D.J., Zuur, A.F., Solan, M., Paton, G.I. and Killham, K. 2010. Factors Affecting Benthic Impacts at Scottish Fish Farms. *Environmental Science & Technology*. 44. 2079-2084.
- Sanford. 2006. Modelling a dynamically varying mixed sediment bed with erosion, deposition, bioturbation, consolidation, and armoring. *Computers & Geosciences*. 1263-1283.
- Wells, A., 2007 Marine fish farm data review. SEPA. 67 pp.

Annex 1. Benthic Flume and Flow Velocity Measurements



SAMS

Survey Report : Benthic Flume and Flow Velocity Measurements

March 2015





DOCUMENT CONTROL

Version History					
Version	Date	Prepared by	Reviewed by	Approved by	Approved as
v03	31 st March, 2015	K Black S Reynolds	M Wright C Amos	K Black	Final

Changes from the Previous Version	
v03	Various internal revisions and suggestions by CL Amos

Recipient	Distribution Method		
	Paper (copies)	PDF	Online
K Black, SAMS, Oban		X	

Holders of controlled copies will automatically be provided with subsequent approved versions of this document when they become available.



CONTENTS

- 1. Introduction 56
 - 1.1 Background to Project 56
- 2. instrumentation and theory 58
 - 2.1 Partrac Voyager Series Benthic Flumes 58
 - 2.2 Introduction to Boundary Layer Flows 65
 - 2.3 The Partrac-SAMS Boundary Layer Rig 71
- 3. SURVEY 1 – August 2013 73
 - 3.1 Flume Deployment Programme 73
 - 3.2 Rig Deployment Programme 76
 - 3.3 Problems 81
- 4. Survey 2 – May 2014 82
 - 4.1 Flume Deployment Programme 82
 - 4.2 Problems 85
- 5. mini-flume pellet mobility studies 86
- 6. settling velocity analysis 87
- 7. data analysis 88
 - 7.1 Grain Size, Dry Bulk Density Data and Organics 88
 - 7.2 Benthic Flume Data 88
 - 7.3 Boundary Layer Flow Data 95
- 8. results 99
 - 8.1 Sediment Bulk Density, Grain Size and Organics 99
 - 8.2 Benthic Flume Data 102
 - 8.3 Boundary Layer Flow Data 115
 - 8.4 Pellet Mobility Studies 124
 - 8.5 Settling Velocity 125
- 9. references 127
- 10. appendix i Sediment photographs 129



LIST OF FIGURES

Figure 1. Compartments and processes within the DEPMOD/AUTODEPOMOD particle tracking model (from Cromey et al., 2002).57

Figure 2. The Partrac 'Voyager II' benthic flume (top) and a schematic cross section.60

Figure 3. Photographs showing the paddle (left), the vertical OBS array (middle) and the Nortek Vectrino acoustic current sensor (right).60

Figure 4. Example sediment concentration (turbidity) time series showing the various phases of an erosion experiment.61

Figure 5. Partrac *Voyager I* benthic flume within a deployment frame. The red cable provides power to the flume; a horizontally mounted OBS turbidity meter is located on the flume outer channel wall on the right hand side. A sideways looking marine camera with integrated LED annulus is on the left (yellow).63

Figure 6. Voyager I benthic flume, communication/power cable and purpose-built control unit.63

Figure 7. Typical flow velocity and shear stress distributions within a turbulent bottom boundary layer (layer thickness is not to scale) (Souce Kim et al., 2000).66

Figure 8. The boundary layer rig showing the Vector ADV (to the right), the Profiler (top left) and a marine altimeter, co-aligned with the Vector (but logger at the top). An TRDI ADCP is mounted on the top of the frame pointing upwards.72

Figure 9. Illustrative vector map (statistical temporal average) for a single velocity (paddle rotation rate) setting (what was the speed ?).....91

Figure 10. Example of echo intensity profile from the Profiler instrument; the red line indicates the seabed. X-axis is time, y-axis is height above bed in decimetres.96

Figure 11. Streamwise current magnitude averaged every 5 seconds (solid red line). Dashed blue lines denote a change in applied voltage.105

Figure 12. Applied voltage (solid red line) and total suspended solids concentration (mg l^{-1} , solid blue line) for Durmyon Bay 2.1 on 29/08/2013.106



Figure 13. Mass of suspended sediment eroded (kg) for Durmyon Bay 2.1 on 29/08/2013.106

Figure 14. (Instantaneous) erosion rates ($\text{kg m}^{-2} \text{s}^{-1}$; computed every 20 s) for Durmyon Bay on 29/08/2013.....106

Figure 15. Depth of erosion (mm) for Durmyon Bay 2.1 on 29/08/2013.107

Figure 16. Suspended sediment concentration (mg l^{-1}) and bed shear stress time series for site DF002.112

Figure 17. Instantaneous erosion rates ($\text{kg m}^{-2} \text{s}^{-1}$); computed every 20 s for site DF002.112

Figure 18. Time series of sediment mass eroded (kg) from site DF002.113

Figure 19. Depth of erosion time series for site DF002.113

Figure 20. Water column profile (ADCP data only) of velocity magnitude at Fiunary 1 site to illustrate boundary layer character; ebb tide phase.118

Figure 21. An example of the vertical variation of flow velocity on a linear and logarithmic scale ($r^2 = 0.97$) at the Ardfuir 1 site.121

Figure 22. Example settling curve for site DF003; note the existence of three, discrete identifiable settling fractions within the sediment mass.125

Figure 1 Relationship between pellet diameter and settling velocity with each point representing the mean of a data set. The mean and standard deviation of all 16 data sets is 10.8 and 2.7 cm s^{-1} , respectively. Source Cromey et al., (2002a).....156

Figure 2 The relationship between drag coefficient of a particle and Reynolds number for particles of varying shape factors settling in still water (Mehta, 2014).158

Figure 3 The threshold for suspension of particles sitting on the seabed (Bagnold, 1966).160

Figure 4 Example settling curve for site DF003; note the existence of three, discrete identifiable settling fractions within the sediment mass.162

Figure 5. Suspended sediment concentration (mg l^{-1}) and bed shear stress time series for site DF002.165



Figure 6 Covariance of the dry bulk density with critical entrainment stress. There is no significant trend in the relationship between these two parameters.166

Figure 7 Excess bed stress ($\tau_0 - \tau_{0,crit.}$) versus erosion rate ε averaged over each velocity/stress time-step on a linear plot.171

Figure 8 The threshold for suspension of particles sitting on the seabed (Bagnold, 1966).173

Figure 9 The threshold Shields parameter for the onset of motion of particles sitting on the flat seabed of similar particles (adapted from Mantz, 1977). Note that the Shields parameter encompasses both the lift and drag forces on the bed material.175

Figure 10 The change in critical Shields parameter with change in relative protrusion (P/d) (after James, 1990). The red line shows the normally-accepted value (0.05) for granular material under turbulent rough flows.177

Figure 11 Field (time-averaged) velocity data plotted up on a Clauser plot. Note $u\tau$ in the axes labels is the friction velocity u^*186

Figure 12 Photographs of surface sediment considered hydraulically transitional-rough from Fuinary 2 (left) and Port na Moine 1 (right).188



LIST OF TABLES

Table 1. Operational parameters used in the Voyager I benthic flume deployments. Note that start and end lid rotation rates are not the induced current velocity at the bed.64

Table 2. Summary of flume deployments.74

Table 3. Summary of erosion run parameters for all flume deployments.....76

Table 4. Settings and deployment details for instruments on the boundary layer rig.77

Table 5. Summary of flume deployments in Survey 2. 'Trial' denotes flume tests where deployment logistics, run testing etc., were done.83

Table 6. Summary of the predictive equations derived from least squares regression analysis of flow calibration data.91

Table 7. Summary of regression equations from the turbidity sensor calibrations (y=concentration, mg l⁻¹, x=instrument readout) for Survey 1.....93

Table 8. Summary of regression equations from the turbidity sensor calibrations (y=concentration, mg l⁻¹, x = instrument readout) for Survey 2.93

Table 9. Summary dry bulk density (ρ_d), particle size (d), porosity (Φ), loss on ignition (LOI) and organic matter OM) from Survey 1 sediment samples.....99

Table 10. Summary dry bulk density (ρ_d), particle size (d), porosity (Φ), loss on ignition (LOI) and organic matter (OM) from Survey 2 sediment samples.101

Table 11. Shear velocity (u_*) and bed shear stress (τ_o) at a range of applied voltage settings for Survey 1.....102

Table 12. Bed shear stress values over the range of lid rotation rates (Ω) and channel depths (H) used in Survey 2.....104

Table 13. Maximum sediment concentration (S_{max}) at the end of each stress time-step. 'Saturated' indicates the OBS sensor is at the upper limit of measurement.....108

Table 14. Total eroded mass (EM_{max}) at the end of each stress time step. No data at discrete voltage / stress steps correspond to OBS sensor saturation...109



Table 15. Maximum eroded depth (z_{max} mm) at the end of each stress time-step. No data at discrete voltage / stress steps correspond to OBS sensor saturation and thus no information on continued erosion depths.110

Table 16. Critical surface erosion threshold stresses and associated regression coefficients. Some sites are classified as having no measureable, or very low critical entrainment stresses, where the regression line essentially goes through or very close to the origin.....111

Table 17 Summary critical entrainment stress values ($N\ m^{-2}$) using a specified, over-background minimum concentration of $10\ mg\ l^{-1}$114

Table 18. Metadata summary for the boundary layer rig deployments.117

Table 19. Measured and computed (theoretical) values for boundary layer thickness.118

Table 20. Summary of boundary classification calculations. The table shows calculations using the grain and flow Reynolds numbers. Two different shear velocity values are used in the calculation of the grain Reynolds number. Data relating to the flow Reynolds number show the maximum and minimum values related to the maximum and minimum flow velocities across the entire rig deployment period plus the value from the 10 minute data record. The two right-hand columns show the grain Reynolds number computed using $d_{50} = 10\ mm$, which is indicative of a pelleted bed.120

Table 21. Bed stress and roughness length estimates from application of the Law of the Wall and TKE methodologies.....122

Table 22. $k_{s\tau}$ values for each site determined from independent values for z_o . Also shown are multipliers of common grain size metrics of use in providing grain Reynolds number inputs ($k_s=f(d_i)$)123

Table 23. Summary of pellet mobility studies.124

Table 24. Summary settling velocity data from deposition phase erosion runs. ...126

Table 1 Summary settling velocity data from deposition phase erosion runs.....162

Table 2 Summary critical entrainment stress values ($N\ m^{-2}$) using a specified, over-background minimum concentration of $10\ mg\ l^{-1}$. Runs in which leakage occurred were not corrected for this anomaly.165

Table 3 Nearfield (Survey 1) and farfield (Survey 2) values of surface critical erosion stress $\tau_{0,crit.}$ at 3 sites.....167



Table 4 Summary values for the friction coefficient ϕ in the surface layers (1) and sub-surface (2).....169

Table 5 Summary of pellet mobility studies.180

Table 6 Summary of boundary classification calculations. The table shows calculations using the grain ($u * ks/\nu$) and flow ($umid, z.z/\nu$) Reynolds numbers. Two different shear velocity values are used in the calculation of the grain Reynolds number. Data relating to the flow Reynolds number show the maximum and minimum values related to the maximum and minimum flow velocities across the entire rig deployment period plus the value from the 10 minute data record. The two right-hand columns show the grain Reynolds number computed using $d_{50} = 10$ mm, which is indicative of a pelleted bed.184

Table 7 Bed stress and roughness length estimates from application of the Wall Law and TKE methodologies to collected flow data.....189



1. Introduction

1.1 Background to Project

DEPOMOD is a particle tracking model used for planning and monitoring of sea cage fish farms and it was initially developed for applications to Atlantic salmonid farms. Predictions of waste faecal and feed deposition and associated benthic impact near the farms can be obtained with site-specific information on the current velocity and direction, depth and husbandry characteristics such as feed input and cage layouts (Figure 1). The model assists with regulation of the farms and provide guidance to the industry on selection of sites with good husbandry characteristics. In the UK, the DEPOMOD model is the basis for the AUTODEPOMOD regulatory software package. Several academic papers have been published describing this work (e.g. Cromey et al., 2002).

SAMS, Oban, have been commissioned by the Scottish Government (under contract REFINING SEA-BED PROCESS MODELS FOR AQUACULTURE SAM/004/12) with the following aims:

- 1) to recode AutoDEPOMOD in Java in a form that will operate independently of third-party software
- 2) to improve the modelling of re-suspension processes informed by a programme of field and laboratory studies.

Partrac Ltd. were sub-contracted by SAMS to provide specialist input into [2.] principally, but within a wider overall remit to provide consultancy on aspects of sediment erosion, transport and deposition, together with marine data acquisition experience.

This report forms a single document summarising all the field and laboratory studies undertaken within this project.

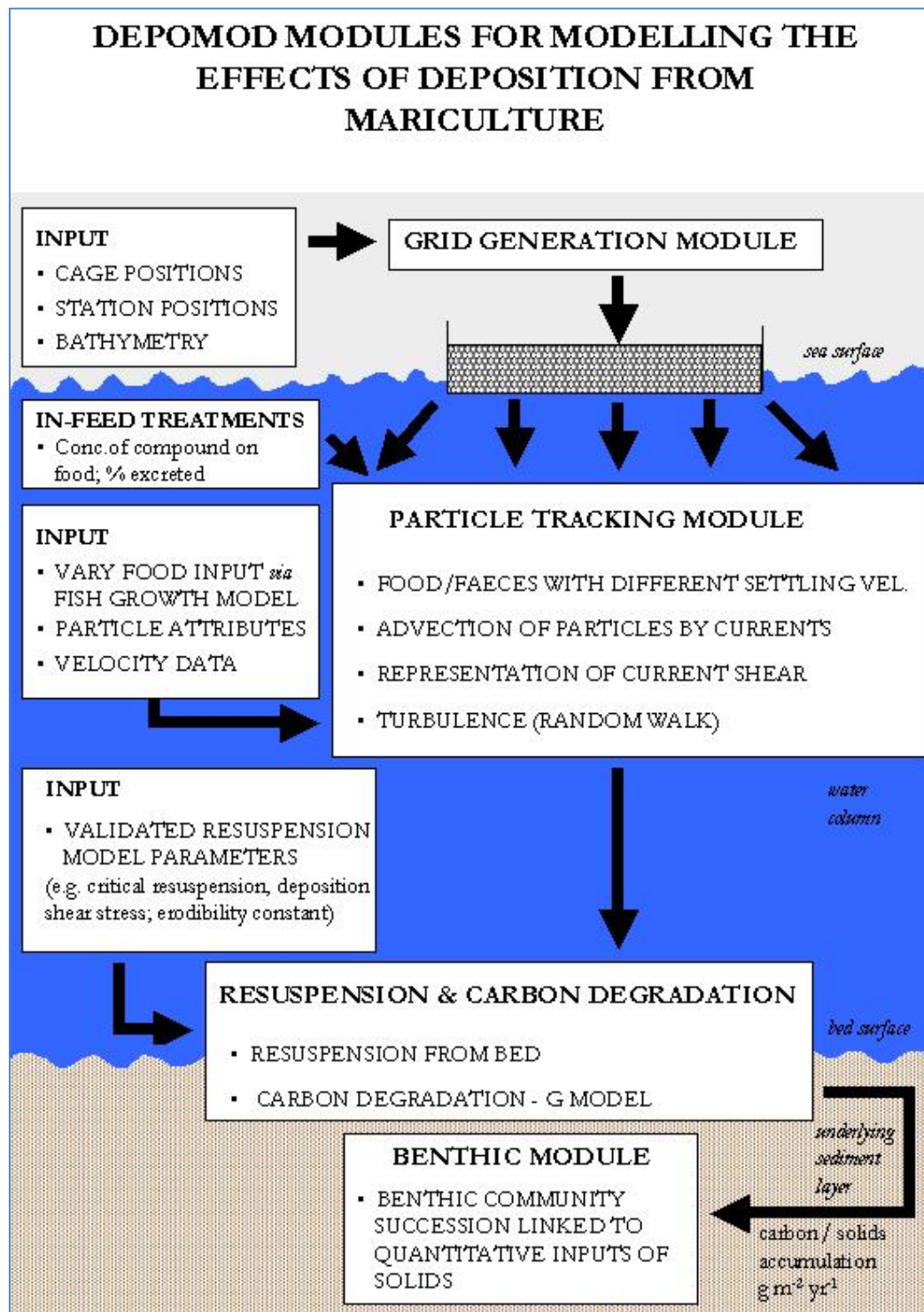


Figure 1. Compartments and processes within the DEPOMOD/AUTODEPOMOD particle tracking model (from Cromey et al., 2002).



2. instrumentation and theory

2.1 Partrac Voyager Series Benthic Flumes

2.1.1 Introduction to Benthic Flumes

Benthic flumes are devices that can be used to apply a controlled flow stress (or velocity) onto the surface of submerged bottom/bed sediments. They have a history extending back to the mid-1980s (Black and Paterson, 1997), and they have been chiefly used previously in intertidal and shallow sub-tidal environments (e.g. Black and Cramp, 1995; Amos et al., 1992, 1996; Houwing and van Rijn, 1992), although Thompson et al., (2011) report benthic flume experiments down to 83 m depth on the UK North Sea shelf. Benthic flumes are considered to be a semi-mature technology.

2.1.2 The Partrac Voyager II Benthic Flume

Partrac own and operate a benthic flume called Voyager II (Figure 2) which was provided for use on the Sir John Murray cruises. It undertook a series of controlled resuspension events in situ. The flume is based on the designs and dimensions of Amos et al. (1992b). It consists of an aluminium channel 0.3 m high (H) and 0.15 m wide (W), with a total diameter (D) of 2.2 m. Eight equidistantly spaced paddles (Figure 2) induce a current via a train drive, driven by a 0.6 hp, 24 V DC submarine motor and gearbox. The lower tip of the set of paddles is ~210 mm above the nominal bed level.

Eight lid sections, each equipped with a lid which can open to allow flushing of water during flume deployment, are arranged on top of the channel and enclose the channel (one section is transparent which allows the paddle drive train to be easily viewed; Figure 2). A 0.07 m wide and 0.005 m thick skirt around the outer channel wall allows the flume to sink ~0.045 m into the bed evenly, and provides for a constant channel depth. Lead weights can be attached to the skirt to ensure penetration on firmer sediments.

The flume is instrumented (see photographs in Figure 3) with 3 optical backscatter sensors (OBS) which measure turbidity at three different heights (centres at 85, 145 and 200 mm above the nominal bed level), a Nortek Vectrino Velocimeter measuring velocity in the along channel (u), across channel (v) and vertical (w) directions 0.15 m above the nominal bed level¹⁰, and an automated syringe sampling system taking calibration samples for the OBS. Data are logged directly to an onboard data logger, and an onboard computer called Arctica Sluut controls the lid rotation frequency (Ω^{11}) and direction.

A Perspex™ window on the internal channel wall allows for submarine video imagery to be recorded. An off-the-shelf JVC high memory, long-play camcorder inside a bespoke submarine housing is fixed to look through the window at an angle, and this provides an oblique view across the sediment surface within the channel. Quality video imagery is possible only up to the point where excessive turbidity is generated by sediment erosion

¹⁰ The Vectrino can be configured to act as an altimeter and return measures of distance to the bed.

¹¹ This may also be referred to as the 'lid rotation rate'.



(mobilisation and suspension). Two sealed LED 24 V submarine lamps, controlled via the Arctica software are used to illuminate the bed surface. One lamp is directed vertically downward through a lid section and one lamp is located adjacent to the camera unit.

The flume can be operated either in autonomous mode or in tethered mode. The former is where the flume runs on onboard batteries and executes a pre-loaded erosion programme and is cast off from the vessel, whereas during the latter (tethered mode) the flume remains tethered to the vessel and is power is supplied from the vessel through a cable which directly drives the motor. Usually in this mode the erosion programme is implemented manually using a 24V DC benchtop mains power supply. Deployment of the flume in tethered mode usually requires the deployment from a dynamically positioned vessel.

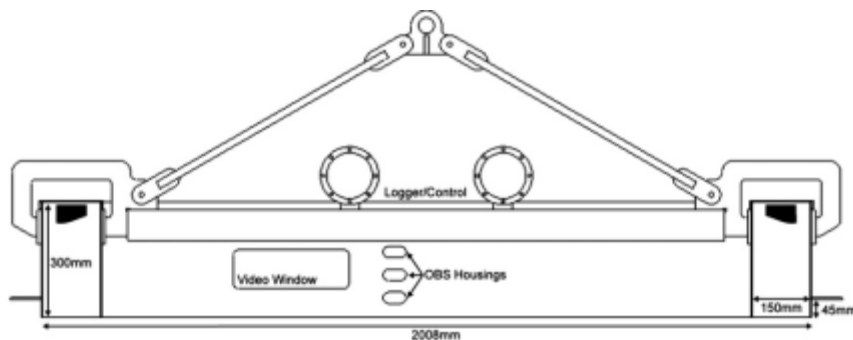
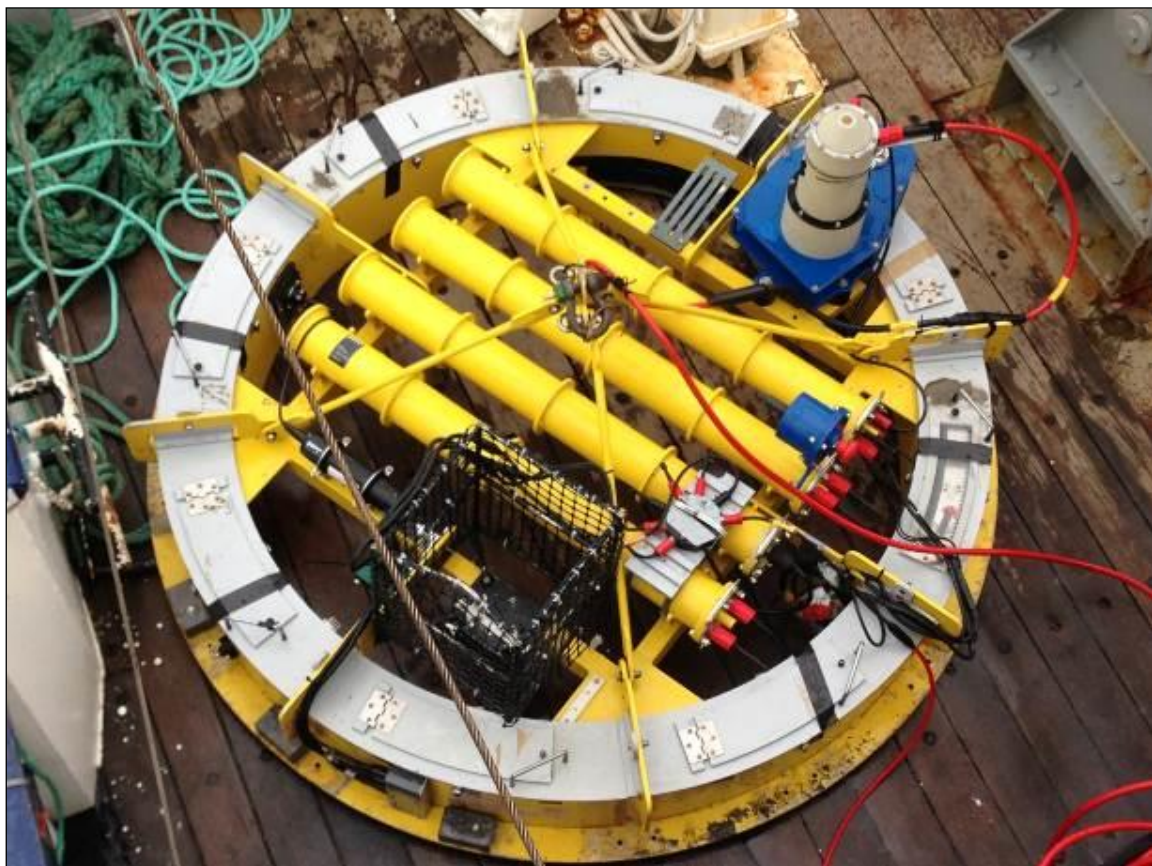


Figure 2. The Partrac 'Voyager II' benthic flume (top) and a schematic cross section.



Figure 3. Photographs showing the paddle (left), the vertical OBS array (middle) and the Nortek Vectrino acoustic current sensor (right).

During deployment the flume is slowly and carefully lowered to the bed; the bow-wave can sometimes create mild resuspension of any low density interfacial sediment, and therefore the flume typically is left to rest for a time period prior to commencement of an erosion experiment. An erosion experiment involves increasing the paddle rotation rate in a stepwise fashion via a series of acceleration ramps, and this is designed to sequentially resuspend and erode the bed (see Amos et al. 1992a; 2003, 2004) and Sutherland et al. (1998a,b). Following completion of the experiment the paddle rotation can either be stopped immediately, ramped down in a single step or decreased in a stepwise fashion to zero (during this time period sediment redeposition will occur). The flume is then recovered. The fundamental parameters of an erosion time series test are:

1. Start time t_0 (s)
2. Landing (on seabed) time t_l (s)
3. Initial wait time t_w (s)
4. Linear acceleration ramp duration t_{acc} (s)
5. Minimum velocity/stress u_{min}/τ_{0min} ($m\ s^{-1}$ or $N\ m^{-2}$)
6. Maximum velocity/stress u_{max}/τ_{0min} ($m\ s^{-1}$ or $N\ m^{-2}$)
7. Velocity/stress increment Δu or $\Delta\tau_0$ ($m\ s^{-1}$ or $N\ m^{-2}$)
8. Duration of steady flow Δt_e (s)
9. Linear deceleration ramp(s) duration t_{dec} (s)
10. Stop time t_{end} (s)
11. Number of increments.



Figure 4. Example sediment concentration (turbidity) time series showing the various phases of an erosion experiment.

Time series of suspended sediment concentration (S ; mg l^{-1} or kg m^{-3} ; Figure 4) and flow velocity \underline{u} (or bed stress, τ_0) form the principal fundamental data sets arising from use of the flume. From these data the following principal metrics (not exhaustive) which characterise seabed stability can be derived:

1. Critical (surface) entrainment velocity/stress $u_{crit.}/\tau_{0crit.}$ (m s^{-1} or N m^{-2})
2. Maximum recorded sediment concentration/dry mass S_{max} (mg l^{-1} or mg or kg)
3. The form of the $[S]$ $\log(\tau_0)$, or $[S]$ $\log(u)$, relationship
4. Various indices of erosion rate ε ($\text{kg m}^{-2} \text{s}^{-1}$) and rate constants M
5. Mass deposition rate D ($\text{kg m}^{-2} \text{s}^{-1}$)
6. ‘Still’ water mean settling velocity ω_s
7. Critical depositional flow velocity/stress $u_{dep.}/\tau_{0dep.}$ (m s^{-1} or N m^{-2})
8. Depth of erosion (mm)
9. Erosion type (I or II)

2.1.3 The Partrac Voyager I Benthic Flume

The flume comprises an annular channel of width 0.12m; this is formed from two concentrically fixed cylinders (radii 0.125 m and 0.245 m), providing an exposed bed area of 0.139 m² (Figure 5). Both the inner and outer cylinders comprise transparent Perspex[®] permitting observation of the sediment bed during erosion. A rotating lid with four shallow paddles mounted at the cardinal points is affixed to the channel top and secured to be watertight. The lid is driven via a submersible, geared electric motor that is mounted on the lid of the flume. Rotation of the lid generates a flow within the channel and therefore also a shear stress on the bottom sediments (comprising skin friction and form drag). The lid rotation frequency (Ω , cm s⁻¹) is controlled directly via software from a purpose-built control unit (Figure 6).

For the purposes of this study (where maximum deployment depths approached 40 m), the entire flume was placed within an aluminum frame to allow the flume to be lifted and lowered into the water column using a deck winch. A ‘skirt’ surrounds the outer frame and this delimits the depth to which the flume is inserted into the sediment; it also provides additional strength and protection. However, this skirt was removed during the study to allow for deeper penetration into the sediment if required.

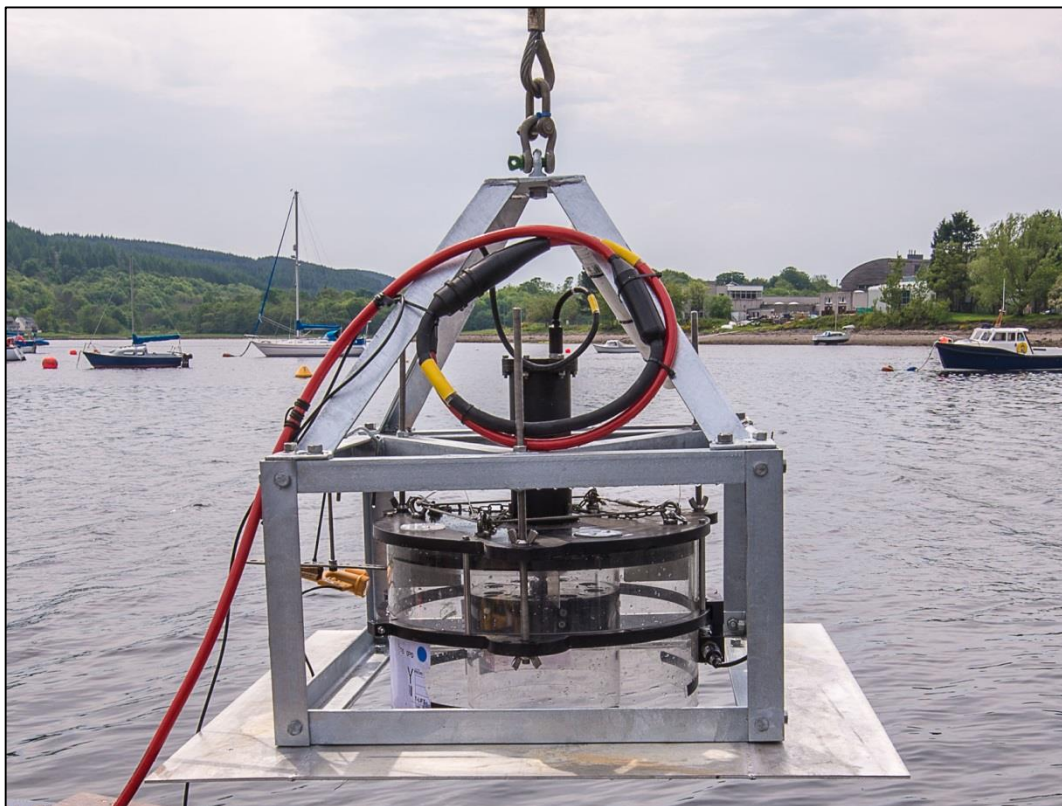


Figure 5. Partrac Voyager I benthic flume within a deployment frame. The red cable provides power to the flume; a horizontally mounted OBS turbidity meter is located on the flume outer channel wall on the right hand side. A sideways looking marine camera with integrated LED annulus is on the left (yellow).

A Seapoint optical backscatter sensor (OBS) interfaced with an RBR data-logger was used to monitor sediment concentration within the annulus and was configured to record turbidity (sediment concentration) at 0.33 Hz continuously during each deployment. The OBS was fixed so that turbidity was recorded directly inside the flume at an elevation of 0.05 m above the sediment bed. The OBS and paddle (lid) rotation frequency (Ω) are both logged providing a time-series of backscatter (NTU) and paddle (lid) rotation frequency, and these data form the fundamental pre-calibration data arising from deployments of the flume.



Figure 6. Voyager I benthic flume, communication/power cable and purpose-built control unit.

During deployment the flume is slowly lowered to the bed. A live feed from a camera looking in towards the flume chamber allows an observer to determine when the flume is on the bed and, to a certain extent, whether or not the flume is sitting in a good enough position to



commence an erosion experiment. The camera, along with pre-measured marks on the outside of the flume wall, also enables the observer to determine the depth that the flume has sunk into the sediment (denoted H , units cm), a crucial parameter in the determination of the bed shear-stress (τ_o) required to entrain sediment. As the flume lands on the bed there is typically a small bow wave and some resuspension of sediment within the flume chamber. As a consequence, sufficient time must be given to allow any resuspended material to settle out before commencing the rotation of the paddles.

Operational variables used in a typical erosion experiment are similar to the Voyager II flume and include start velocity, end velocity, step-wise rotation frequency increments, constant velocity increment duration and ramping rate between increments, all of which can be pre-determined prior to a deployment. Paddle rotation is increased in a stepwise manner through a series of acceleration ramps with the purpose of sequentially resuspending and eroding the bed (see Amos et al. 1992a; 2003; 2004 and Sutherland et al. 1998a,b.). Once the end velocity has been reached, the paddles are stopped immediately allowing for sediment deposition to occur. The operational parameters used during each deployment of this study are shown in Table 1.

Table 1. Operational parameters used in the Voyager I benthic flume deployments. Note that start and end lid rotation rates are not the induced current velocity at the bed.

Settlement Time (minutes)	Start Lid Rotation Rate Ω (cm s^{-1})	End Lid Rotation Rate Ω (cm s^{-1})	Lid Rotation Rate Velocity Increment Δ (cm s^{-1})	Step Duration (minutes)	Ramp Duration (minutes)
10	0	30	2	5	1

Time series of suspended sediment concentration (S ; mg l^{-1} or kg m^{-3}) and flow velocity u (or bed stress, τ) form the principal fundamental post-calibration data sets arising from use of the flume. From these data the following principal metrics (not exhaustive), which characterise seabed stability can be derived:

1. Critical (surface) entrainment velocity/stress $u_{crit.}/\tau_{0crit.}$ (m s^{-1} or N m^{-2})
2. Maximum recorded sediment concentration/dry mass S_{max} (mg l^{-1} or mg or kg)
3. The form of the $[S]$ $\log(\tau)$, or $[S]$ $\log(u)$, relationship
4. Various indices of erosion rate ε ($\text{kg m}^{-2} \text{s}^{-1}$) and rate constants M
5. Mass deposition rate D ($\text{kg m}^{-2} \text{s}^{-1}$)
6. ‘Still’ water mean settling velocity ω_s
7. Critical depositional flow velocity/stress $u_{dep.}/\tau_{0dep.}$ (m s^{-1} or N m^{-2})

2.2 Introduction to Boundary Layer Flows

The flow of water near a solid boundary has a distinct structure known as the boundary layer. An important aspect of a boundary layer is that the velocity of the fluid (u) goes to zero at the boundary. At some distance above the boundary the velocity reaches a constant value (Figure 7) called the free stream velocity u_∞ . Between the bed and the free stream, the velocity varies over the vertical co-ordinate. The height of the boundary layer, δ , is typically defined as the distance above the bed at which $u(\delta) = 0.99u_\infty$ (Douglas et al., 1986).

The bottom boundary layer (BBL) can be subdivided into four regions (see Figure 7):

- (i) viscous sub-layer (thickness $\delta_{\text{visc}} = 11.6\mu/u_*$) representing a thin laminar flow layer just above the bottom - in this layer there is almost no turbulence and the viscous shear stress is constant. It is only present under turbulent smooth flows (Tennekes and Lumley, 1972);
- (ii) transition layer, where viscosity and turbulence are equally important and the flow is turbulent;
- (iii) turbulent logarithmic layer, where the viscous shear stress can be neglected and the turbulent shear stress is constant and equal to the bottom shear stress; and,
- (iv) turbulent outer layer, where velocities are almost constant because of the presence of large eddies, which produce strong mixing of the flow and shear stress gradually reducing to zero at the free stream (outer edge of the boundary layer). In a well-mixed fully developed turbulent flow over a rough channel bed, the outer turbulent layer covers approximately 80 per cent of the BBL thickness (Granger, 1985).

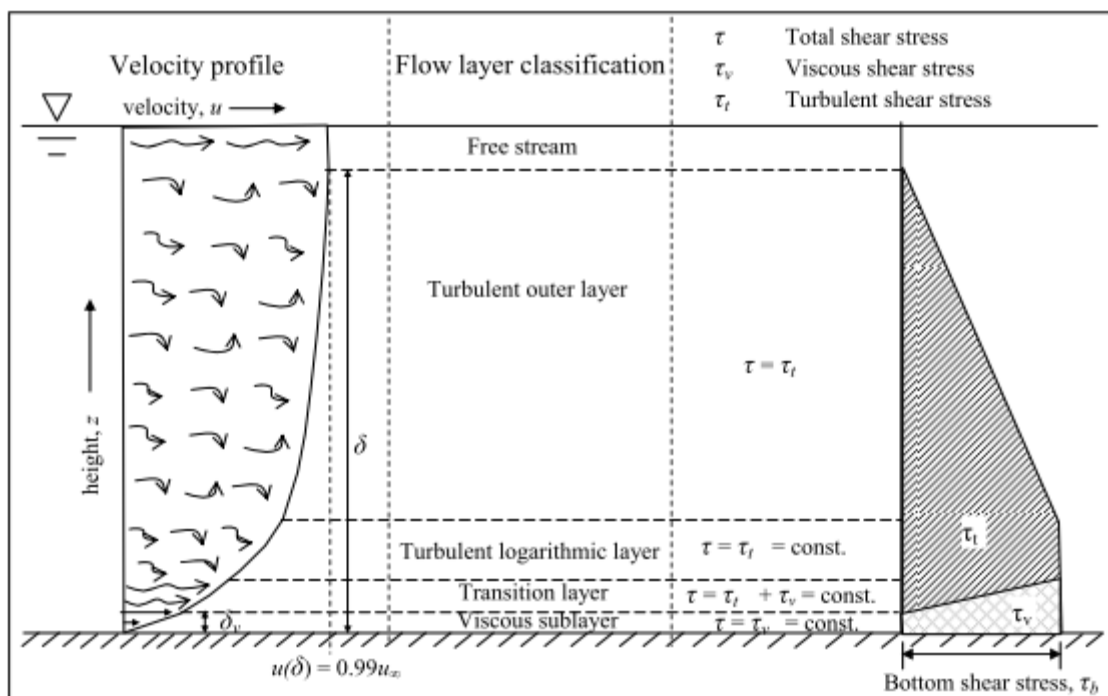




Figure 7. Typical flow velocity and shear stress distributions within a turbulent bottom boundary layer (layer thickness is not to scale) (Souce Kim et al., 2000).

A typical phenomenon of turbulent flow is the fluctuation of velocity called the Reynolds decomposition. The instantaneous velocity consists of a mean and a fluctuating component, and can be written as follows:

Equation 1

$$U = u + u'; \quad V = v + v'; \quad W = w + w'$$

where U , V and W are instantaneous velocities; u , v and w are time-averaged velocities; and u' , v' and w' are instantaneous velocity fluctuations in longitudinal, transverse and vertical directions, respectively. Shear stress in laminar flow is defined as:

Equation 2

$$\tau_v = -\mu \frac{du}{dz}$$

where τ_v is the viscous dominated shear stress; ρ is the density of fluid; μ is the absolute or dynamic viscosity of the fluid; and z is the elevation above the bed. On the other hand, a shear stress resulting from a turbulent flow (as found in most marine settings) is defined as:

Equation 3

$$\tau_t = \eta \frac{du}{dz}$$

where τ_t is the turbulent shear stress, and η is a turbulent mixing coefficient (often called eddy viscosity). The eddy viscosity is not a property of the fluid like ρ and ν , but is a function of the flow (Tennekes and Lumley, 1972). Turbulent velocity fluctuations generate momentum fluxes resulting in shear stresses (called Reynolds stresses) between adjacent parts of a flow (Tennekes and Lumley, 1972). The Reynolds stress (turbulent shear stress) is defined as:

Equation 4

$$\tau_1 = -\rho \overline{u'w'}$$

This can be measured with high precision velocity recording devices such as Acoustic Doppler Velocimeter and Laser Doppler systems. The turbulence shear stress within the log layer is equated with the bed shear stress when turbulence is measured within the constant shear stress region (Figure 7). This is an important assumption for investigations into near-bed flows and bed stress estimation. It is under some debate at the moment, and the literature is somewhat mixed about its existence and character in turbulent benthic boundary layers.





Prandtl (1926) introduced the mixing length concept and derived the logarithmic velocity profile (also known as von-Kármán – Prandtl equation or Universal Law of the Wall) for the turbulent logarithmic layer. It is derived from the fundamental relationship, seen in so-called ‘Clauser plots’, where $\frac{u_z}{u_*}$ is regressed against Reynolds number. Under turbulent rough flows the following equation results:

Equation 5

$$u(z) = \frac{u_*}{\kappa} \ln\left(\frac{z}{z_0}\right)$$

where u_* is the shear velocity defined as $u_* = \sqrt{\tau_0/\rho}$, τ_0 is the bed shear stress; z_0 is the elevation where mean horizontal velocity is zero, usually known as roughness length; and κ is the von-Kármán constant = 0.4. The range of heights for which equation 5 is valid is from a few cm above the bed to 20-30% of the boundary layer thickness in deep water (say, 20 – 30 m; Soulsby, 1997). Various expressions have been proposed for the velocity distribution within the transitional layer and the turbulent outer layer, none of which is widely accepted (Granger 1985; Crowe et al., 2005).

2.2.1 Techniques for estimating bed stress (τ_0)

Commonly employed methods to obtain the bed stress from velocity data include:

- Log-profile (LP – Universal Law of the Wall);
- Reynolds stress (RS);
- Turbulent Kinetic Energy (TKE); and
- Inertial Dissipation (ID) methods.

The suitability, assumptions and limitations of these methods have been critically reviewed by Kim et al. (2000) and Pope et al. (2006). These authors concluded that the TKE approach was the ‘most consistent’ and offered most promise for future development. More recently Ali and Lemckert (2012) summarise a field inter-comparison which found reasonably good agreement across all approaches. However, they have suggested simultaneous use of several methods to estimate bed shear stress where possible, as all of these methods have both advantages and disadvantages; in this way, likely sources of errors can be identified.

Within this project the LP and TKE methods have been utilised to estimate bed stress. The following provides a brief overview for each of these methods.

The LP method fits mean flow velocity and height data into the Kármán-Prandtl equation (Equation 5) and estimates shear velocity (u_*) and roughness length (z_0). The relationship is derived from the assumption that $z_0 = V/u_*$ (in equation 5):

The shear velocity is used to calculate bed shear stress from:

Equation 6

$$\tau_o = \rho \bar{u}_*^2$$

One of the central tenets of the LP approach is that the theory is strictly valid only for steady flows (Cheng et al., 1999; Pope et al., 2006) and thus a time-series must be divided into quasi-stationary time periods (about 10 minutes under most tidal settings). Another fundamental feature of the LP method is that it is dependent upon precise knowledge of the elevations above the bed at which the sequence of current velocities are measured (Kabir and Torfs, 1992; Biron et al., 1998), but this is of less concern when modern acoustic profilers set at a known elevation above the seabed are used to collect velocity data. The LP method is sensitive to the estimation of Z_o : It can be expected to vary with varying bottom roughness and also with flow Reynolds number.

Turbulent Kinetic Energy (TKE) is a measure of the absolute intensity of the turbulent velocity fluctuations about the mean velocity i.e. the variances of the flow within an XYZ co-ordinate system. It assumes that all the momentum flux to the bed is transmitted by the turbulent eddies of the flow. Hence it is defined as:

Equation 7

$$TKE = \frac{1}{2} \rho (\overline{u^2} + \overline{v^2} + \overline{w^2})$$

Simple relationships between TKE and shear stress have been formulated in turbulence models (Galperin et al., 1988), while further studies (Soulsby and Dyer, 1981; Stapleton and Huntley, 1995) have shown the ratio of TKE to shear stress is constant, i.e.:

Equation 8

$$\tau_1 = C_1 TKE$$

The proportionality constant C_1 was found to be 0.20 (Soulsby and Dyer, 1981), while $C_1 = 0.19$ has been adopted by others (Soulsby, 1983; Stapleton and Huntley, 1995; Thompson et al., 2003). The main advantage of the TKE method over the LP method is that the sensor can be positioned well within the logarithmic/constant stress layer, avoiding any uncertainties, and it does not require accurate knowledge of elevation above the bed, and is therefore less sensitive to conditions, where sediment erosion and deposition can alter sediment levels by several millimetres or more. Furthermore, in some settlings e.g. inter-tidal field studies, some tilting of acoustic (profiling) sensors is almost inevitable, and this method is much less sensitive to tilting. It requires that the turbulence is measured in the constant stress layer. It also assumes no turbulence dampening within the viscous sub-layer or due to suspended sediment induced density stratification.



However, there are some potential disadvantages to the use of the TKE method. Firstly, the exact limits and dimensions of the sampling volume must be known so when measurements are made within the BBL (near the bed) the sampling volume is not mistakenly positioned partially within the bed. Secondly, an inherent feature of all Doppler-based backscatter systems is Doppler noise, which is attributable to several sources, including positive and negative buoyancy of particles in the sampling volume; small-scale turbulence (at scales less than that of the sampling volume); and acoustic beam divergence, which in total may lead to high-biased estimates of turbulent energy from acoustic doppler devices (Nikora and Goring, 1998). Finally, accelerating and decelerating flows can cause errors in the TKE approach just as in the LP method, and the pre-condition of non-stationarity is important.

2.2.2 Technique for estimating roughness length (z_0)

While fluid flows over a surface, it is subject to frictional drag termed skin friction (related to grain size) and form drag related to pressure differences over roughened beds (it is manifest and described by the scalar called bed roughness, z_0). The total drag force at the bed is balanced by the velocity gradient (change in momentum) within the benthic boundary layer. This concept is encapsulated within the Law of the Wall. The chief purpose of collection of near bed flow data for this project was to define the bed shear stress through the hydraulic roughness metric. The TKE method is adjusted for z_0 subject to a **smooth boundary** using following equation:

Equation 9

$$z_0 = \frac{v}{9u_*}$$

For a **rough boundary**, information on Vector (flow velocity) measurement height ($z=0.05$ m), the corresponding mean flow velocity at that height (u_z), u^* and a value for the constant kappa ($\kappa=0.4$) is used:

Equation 10

$$z_0 = \frac{z}{e \frac{\kappa u_z}{u_*}}$$

However, the (hydraulic) roughness length z_0 can be directly estimated from recorded velocity profiles using Equation 5 (the LP method). The velocities and corresponding elevations measured from a water column are plotted on log-linear graph, and roughness height and shear velocity are obtained from curve fitting (Wilkinson, 1986).



2.3 The Partrac-SAMS Boundary Layer Rig

A boundary layer rig, based upon the frame structure of a benthic lander, was used to collect boundary layer flow data (Figure 8). The rig comprises an aluminium frame in a triangular configuration approximately 2.1 m high. Three cross-members ~ 1m above the bed serve as points to mount a downward looking Nortek Vector 3D instrument, a Nortek 2 MHz Aquaprofiler mounted to look downwards and an NKE 1MHz Marine Altimeter. On the uppermost triangular frame a upward looking TRDI 600kHz ADCP was mounted. Each of these instruments is powered by batteries and is self-logging. The ADCP was set to log continuously from the outset of the cruise.

The Vector 3D is a point flow velocity sensor, which collects high-resolution velocity and pressure data in all 3 dimensions (u , v , w). The Vector was vertically mounted with the probe at a distance of 0.2 m from the base of the frame giving a sampling volume at 0.05 m above the bed.

The horizontally mounted Aquaprofiler measured velocity within the lowermost 0.9 m of the water column. The instrument was configured with a 0.1 m blanking distance and 0.1 m cell sizes. Velocity data (nominally) were collected at the following distances above the seabed: 0.7, 0.6, 0.5, 0.4, 0.3, 0.2 and 0.1 m above the bed (note for the purposes of examining the logarithmic distribution of flow velocity with height above the bed, the data from the Vector [0.05 m ab] was used, in addition).

The Marine Altimeter sonar head unit was clamped to the rear of the Vector instrument thereby providing data useful in judging the datum of the measurement volume above the bed.

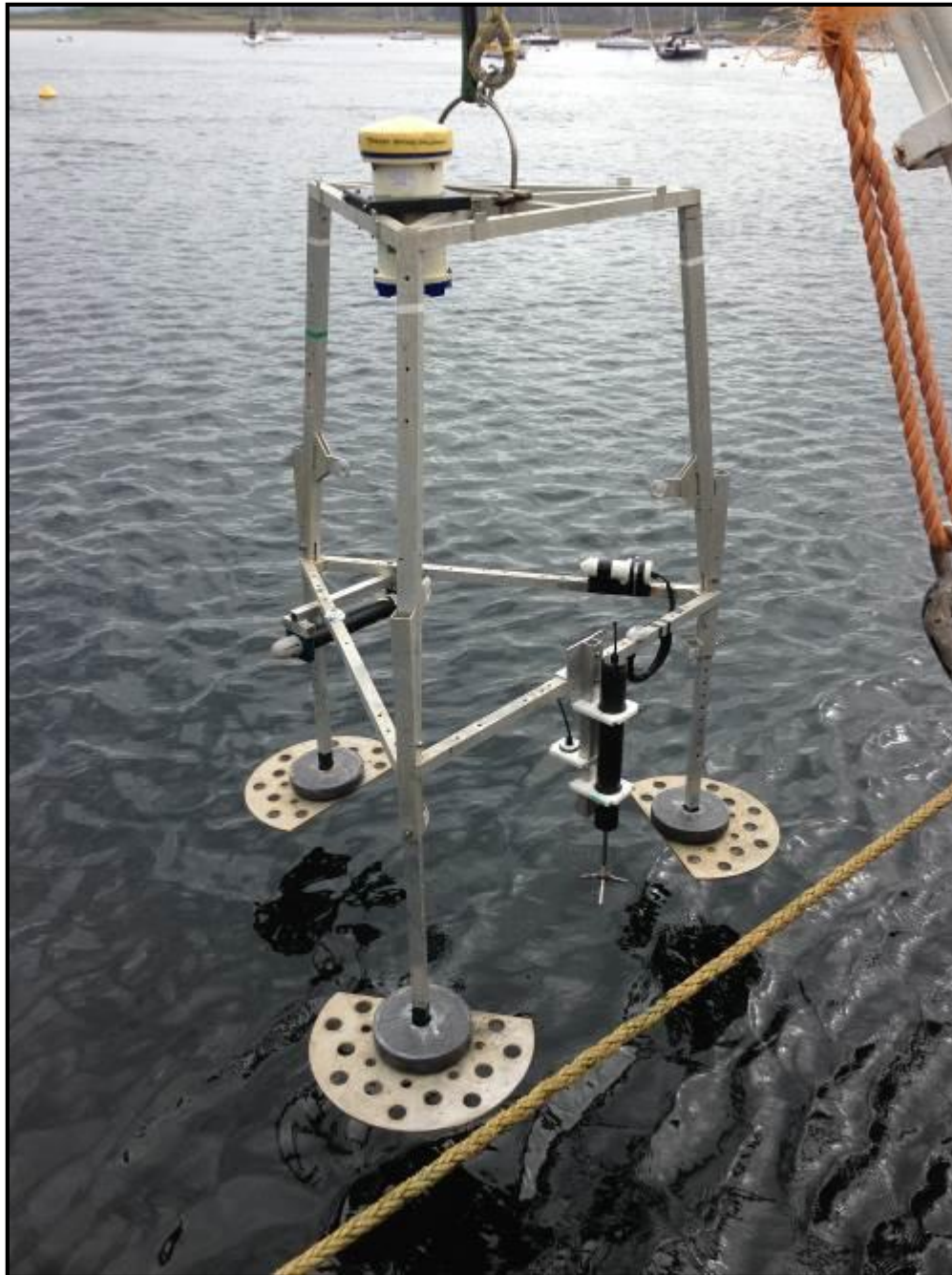


Figure 8. The boundary layer rig showing the Vector ADV (to the right), the Profiler (top left) and a marine altimeter, co-aligned with the Vector (but logger at the top). An TRDI ADCP is mounted on the top of the frame pointing upwards.



3. SURVEY 1 – August 2013

3.1 Flume Deployment Programme

Table 2 provides a summary of all flume deployments. Altogether 28 scientific deployments (not including sea trials, 31 if included) were made. The principal issue associated with deployment of Voyager 2 in tethered mode is that the vessel remains absolutely or nearly stationary. The survey vessel Sir John Murray was not equipped with a dynamic positioning system and susceptible to motion induced by the current flows and, more importantly, windage on the vessel structure. Overall the metocean conditions were very good throughout the survey and only 1 deployment (Fiunary 1.2) had to be aborted (the deployment was repeated).

The sequence of events for each flume deployment was identical and as follows; the Flexilogger was switched on and the time (BST) noted (this corresponds to an elapsed time of 0/test start). The flume is lifted off the deck and the time at which it is first submerged in the sea surface noted. It is then carefully lowered to the seabed and the time at which it lands on the bottom noted. The flume is then left for a period (initially 1 minute but then later changed to 5 minutes). A series of discrete step-wise increasing paddle rotation frequencies Ω_i was then applied, each separated by a 30 second acceleration ramp (see Figure 4). The following discrete power settings corresponding to each Ω_i were applied to every experimental run: 8, 11, 14, 17, 21, 21.5. Table 3 provides a summary of the erosion test parameters for all flume deployments.

At the end of the final power setting a 30 second ramp decreased power to zero. The flume was then lifted off the bottom (time noted), recovered to the surface (time noted) and finally lifted inboard (time noted). Usually the data were then downloaded and the flume re-deployed, but on some sites the flume was lifted to 5 m above the bed, held there for 10 minutes and then immediately re-deployed without recovery.

The OBS sensor gain (sensitivity) is controlled by the particular cable used to connect it to the datalogger. Following a series of tests at Scallastle Bay it became clear that the cable providing the highest gain should be used. The middle OBS sensor was wired up with this cable; data only from this sensor/cable combination are presented in this report (other sensors saturated very early during runs).

Table 2. Summary of flume deployments.

Date	Site	Water Depth (m)	Latitude	Longitude	Test Number	In Water	On Deck	Sediment Description
20/08/13	Scallaste Bay 1.1	~20 m	56 29.504	05 44.705	001	15:58	16:28	Quite firm muddy sand
20/08/13	Scallaste Bay 1.2				002	16:58	17:21	
21/08/13	Bloody Bay 1.1	32.2 m	56 38.46	06 05.013	003	11:21	12:00	Soft Fine mud
21/08/13	Bloody Bay 1.2				004	12:04	12:47	
21/08/13	Bloody Bay 2.1	34.7 m	56 38.730	06 6 6.240	005	15:02	15:43	Soft Fine mud
21/08/13	Bloody Bay 2.2				006	15:51	16:31	
22/08/13	Fiunary 1.1	35 m	56 23.432	05 55.066	007	08:49	09:27	Description lost
22/08/13	Fiunary 1.2				008	Aborted due to vessel motion		
22/08/13	Fiunary 1.2(a)				009	09:48	10:28	
22/08/13	Fiunary 2.1	30 m	56 33.632	05 55.818	010	13:14	13:53	Description lost
22/08/13	Fiunary 2.2				011	13:55	14:35	
23/08/13	Shuna Castle Bay 1.1	24 m	56 13.866	05 35.773	012	07:55	08:39	Description lost
23/08/13	Shuna Castle Bay 1.2				013	08:40	09:19	
23/08/13	Shuna Castle Bay 2.1	33 m	56 13.506	05 35.287	014	10:48	11:29	Description lost
23/08/13	Shuna Castle Bay 2.2				015	11:30	12:08	
26/08/13	BDNC 1.1	31.4 m	56 10.682	05 35.359	016	13:05	13:45	Slightly coarse silt mud
26/08/13	BDNC 1.2				017	13:48	14:46	
26/08/13	BDNC 2.1	14.7 m	56 11.191	05 34.950	018	16:20	17:01	Fine silts
26/08/13	BDNC 2.2				019	17:26	18:10	
27/08/13	Ardfuir 1.1	23.9 m	56 6.776	05 34.289	020	10:49	11:38	Sandy mud; muddy sand
27/08/13	Ardfuir 1.2				021	11:54	12:43	
27/08/13	Ardfuir 2.1	Data not available			022	14:13	15:00	Very coarse sediment admixture; poorly sorted with stones
27/08/13	Ardfuir 2.2				023	16:52	17:40	
28/08/13	Port Na Moine 1.1				024	08:59	09:59	

Date	Site	Water Depth (m)	Latitude	Longitude	Test Number	In Water	On Deck	Sediment Description
28/08/13	Port Na Moine 1.2				025	11:49	12:41	Fine mud with shells + terrestrial debris; sulphides and numerous worm tubes
28/08/13	Port Na Moine 2.1	23.4 m	56 09.090	05 32.365	026	14:24	15:07	Gel, cohesive muds, lots of worm tubes, leaves etc; some shells
28/08/13	Port Na Moine 2.2	23.4 m	56 09.090	05 32.365	027	15:24	16:12	
29/08/13	Durmyon Bay 1.1	28.8 m	55 42.252	05 42.726	028	08:28	09:24	Fine-cse silt, and muddy sand
29/08/13	Durmyon Bay 1.2				029	10:02	10:57	
29/08/13	Durmyon Bay 2.1	Data not available			030	11:43	12:32	Cohesive, admixed, lots of worm tubes, ext bioturb; organic
29/08/13	Durmyon Bay 2.2				031	12:35	13:32	

Table 3. Summary of erosion run parameters for all flume deployments.

Metric	Setting
Start time t_0	n/a
Landing (on seabed) time t_l	n/a
Initial wait time t_w	60 s, changed to 300 as of 21/08/13
Linear acceleration/deceleration ramp duration $t_{acc/decc}$	30 s
Minimum stress τ_{0min}	0.4198 N m ⁻²
Maximum stress τ_{0max}	2.0323 N m ⁻²
Stress increment $\Delta\tau_0$	N m ⁻² 0.420 0.826 1.119 1.786 1.851 2.032
Duration of steady flow Δt_e	300 s

3.2 Rig Deployment Programme

Table 4 provides a summary of all boundary layer rig deployments. Altogether 16 deployments were made (not including sea trials). The instruments collecting flow (current velocity) data were configured as follows:

Aquaprofiler:- A velocity profile was measured every 20 seconds during each of the deployments with the exception of two overnight deployments at Shuna Castle Bay and Ardfiur (22/08/13 – 23/08/13 and 27/08/13 -28/08/13, respectively). At Shuna Castle Bay a 300 second profile was employed and at Ardfiur the interval was 120 seconds. An ENU coordinate system was used during all deployments.

Vector 3D:- Velocity data were acquired at a rate of 16 Hz during every deployment. The Vector logged continuously with a 10 second interval every half-hour with the exception of two overnight deployments at Shuna Castle Bay and Ardfiur (22/08/13 – 23/08/13 and 27/08/13 -28/08/13, respectively) where the instrument logged data without an interval. The coordinate system used throughout the survey was ENU.

TRDI ADCP:- The instrument was set to record data continuously (i.e. it was not switched off when out of the water). The instrument was configured to record 25 x 2m bins with 2 minute ensembles and 50 pings/ensemble.

Altimetry:- The Altimeter instrument was set to record data at 0.1 Hz.

Table 4. Settings and deployment details for instruments on the boundary layer rig.

Date (dd/mm/yy)	Site	Instrument	Position / depth	Sampling Regime	Instrument start time (BST, hh:mm)	Instrument end time (BST, hh:mm)	Time in water (BST)	Time out of water (BST)
19/08/13	DML Pontoon	Vector ADV	N/A	16 Hz, continuous sampling, XYZ coords.	15:30	17:37	15:30	17:28
		Aquadopp Profiler		10 s profile interval, 0.1m cells, 0.1m blanking, ENU coords.	15:45	18:10		
		Altimeter		N/A	N/A	N/A		
		ADCP						
19/08/13	Scallaste Bay 1.1	Vector ADV	56° 29.450°N 0544.729W 17m	16 Hz, continuous sampling, ENU coords.	11:30	14:13	11:37	13:30
		Aquadopp Profiler		10 s profile interval, 0.1m cells, 0.1m blanking, ENU coords.	11:30	14:08		
		Altimeter		N/A	N/A	N/A		
		ADCP						
20/08/13	Scallaste Bay 1.2	Vector ADV	56 29.450N 05 44.729W 17m	16 Hz, continuous sampling, ENU coords.	15:45	18:16	15:42	18:10
		Aquadopp Profiler		20 s profile interval, 0.1m cells, 0.1m blanking, ENU coords.	15:45	18:29		
		Altimeter		1 measurement/10 s	11:00	21:09 on 26/08		
		ADCP						
21/08/13	Bloody Bay 1.1	Vector ADV	56 38.56N 06 05.39W 30.0m	16 Hz, continuous sampling, ENU coords.	11:05	13:40	11:01	13:35
		Aquadopp Profiler		20 s profile interval, 0.1m cells, 0.1m blanking, ENU coords.	11:05	13:54		
		Altimeter		1 measurement/10 s	11:00	21:09 on 26/08		
		ADCP						
21/08/13	Bloody Bay 1.2	Vector ADV	56 38.704N 06 06.117W 34m	16 Hz, continuous sampling, ENU coords.	14:15	17:19	14:04	17:12
		Aquadopp Profiler		20 s profile interval, 0.1m cells, 0.1m blanking, ENU coords.	14:15	17:34		
		Altimeter		1 measurement/10 s	11:00	21:09 on 26/08		
		ADCP						

Date (dd/mm/yy)	Site	Instrument	Position / depth	Sampling Regime	Instrument start time (BST, hh:mm)	Instrument end time (BST, hh:mm)	Time in water (BST)	Time out of water (BST)
22/08/13	Fiunaray 1.1	Vector ADV	56 32.432N 05° 55.066'W 35m	16 Hz, continuous sampling, ENU (East-North-Upoords.	08:15	10:41	8:16	10:30
		Aquadopp Profiler		20 s profile interval, 0.1m cells, 0.1m blanking, ENU coords.	08:15	10:56		
		Altimeter		1 measurement/10 s	11:00 on 21/08	21:09 on 26/08		
		ADCP						
22/08/13	Fiunaray 1.2	Vector ADV	56 33.617N 05 55.662W 30m	16 Hz, continuous sampling, ENU coords.	11:20	15:04	11:23	14:45
		Aquadopp Profiler		20 s profile interval, 0.1m cells, 0.1m blanking, ENU coords.	11:20	15:29		
		Altimeter		1 measurement/10 s	11:00 on 21/08	21:09 on 26/08		
		ADCP						
22/08/13	Shuna Castle Bay 1.1	Vector ADV	56 13.799N 05 35.691W 23m	16 Hz, continuous sampling, ENU coords.	19:30	09:32 on 23/08	19:15	9:29 on 23/08
		Aquadopp Profiler		300 s profile interval, 0.1m cells, 0.1m blanking, ENU coords.	19:30	10:05 on 23/08		
		Altimeter		1 measurement/10 s	11:00 on 21/08	21:09 on 26/08		
		ADCP						
23/08/13	Shuna Castle Bay 1.2	Vector ADV	56 13.435N 05 35.287W 33m	16 Hz, continuous sampling, ENU coords.	10:30	12:34	10:28	12:22
		Aquadopp Profiler		20 s profile interval, 0.1m cells, 0.1m blanking, ENU coords.	10:30	12:27		
		Altimeter		1 measurement/10 s	11:00 on 21/08	21:09 on 26/08		
		ADCP		Overnight deployment				
26/08/13	BDNC 1.1	Vector ADV	56 10.682N 05 35.359W 31.4m	16 Hz, continuous sampling, ENU coords.	12:45	14:56	12:52	14:54
		Aquadopp Profiler		20 s profile interval, 0.1m cells, 0.1m blanking, ENU coords.	11:45	15:14		
		Altimeter		1 measurement/10 s	11:00 on 21/08	21:09 on 26/08		
		ADCP						
26/08/13	BDNC 1.2	Vector ADV	56 11.146N 05	16 Hz, continuous sampling, ENU coords.	15:30	18:25	15:32	18:22
		Aquadopp Profiler		20 s profile interval, 0.1m cells, 0.1m blanking, ENU coords.	15:30	18:53		

Date (dd/mm/yy)	Site	Instrument	Position / depth	Sampling Regime	Instrument start time (BST, hh:mm)	Instrument end time (BST, hh:mm)	Time in water (BST)	Time out of water (BST)
		Altimeter	34.968W	1 measurement/10 s	11:00 on 21/08	21:09 on 26/08		
		ADCP	18.0m					
27/08/13	Ardfuir 1.1	Vector ADV	56 06.861N	16 Hz, continuous sampling, ENU coords.	08:15	12:55	08:15	12:53
		Aquadopp Profiler	05	20 s profile interval, 0.1m cells, 0.1m blanking, ENU coords.	08:15	13:28		
		Altimeter	34.234W	1 measurement/10 seconds	21:00 on 26/08	10:28 on 28/08		
		ADCP	29.1m					
27/08/13	Ardfuir 1.2	Vector ADV	56 07.233N	16 Hz, continuous sampling, ENU coords.	14:00	17:54	13:42	17:50
		Aquadopp Profiler	05	20 s profile interval, 0.1m cells, 0.1m blanking, ENU coords.	13:37	18:18		
		Altimeter	33.904W	1 measurement/10 s	21:00 on 26/08	10:28 on 28/08		
		ADCP	24m					
27/08/13	Ardfuir 1.3	Vector ADV	56 07.277N	16 Hz, continuous sampling, ENU coords.	17:45	07:39 on 28/08	18:30	07:36 On 28/08
		Aquadopp Profiler	05	120 s profile interval, 0.1m cells, 0.1m blanking, ENU coords.	17:45	08:25 on 28/08		
		Altimeter	33.973W	1 measurement/10 seconds	11:00 on 21/08	10:28 on 28/08		
		ADCP	32.3m	Overnight deployment				
28/08/13	Port Na Moine 1.1	Vector ADV	56 09.519N	16 Hz, continuous sampling, ENU coords.	09:00	13:49	08:48	13:30
		Aquadopp Profiler	05	20 s profile interval, 0.1m cells, 0.1m blanking, ENU coords.	09:00	13:59		
		Altimeter	31.962W	1 measurement/10 s	08:15	10:26		
		ADCP	23.4m					
28/08/13	Port Na Moine 1.2	Vector ADV	56 09.117N	16 Hz, continuous sampling, ENU coords.	14:30	16:26	14:13	16:22
		Aquadopp Profiler	05	20 s profile interval, 0.1m cells, 0.1m blanking, ENU coords.	14:30	16:38		
		Altimeter	32.370W	1 measurement/10 s	no data	no data		
		ADCP	24m					

Date (dd/mm/yy)	Site	Instrument	Position / depth	Sampling Regime	Instrument start time (BST, hh:mm)	Instrument end time (BST, hh:mm)	Time in water (BST)	Time out of water (BST)
28/08/13	Durmyon Bay 1.1	Vector ADV	55 42.157N 05 42.789W 29.3m	16 Hz, continuous sampling, ENU coords.	08:30	11:11	08:15	11:09
		Aquadopp Profiler		20 s profile interval, 0.1m cells, 0.1m blanking, ENU coords.	08:30	11:24		
		Altimeter		1 measurement/10 s				
		ADCP						
28/08/13	Durmyon Bay 1.2	Vector ADV	55 41.654N 05 43.112W 17.5m	16 Hz, continuous sampling, ENU coords.	11:45	13:49	11:35	13:41
		Aquadopp Profiler		20 s profile interval, 0.1m cells, 0.1m blanking, ENU coords.	11:31	14:53		
		Altimeter		1 measurement/10 s	08:06	14:51		
		ADCP						



3.3 Problems

Several issues arose which modified the collection of data using Voyager II. Firstly, both the main and spare circuit board which controls automated (autonomous) operation of the flume failed, we think due to a power surge. Therefore the flume was not able to be deployed and cast off as originally intended. The flume was thus modified to be run in tethered mode, in which a power cable is permanently connected directly to the motor. An 80 m long power cable was used to achieve this, and mains power delivered to the flume via a 24V DC bench-top power supply (see Figure 2, red cable). Note the two sealed LED submarine lamps and the onboard water sampler (used to collect samples to calibrate the OBS sensors) could not be used as these are powered from the circuit board system. Therefore no underwater video footage could be collected (insufficient light). In order to calibrate the OBS sensors surface scrapes from bottom sediment samples were collected using a van Veen grab, bagged and frozen. A calibration of the OBS was performed under controlled conditions *post hoc*.



4. Survey 2 – May 2014

4.1 Flume Deployment Programme

Table 5 provides a summary of all flume deployments. A total of 14 deployments (20 deployments including trials and those where sediment/bathymetry was unsuitable) were carried out. A grab sample, using a small Van-Veen grab was taken prior to each deployment in order to determine the suitability of the sediment type. Deployments occurred with the vessel, RV Seol Mara, tied-up alongside moored fish farm cage groups. This allowed for a stable position to be maintained for the deployment duration. Conditions during the entire deployment were on the whole very good, however one deployment at Shuna Castle Bay was aborted as the heave of the vessel, due to wind-waves, caused the flume to ‘bounce’ on the seabed. This deployment was subsequently repeated.

The sequence of events for each of the deployments was identical: a grab sample was taken and photographed to determine the suitability of the sediment; the RBR data-logger and OBS sensor were switched on and the time in GMT was recorded; the flume was slowly lowered to the seabed and the time of landing and depth at which the flume sank into the sediment (H) were observed and noted; the camera feed was then monitored until all resuspended material had settled; the experimental programme detailed in Table 1 was then started.

At the end of each of the deployment programmes, the paddle rotation was stopped. There was a period of two to three minutes to allow for redeposition of suspended sediments before a ‘speed test’ was carried out, whereby the paddle velocity was ramped at a stable rate from 0 cm s^{-1} to 30 cm s^{-1} to 0 cm s^{-1} over a two minute period. The flume was then recovered onto deck and the logger stopped and data downloaded.

Table 5. Summary of flume deployments in Survey 2. 'Trial' denotes flume tests where deployment logistics, run testing etc., were done.

Date (dd/mm/yy)	Site	Water Depth	Latitude	Longitude	Deployment Number	Time on Bed (GMT, hh:mm)	Time on Deck (GMT, hh:mm)	Notes
20/05/14	Dunstaffnage D1	39m	56° 27.089'N	05° 27.863'W	01	13:35	14:31	Trial
20/05/14	Dunstaffnage D2	39m	56 27.014	05 28.010	02	15:17	16:09	Trial
21/05/14	Port Na Cro	40m	56 13.661	05 36.817	03	-	-	Too Rocky
21/05/14	Shuna Castle Bay - SCB001a	23m	56 13.653	05 35.546	04	12:31	12:20	Trial
21/05/14	Shuna Castle Bay – SCB001b	23m	56 13.653	05 35.546	05	13:56	15:40	Good Sediment
22/05/14	Shuna Castle Bay – SCB001	24m	56 13.654	05 35.544	06	09:50	11:20	Frame bounced
22/05/14	Shuna Castle Bay – SC001	23m	56 13.556	05 35.503	07	12:04	13:48	Good Sediment
23/05/14	Port Na Gillie – PNG001	29m	56 12.945	05 35.258	09	09:42	11:18	Good Sediment
23/05/14	Port Na Gillie – PNG002	23m	56 12.771	05 35.297	10	11:43	13:25	Good Sediment



Date (dd/mm/yy)	Site	Water Depth	Latitude	Longitude	Deployment Number	Time on Bed (GMT, hh:mm)	Time on Deck (GMT, hh:mm)	Notes
26/05/14	BDNC001	27m	56 11.021	05 35.176	11	11:30	13:24	Good Sediment
26/05/14	BDNC002	37.5m	56 10.827	05 35.156	12	14:20	16:02	Good Sediment; but flume leaked
27/05/14	Port Na Moine – PNM001	31m	56 09.429	05 32.057	13	10:36	12:17	Good Sediment, but flume leaked
27/05/14	Port Na Moine – PNM002	36m	56 09.254	05 32.194	14	12:38	14:22	Good Sediment
28/05/14	BDNC003	36m	56 10.831	05 35.158	15	09:44	11:30	Good Sediment, but flume leaked
29/05/14	Dunstaffnage Bay – DF001	41m	56 27.010	05 28.116	16	08:32	10:14	Good Sediment
29/05/14	Dunstaffnage Bay – DF002	38m	56 27.094	05 27.858	17	11:27	13:11	Good Sediment
29/05/14	Dunstaffnage Bay – DF003	39m	56 27.069	05 27.895	18	13:33	15:15	Good Sediment
30/05/14	Scallastle Bay – SB001	20m	56 29.464	05 45.205	19	09:24	11:14	Good Sediment
30/05/14	Scallastle Bay – SB002	23m	56 29.539	05 45.494	20	11:40	13:26	Good Sediment, but flume leaked



4.2 Problems

Leakage of the flume annulus was observed at the following sites: BDNC002; BDNC003; PNM001; and SB002. This was likely due to an obstacle on the seabed, such as a stone. There are procedures to correct the data for leakage (Amos et al., 1992a), however these were not pursued in this case.



5. mini-flume pellet mobility studies

Kenny Black (SAMS) supplied Partrac with two different samples of feed pellet material. Pellets 4-5 mm and pellet 11-12 mm in diameter were provided. Studies were performed using the mini-flume to establish the critical traction stress, and general mobility stress, for each sample.

The mini-flume was set exactly as used in the field studies within a laboratory tank. A smooth false floor made of high density foam with a very fine sandpaper upper surface was used to create a firm bed at H=15 cm. For each pellet size, two situations were created within the annulus. On one side a sample of neat pellets was laid onto the bed and smoothed; on the other side of the flume a batch of pellets was glued into a pit into the foam base of depth equivalent to the pellet diameter, and then a sample of pellets was laid onto the glued patch and smoothed. This provides information on the stress required to initiate pellet movement on a) a smooth bed and b) on a rough bed of similar particles.

Flume Test 25 (the same as the field test) was used to impart a shear stress on the pellets. Data on the moment (stress) of first movement, and the moment (stress) of 'weak, general movement' was obtained visually.



6. settling velocity analysis

The time-series flume data contain information on the mass deposition rates, and therefore also settling velocity, of eroded bottom sediments. This is due to the fact that at the end of every erosion run the flume is switched off allowing deposition of resuspended sedimentary material (nominally in still water), which is reflected in a decay in the turbidity time series. For the mini-flume runs in addition, the 'SPEED' test was run which gave rise to a second deposition phase. The 'SPEED' test is a separate test which increases the lid (paddle) rotation rate from zero monotonically up to 30 RPM, at which time the flume is switched off; the test rapidly induces sediment erosion up to generally higher concentrations. Turbidity is logged through this test providing a second, elevated concentration deposition profile.

This analysis is of use to modelling attempts, which require information on the size/density/settling velocity of eroded particles/aggregates in order to redistribute the particles in the flow. However, presently it is not possible to readily predict the hydraulic character of eroded sediments from first principles, in which case measurements (such as these) are required.



7. data analysis

7.1 Grain Size, Dry Bulk Density Data and Organics

Grain size analysis and dry bulk density determinations were undertaken by SAMS. Dry bulk density was determined by defrosting frozen sediment samples from surface (0-1 cm and 1-2 cm) core slices and combining these into a single sample. These samples were then homogenised and 10 ml placed into cut-off 10 ml syringes. These 10 ml samples were placed into pre-weighed weigh boats, weighed, and dried for 24 h at 60°C, and reweighed. Dry bulk density (ρ_d) was then calculated as dry wt/volume (kg m^{-3}). Loss on ignition (LOI) is carried out in a temperature monitored muffle furnace. Approximately 0.5 g of dried, ground and sieved sediment sample is weighed precisely into a crucible. Crucibles with sediment are then ashed (250°C for 16 hours). When cooled, the crucibles are reweighed. Sediments are then heated to 500°C (Loh, 2005) for 16 hours. When cool, they are weighed again. Organic matter (OM) % is computed from data provided within the LOI methodology.

7.2 Benthic Flume Data

7.2.1 Bed Shear Stress Calculation for Voyager II

Bed shear stress is the parameter which is most commonly used in issues of sediment transport. (Mean) flow velocity (0.13 m above the bed) data ($u, v, w, \text{m s}^{-1}$) (in conjunction with applied voltage - Ω data) were collected within the annular flume under clear water conditions. These were filtered for quality following procedures recommended by Nortek. Data with a signal to noise ratio (SNR) lower than 15 and/or a correlation less than 85% were discarded. Mean shear velocity (\bar{u}_* , m s^{-1}) was calculated from the (mean) flow velocity measurements (\bar{u}) using the following empirical relationship (obtained from collaborative calibration studies by Partrac and NOCS):

Equation 11

$$\bar{u}_* = 0.0167 + 0.097\bar{u}, \text{m s}^{-1}$$

This equation is valid for a smooth bed over a full operating range of current speeds. The corresponding value for bed shear stress was derived using the expression

Equation 12

$$\tau_o = \rho \bar{u}_*^2$$

Because the shear velocity / bed stress calibration was derived from clear water studies, and it is known that the presence of sediment in suspension can feedback and reduce bed stress (so-called drag reduction) it is necessary to correct for the evolution of high suspended sediment concentrations during erosion runs. The change in bed stress is a function both of the sediment concentration and the bed stress imposed by paddle rotation. The equation which can be used to revise the bed stress in the presence of suspended sediment was provided by Amos et al., (1992b):





Equation 13

$$u_{*s} = u_* - (0.2267[\log_{10}S] \left\{ \frac{u_*}{6.35} \right\}), \text{ m s}^{-1}$$

7.2.2 Bed Shear Stress Calculation for Voyager I

A flow calibration exercise was performed using a) a laser-PIV system and b) the Nortek ADV 3D point sensor (see Figure 3); the laser PIV system provided detailed, mean sectional azimuthal and resultant flow velocity @ 0.05 m above the bed, which is useful given the ultra-high resolution and 2D areal coverage of the flume, whereas the ADV sensor provided high temporal resolution data which can be processed to provide an estimate of bed stress. The measurement volume of the ADV was ~1-2 mm above the flume artificial bed.

A 2-D Dantec Flow Map PIV system was utilized to determine the detailed flow velocity field within the flume annulus. The PIV method measures the horizontal azimuthal (U_θ) and radial velocity (U_r) fields at a given height above the bed in great spatial detail within the annulus. A major advantage of this measurement technique is that it is non-intrusive and it provides a synoptic map of velocity fields at any chosen elevation within the fluid disturbance field. The technique employs a double-pulsed laser light source, suitably aligned to generate a light sheet at any plane within the flow. In the present experiments, the axis of the flume was vertical and the light sheet was adjusted to be horizontal, illuminating the flow at a prescribed, constant elevation level in the fluid. To avoid problems with limitations of the field of view of the optical components of the PIV system and to exploit the symmetrical property of the flume system, a measurement area incorporating one-quarter of the total annular channel plan area was chosen. A CCD camera and 45° mirror arrangement was employed to record velocity field data from below the channel for a duration of 30 s at each predetermined elapsed time after initiation of the paddle motion. To optimise the PIV system the seawater within the channel was initially seeded with Iriodin 100 (Silver Pearl) tracer particles. Calibration grids were placed at the prescribed elevations prior to an experimental run, thereafter being removed before the paddle forcing was initiated.

Post-processing and analysis of the recorded flow fields was carried out using the Flow Manager 3D-PIV software package (used in 2-D mode) and data generated are presented in a polar coordinate field (i.e. x-y co-ordinates are references to the axis of rotation).

Experimental runs were carried out for four different flume depths ($H = 0.20\text{ m}, 0.25\text{ m}, 0.30\text{ m}, 0.34\text{ m}$), in which for each case, the lid rotation (paddle) rate Ω was increased incrementally by $\Delta\Omega = 2$ from 0 to 30 cm s^{-1} (as in the field tests). In these runs, the duration t_{acc} of the linear acceleration ramp process was 60 s and the time interval Δt_s was fixed at 300 s; for each increase in paddle speed, measurements of the fluid velocity field were taken continuously for an interval of 30 s, starting at 240 s after the end of the ramping process (i.e. 240 s from the start of each constant paddle speed phase).



An example of the filtered data output showing the spatial distribution of flow vectors is given in Figure 9. The velocity data represent time-averaged values of horizontal velocity over the 30 s acquisition interval.

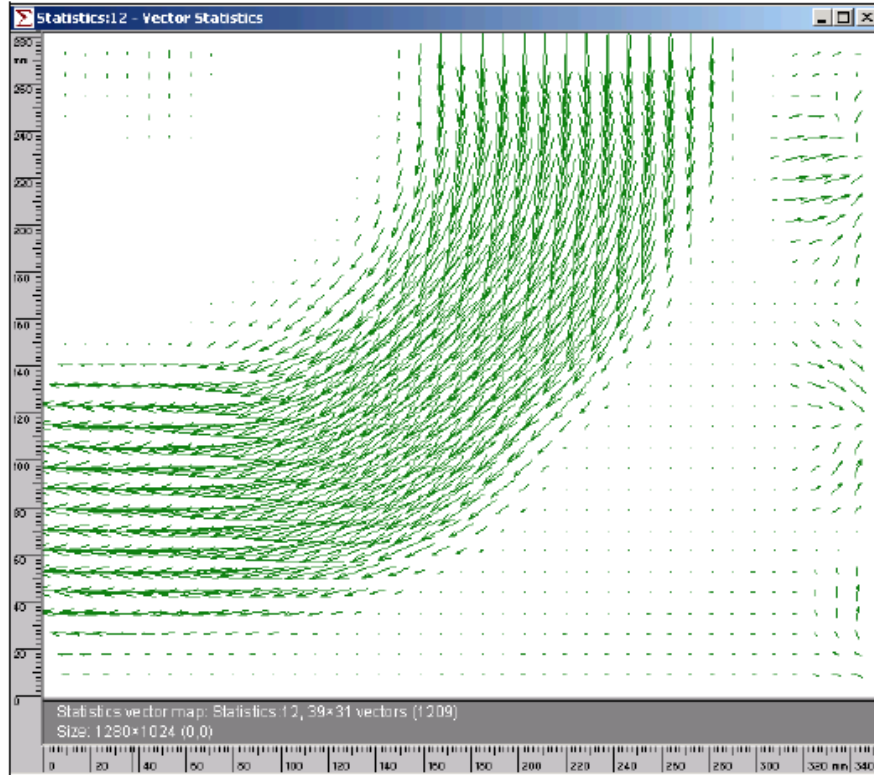


Figure 9. Illustrative vector map (statistical temporal average) for a single velocity (paddle rotation rate) setting (what was the speed ?).

The PIV method measures the horizontal azimuthal (U_{θ}) and radial velocity (U_r) fields; the resultant horizontal velocity at any point is given by $U_R^2 = U_r^2 + U_{\theta}^2$ and the horizontal sectional average value ($U_{R,ave}$) is calculated as $\Sigma U_R/n$ where n is the number of data points along a flow transverse transect from the inner to the outer wall. $U_{R,ave}$ is the velocity metric of interest to the use of the flume in this study.

From this data, relationships between the rotation rate Ω of the paddles (i.e. lid rotation rate) through an erosion test and $U_{R,ave}$ for each of the four values of channel depth (H) were formed. Table 6 summarises the relationship between these two variables following linear least squares regression analysis of the raw data. These equations can thus be used to transform field measurements of Ω into channel flow velocities.

Table 6. Summary of the predictive equations derived from least squares regression analysis of flow calibration data.

H (cm)	Regression equation	r ²
35	$U_{R,ave} = 0.0081\Omega - 0.0109$	0.99
30	$U_{R,ave} = 0.0079\Omega - 0.0186$	0.99



25	$U_{R,ave} = 0.0071\Omega - 0.0175$	0.99
20	$U_{R,ave} = 0.0067\Omega - 0.094$	0.98

For each of the sediment to lid distances (H) used in the field (H=15, 20, 25 cm only) the lid rotation frequency Ω was transformed to a bed stress (τ_o) using approach b) (above) (the TKE methodology from the ADV time series data; see Section 2.2.1) using Equation 8. Finally, Equation 13 was applied to the stress time series to account for stress reduction due to evolving high sediment concentrations.

7.2.3 Turbidity Sensor Calibrations

The on-board OBS (turbidity) sensors record raw data as a voltage; this requires conversion into scientific (sediment concentration) units (here $mg\ l^{-1}$). A series of calibrations was undertaken using surface scrapes (upper 1 cm) from bottom sediment samples collected at each site using a van Veen grab. Samples were collected, bagged and frozen during both surveys (photographs of each grab were taken (see Appendix I). For each calibration concentration reference standards were made by mixing a known dry mass of sediment into a known volume of seawater. Eight standards were made up for each site. The OBS sensor was sequentially exposed to these suspensions, and least-squares regression analysis (Fowler et al., 1989) used to generate an equation relating sensor voltage to sediment concentration. Table 7 summarises the regression equation for each site from Survey 1 and Table 8 from Survey 2.

Table 7. Summary of regression equations from the turbidity sensor calibrations (y =concentration, mg l^{-1} , x =instrument readout) for Survey 1.

Site Name	Equation	r^2
Bloody Bay 1	$y = 0.0463x - 1.4577$	0.95
Bloody Bay 2	$y = 0.0450x + 0.1689$	0.95
Fiunary 1	$y = 0.1844x - 13.0195$	0.95
Fiunary 2	$y = 0.1640x - 11.0471$	0.85
Shuna Castle Bay 1	$y = 0.0427x + 9.8368$	0.74
Shuna castle Bay 2	$y = 0.1055x - 2.7369$	0.98
BDNC 1	$y = 0.0489x + 0.2655$	0.93
BDNC 2	$y = 0.0785x - 2.9269$	0.93
Ardfuir 1	$y = 0.1338x - 5.7198$	0.88
Ardfuir 2	$y = 0.0729x - 0.7424$	0.97
Port na Moine 1	$y = 0.0153x + 3.6996$	0.67
Port na Moine 2	$y = 0.1026x - 2.0047$	0.98
Durmyon Bay 1	$y = 0.1349x - 4.1568$	0.96
Durmyon Bay 2	$y = 0.1203x - 1.2797$	0.99

Table 8. Summary of regression equations from the turbidity sensor calibrations (y =concentration, mg l^{-1} , x = instrument readout) for Survey 2.

Site Name	Equation	r^2
BDNC001	$y = 2.0121x - 46.64$	0.97
BDNC002	$y = 2.1749x - 17.75$	0.98
BDNC003	$y = 1.9543x + 0.0462$	0.99
Dunstaffnage 001	$y = 1.5146x - 29.7022$	0.96
Dunstaffnage 002	$y = 1.9612x - 36.1864$	0.91
Dunstaffnage 003	$y = 1.2575x + 3.8008$	0.83
Port na Gillie 001	$y = 2.3027x - 85.8541$	0.96
Port na Gillie 002	$y = 2.1808x - 37.2986$	0.99
Port na Moine 001	$y = 0.8945x + 38.2554$	0.71
Port na Moine 002	$y = 2.3857x - 24.4069$	0.90
Scallastle Bay 002	$y = 1.2128x - 36.2136$	0.88
Scallastle Bay 001	$y = 1.5521x - 9.4223$	0.98
Shuna Castle Bay 002	$y = 2.0381x - 31.1336$	0.99
Shuna Castle Bay 001B	$y = 1.4320x + 11.9877$	0.96

7.2.4 Time Series Data Analysis

The SPM time series (S) for both surveys were initially inspected visually for quality and any obvious outliers were edited out (a QC log was kept of this process). Any background (pre-existing i.e. generated by flume touchdown) turbidity was subtracted.

For all time series the data was time averaged every 20 s to eliminate high frequency short-term variability in the record (Widdows et al., 2007). A record of the maximum sediment concentration (S_{max}) per time-step (Δt) was made.



The SPM time series was then transformed into engineering units (kg m^{-3}) and four further time series created. These are:

- (i) eroded mass (EM, kg) time series created (using the flume volume $V = 0.261 \text{ m}^3$),
- (ii) instantaneous erosion rate (IER, $\text{kg m}^{-2} \text{ s}^{-1}$) time series (using the values for flume area and the time interval between successive data points 20 s),
- (iii) a cumulative EM time series (CEM, kg), from which a record of the total mass of sediment eroded EM_{max} per time step (Δt) was made; and
- (iv) an erosion depth (z) estimation defined by $z = \text{EM}/\rho_s \cdot A$ (values for ρ_s were taken from measures of surface dry bulk density made on samples collected at each site; see Section 6.1). A record was kept of the maximum depth of erosion (z_{max}) per time-step, Δt .

Values of initial erosion rate (IER) were then calculated. IER is defined as the erosion rate averaged over the first minute of any given time step i.e. erosion rate average over the first minute after the bed stress ramp has been applied. This differs from previous work where the erosion rate was defined over the average interval. Additional analyses of erosion time series were undertaken for the purposes of this study but are not included in this report.

7.2.5 Derivation of Critical Entrainment Stress

The critical surface erosion threshold of marine sediments τ_{0crit} is the bed stress τ_0 (or flow velocity) which just induces sediment transport. According to whether the sediments are fine (e.g. silts and clays) or coarse (sands and gravels) such a stress will induce, in general, entrainment directly into suspension or motion as bedload, respectively. For fine sediments, therefore, evidence for the threshold condition is the increase in S in the overlying water.

In spite of a wealth of studies on sediment erosion over the last 60 years and a general agreement on the foregoing definition, there is no consensus in relation to an appropriate and unequivocal methodological approach to determination of τ_{0crit} . and there are some useful publications which investigate and compare the various suggested methods e.g. Sutherland et al. (1998a). For present purposes there is a need for a method which can be applied across all flume deployments (or at least a survey specific methodology) and be used in a comparative way to view differences in sediment stability; preferably the method should embody a reproducible statistical approach rather than a subjective approach.



Voyager II Large Benthic Flume

A number of approaches were attempted to explore the best methodology for defining erosion threshold, including that outlined by Widdows et al. (2007) which uses least square regression analysis on data arranged as \log_{10} (maximum suspended particulate matter per time step, S_{max}) vs. bed shear stress. However, the method based upon the use of erosion depth, used by Mehta and Partheniades (1982), was found to be the most robust and stable method; this method is based upon the premise of Type I (asymptotic) erosion occurring at all applied stress time-steps. If this is true then one can assume that the bed shear stress τ_0 is equivalent to the aggregate shear strength at a given depth in the sediment at which erosion ceases. The surface critical entrainment stress (τ_{0crit}) is derived by extrapolation of a least squares best fit line to the surface (i.e. erosion depth = zero).

Voyager I Small Benthic Flume

The second survey *Voyager I* data differ from that collected by the Voyager II flume in that many more bed stress time-steps are used per erosion run. This offers an opportunity to directly inspect the concentration time series and to read directly the stress where sediment first appears in suspension i.e. the condition relating to the critical entrainment condition. In order to have a consistent definition across all data sets, it is necessary to specify the concentration at which the critical condition is judged to have occurred, and for these studies we chose 10 mg l^{-1} . Such an approach and number was advocated by Widdows et al., (1998) for intertidal mudflat sediments. Thus, τ_{0crit} is defined as the “bed stress when the concentration of sediments within the annulus is first observed to be 10 mg l^{-1} ”. As part of this operational definition, we take not a single data point but rather when 10 consecutive data points (equivalent to 30 s) collectively are $> 10 \text{ mg l}^{-1}$.

7.3 Boundary Layer Flow Data

The primary objective of the research project is to determine the hydraulic roughness of the bed (z_0), which is a function of the bed material type, the physical roughness, and the boundary layer fluid and flow properties. The Universal Law of the Wall can be used using Profiler (plus Vector) data, with checks, whereas for all other methods the bed stress needs to be calculated and then z_0 derived.

Initially, an accurate estimate of the bed datum through the deployment was measured using the marine altimeter (Figure 8). In addition, the echo amplitude of the Profiler (Figure 10) was used to provide information on data quality of each data bin and to isolate the lowermost velocity datum that could be used in any analysis.

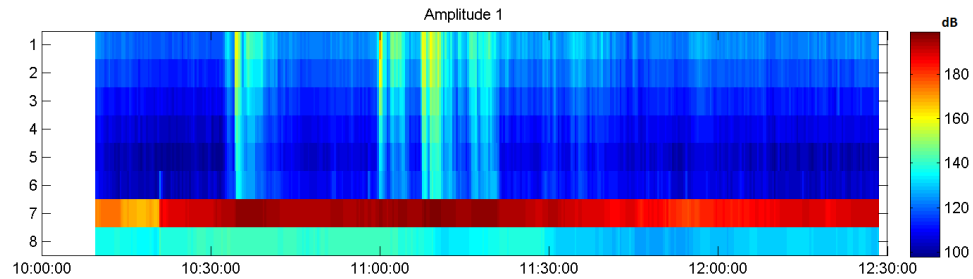


Figure 10. Example of echo intensity profile from the Profiler instrument; the red line indicates the seabed. X-axis is time, y-axis is height above bed in decimetres.

The data from each of the separate instruments (ADCP, Profiler, Vector) was initially inspected holistically to ascertain the profile of velocity through the entire water column. An estimate of the boundary layer thickness (δ) was made from this data using the criterion where $\delta=0.99u_{\infty}$ where u_{∞} is the free-stream flow velocity, and this was augmented by a theoretical estimate (after Bowden (1978) as follows:

Equation 14

$$\delta = 0.4 \frac{u_*}{f}$$

where f is the Coriolis parameter, defined as: $f=2 \omega \sin(\theta)$, ω is the rate of angular rotation of the Earth, and θ is the latitude.

Where the boundary layer extended to the sea surface it was classified as ‘depth-limited’.

A check was then made to ascertain that the time stamp for the various instruments were time synchronised and errors associated with different averaging regimes and instrument settings did not create any issues. Data records for the Profiler and the Vector were then filtered for quality following procedures recommended by Nortek. Data with a signal to noise ratio (SNR) lower than 15 and/or a correlation less than 85% were discarded. The variation in water depth through the rig deployment for each site was derived from the Vector pressure sensor data using standard formulae (UNESCO Technical Papers in Marine Science No. 44).

For each deployment of the rig a 10 minute record was identified within each deployment period for the evaluation of bed stress and associated parameters. Initially a check was made for stationarity, and a mean water depth (h_{mean}) and average flow velocity established at mid-depth (u_{mid}) over this interval.

A check on the ratio of Vector measurement volume height (0.05 m above the bed) in relation to the boundary layer thickness (δ) was made where a value <0.1 indicate validity of the approach (Soulsby, 1983). The Law of the Wall (LP) is valid only if the data points used are



approximately within the lowest 20-30% of the boundary layer where the stress is notionally constant with height above the bed (the so called constant stress layer, Soulsby, 1983), and thus attention was given to the heights of the measurements (the bottom-most value from the Vector was included in the LP methodology) during regression analysis. Further, according to Dyer (1985) it is possible to use the Universal Law of the Wall for all $Re > 3.5$, even though the flows are considered transitional below $Re = 70$. Following these checks bed stress (τ_o), and its sister parameter the friction velocity (u_*) were computed using both the TKE and LP methodologies. A value of 0.19 was used for the coefficient C_1 (see equation 8) in the TKE method.

Two different versions of the Reynolds number: a ‘grain’ Reynolds number = u_*k_s/ν , where k_s was taken as equal to $1.1d_{90}$ (after Soulsby, 2007, d_{90} is the 90th percentile grain diameter and values from size analysis of bottom sediments were used; see Section 5.1), and ν is the kinematic viscosity @10°C = $1.212 \times 10^{-6} \text{ m}^2 \text{ s}^{-1}$; and a ‘flow’ Reynolds number ($u_{mid}(z) \cdot z/\nu$ where z is a mid-depth datum). u_* values from both the TKE and LP methods were used within these formulae to provide some redundancy. The Reynolds numbers were calculated to aid classification of the boundary as hydrodynamically rough, transitional, or smooth according to the criteria below;

- i. $u_*k_s/\nu > 70$ rough turbulent
- ii. $u_*k_s/\nu < 5$ smooth turbulent
- iii. $u_*k_s/\nu < 70$ transitional
- iv. $\bar{u}_{mid,z} \cdot z/\nu > 500,000$ rough turbulent
- v. $\bar{u}_{mid,z} \cdot z/\nu > 500,000$ smooth turbulent

In addition, the grain Reynolds number was computed for a typical pellet maximum diameter (10 mm, i.e. $k_s = 2.5 \times 0.010 \text{ m}$) in order to compare the boundary classification at each site for a coarser particle.

z_o within the LP methodology is given by the intercept on the y-axis on a plot of $\log(z)$ versus velocity. This value has been tabulated with the regression correlation coefficient (r^2) and associated shear velocity and bed stress values. z_o within the TKE methodology was derived using different equations according to whether the boundary classification came out as smooth or transitional – rough. For a smooth classification equation 9 is used, for a rough classification equation 10 is used.

Further, if an independent measure of z_o is available, there is a means of computing k_s (the bed ‘grain’ roughness) which is always difficult to determine:

Equation 15

$$Z_o = k_s \exp\left(\frac{-B}{2.5}\right)$$



where $B = 8.5$ (found experimentally for fully turbulent or transitional boundaries) or 5.5 (found experimentally for smooth boundaries) (Tennekes and Lumley, 1972).



8. results

8.1 Sediment Bulk Density, Grain Size and Organics

Table 9 presents the data from density, size and porosity analysis from Survey 1.

Table 9. Summary dry bulk density (ρ_d), particle size (d), porosity (Φ), loss on ignition (LOI) and organic matter OM) from Survey 1 sediment samples.

Site Name	Sample Type	Sediment Name	d ₁₀ (µm)	d ₅₀ (µm)	d ₉₀ (µm)	Dry Bulk Density ρ_d (kgm ⁻³)	Porosity (Φ) %	LoI (%)	OM (%)
Bloody Bay 1	Trimodal, Very Poorly Sorted	Fine Sandy Very Coarse Silt	4.605	35.020	244.500	553	79	9.8	10.0
Bloody Bay 2	Polymodal, Very Poorly Sorted	Very Coarse Sandy Coarse Silt	4.055	19.600	1129.000	488	82	11.6	11.6
Fiunary 1	Bimodal, Poorly Sorted	Medium Silty Fine Sand	17.230	165.900	283.400	1001	62	4.0	4.3
Fiunary 2	Trimodal, Very Poorly Sorted	Very Coarse Sandy Medium Silt	3.057	12.990	2945.600	871	67	3.9	4.0
Shuna Castle Bay 1	Polymodal, Very Poorly Sorted	Very Coarse Sandy Coarse Silt	3.955	20.680	1237.100	354	87	10.6	10.4
Shuna Castle Bay 2	Polymodal, Very Poorly Sorted	Very Coarse Sandy Fine Silt	1.928	8.551	1141.500	638	76	6.8	7.2
BDNC 1	Polymodal, Very Poorly Sorted	Fine Sandy Coarse Silt	4.810	27.990	238.600	707	73	9.0	9.2
BDNC 2	Polymodal, Very Poorly Sorted	Very Coarse Sandy Medium Silt	2.807	13.200	1265.600	664	75	8.8	8.7
Ardfuir 1	Polymodal, Very Poorly Sorted	Fine Silty Fine Sand	3.731	108.900	624.400	990	63	4.6	4.3



Site Name	Sample Type	Sediment Name	d ₁₀ (µm)	d ₅₀ (µm)	d ₉₀ (µm)	Dry Bulk Density ρ_d (kgm ⁻³)	Porosity (ϕ) %	LoI (%)	OM (%)
Ardfuir 2	Polymodal, Poorly Sorted	Fine Silty Sandy Coarse Gravel	Poor data			920	65.24	8.5	8.7
Port Na Moine 1	Polymodal, Very Poorly Sorted	Coarse Silty Very Coarse Sand	6.574	75.600	18882.300	382	86	12.9	13.1
Port Na Moine 2	Polymodal, Very Poorly Sorted	Fine Gravelly Very Coarse Silt	3.900	60.300	2900.600	486	82	12.9	13.1
Durmyon Bay 1	Unimodal, Poorly Sorted	Very Coarse Silty Fine Sand	13.710	144.100	296.700	1149	57	No data	
Durmyon Bay 2	Polymodal, Very Poorly Sorted	Very Coarse Sandy Coarse Silt	5.297	32.360	1150.900	888	66		

Table 10 presents the data from density, size and porosity analysis from Survey 2.

Table 10. Summary dry bulk density (ρ_d), particle size (d), porosity (Φ), loss on ignition (LOI) and organic matter (OM) from Survey 2 sediment samples.

Site Name	Sample Type	Sediment Name	d_{10} (μm)	d_{50} (μm)	d_{90} (μm)	Dry Bulk Density ρ_d (kg m^{-3})	Porosity (Φ) (%)	LoI (%)	OM (%)
Shuna Castle Bay 001B	Bimodal, Poorly Sorted	Very Fine Sandy Very Coarse Silt	4.763	39.82	143.9	750	71.71	14.2	17.6
Port na Gillie 001	Polymodal, Very Poorly Sorted	Very Fine Sandy Coarse Silt	3.640	41.41	602.0	790	70.08	12.5	14.4
Port na Gillie 002	Unimodal, Very Well Sorted	Very Well Sorted Very Coarse Sand	1212.9	1525.0	1754.1	750	71.84	16.0	17.2
BDNC 001	Trimodal, Very Poorly Sorted	Very Fine Sandy Very Coarse Silt	3.751	29.67	182.0	400	85.05	10.9	13.6
BDNC 002	Bimodal, Very Poorly Sorted	Very Fine Sandy Very Coarse Silt	4.017	32.61	176.7	780	70.72	18.5	18.2
BDNC 003	Polymodal, Very Poorly Sorted	Fine Sandy Medium Silt	2.641	32.93	265.8	770	70.90	13.0	10.6
Port na Moine 001	Trimodal, Very Poorly Sorted	Medium Silty Fine Sand	4.484	67.97	388.5	630	76.23	6.2	5.9
Port na Moine 002	Unimodal, Very Poorly Sorted	Very Coarse Silty Fine Sand	6.810	84.86	344.9	820	69.14	26.1	23.8
Dunstaffnage Bay 001	Polymodal, Very Poorly Sorted	Medium Silty Medium Sand	4.656	101.2	417.1	820	69.03	20.7	22.1
Dunstaffnage Bay 002	Bimodal, Very Poorly Sorted	Very Coarse Silty Fine Sand	10.02	175.3	413.3	810	69.50	18.2	30.4
Dunstaffnage Bay 003	Bimodal, Very Poorly Sorted	Very Coarse Silty Fine Sand	5.085	82.21	308.7	810	69.35	23.4	18.4
Scallastle Bay 001	Bimodal, Very Poorly Sorted	Very Coarse Silty Fine Sand	6.840	74.19	372.9	750	71.77	22.5	23.2
Scallastle Bay 002	Unimodal, Poorly Sorted	Very Coarse Silty Fine Sand	8.641	100.5	304.2	790	73.10	16.0	15.9



8.2 Benthic Flume Data

8.2.1 QC Summary

Survey 1

In general Survey 1 resulted in good quality time series being obtained. It was noted on a general level that the highest applied velocity (whilst a smaller stress increment relatively) may not have increased internal flow velocities proportionately and induced additional seabed erosion i.e. there may have been a cavitation or similar flow coupling issue at high Ω . Inspection of individual time series was therefore important throughout.

There were issues in some records relating to saturation of the OBS sensor; this arises when erosion is so severe it exceeds the measurement limit of the sensor. Since the erosion characteristics of the sediments cannot be known in advance and the maximum (most sensitive) gain of the sensor was utilised, this is not avoidable (note saturation is itself evidence of bed erodibility and the stress at which this occurs can be quantitatively).

Several datasets were poor and not amenable to analysis:

- Shuna Castle Bay 2.1 – Data file corrupted
- Durmyon Bay 1.1 – Time stamp issue in data record
- Flume likely on a cobble/topographic high (leakage)

Survey 2

Overall, good quality time series were obtained from Survey 2. Of the 14 deployments, nine sites provided usable time-series. It is not possible to fully determine the reason for the poor data sets but it is most likely a consequence of leakage from the flume due to an obstruction between the bottom of the flume chamber and the seabed, this could be a large pebble or a topographic feature on the seabed that prevented the flume from settling into the sediment correctly, and is difficult to avoid.

8.2.2 Bed Stress Data

Table 11 gives the shear velocity and bed shear stress values for the range of discrete applied voltages used during the erosion experiments within Survey 1. Table 12 provides comparable data for Survey 2, for H=15, 20, and 25 cm.

Table 11. Shear velocity (u_*) and bed shear stress (τ_0) at a range of applied voltage settings for Survey 1.

	Shear velocity and bed shear stress values for applied voltage settings					
Applied voltage (volts)	8	11	14	17	20	21.5
Shear velocity $u_* u_*$ (ms^{-1})	0.0202	0.0284	0.0330	0.0417	0.0424	0.0445
Bed shear stress τ_0 (Nm^{-2})	0.4198	0.8263	1.1189	1.7857	1.8505	2.0323



Table 12. Bed shear stress values over the range of lid rotation rates (Ω) and channel depths (H) used in Survey 2.

	Flume Paddle RPM (rotation rate)															
	Ω (cm s ⁻¹)															
	0	2	4	6	8	10	12	14	16	18	20	22	24	26	28	30
Bed shear stress τ_0 (Nm ⁻²) at H = 15 cm	0.000	0.000	0.000	0.007	0.017	0.026	0.036	0.046	0.055	0.065	0.075	0.084	0.094	0.104	0.113	0.123
Bed shear stress τ_0 (Nm ⁻²) at H = 20 cm	0.000	0.003	0.005	0.007	0.009	0.011	0.013	0.014	0.016	0.018	0.020	0.022	0.024	0.026	0.028	0.030
Bed shear stress τ_0 (Nm ⁻²) at H = 25 cm	0.000	0.000	0.001	0.002	0.004	0.005	0.006	0.007	0.009	0.010	0.011	0.012	0.013	0.015	0.016	0.017

8.2.3 Results of Survey 1

As seabed erosion within the flume annulus occurs, sediments are entrained into suspension during each time step (i.e. during each applied constant voltage/velocity/stress). Figure 15 show examples of time series information from the Durmyon Bay 2.1 site. It shows the velocity / applied voltage time series (Figure 11), concentration time series (Figure 12), the eroded mass time series (Figure 13), the instantaneous erosion rate time series (Figure 14) and the corresponding eroded depth time series (Figure 15, which mirrors the former two time series effectively). In this specific example, increases in flow velocity within the annulus induce step-wise erosion and concentration values rise to a maximum of ca. 330 mg l^{-1} . Sediment deposition is evident when the motor is switched off (data not treated here). Peak (instantaneous) erosion rates rise systematically with increases in applied bed shear stress to ca. $5 \times 10^{-4} \text{ kg m}^{-2} \text{ s}^{-1}$ and the pattern of erosion depicts consistent Type I (asymptotic) erosion. The maximum erosion depth is $\sim 0.12 \text{ mm}$.

From these data a range of useful summary metrics can be derived, which are of use in the inter-comparison of seabed stability across sites. Table 13 summarises the maximum sediment concentration at the end of each time step across all sites (S_{max} ; units kg m^{-3}) and Figure 13 and 15 provide the same but for the respective parameters total eroded dry mass (EM_{max} , units kg) and maximum erosion depth (z_{max}). Table 14 summarises the eroded mass (kg) across all stations; Table 15 summaries the maximum eroded depth across all stations; table 16 summarises derived critical entrainment stress values ($\tau_{\text{crit.}}$) for all sites. Some sites are classified as having no measureable, or very low critical entrainment stresses, where the regression line essentially goes through or very close to the origin. $\tau_{\text{crit.}}$ values range from zero to 0.73 N m^{-2} . The range of values falls within the normal range of expected values for near-shore and estuarine muds.

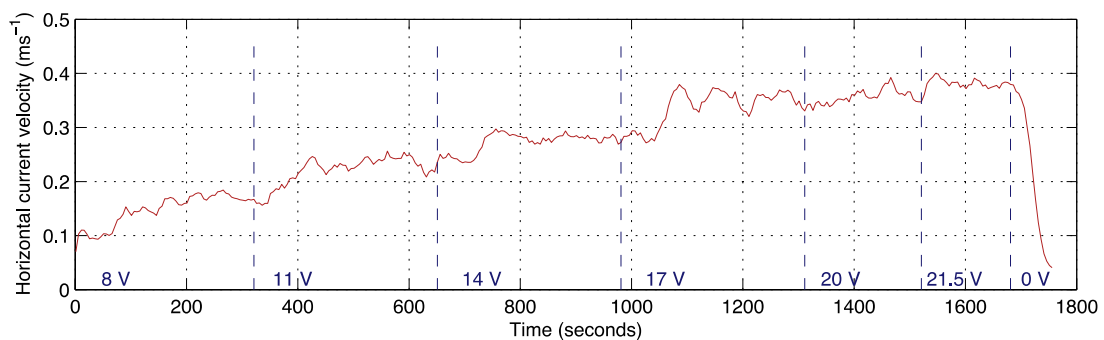


Figure 11. Streamwise current magnitude averaged every 5 seconds (solid red line). Dashed blue lines denote a change in applied voltage.

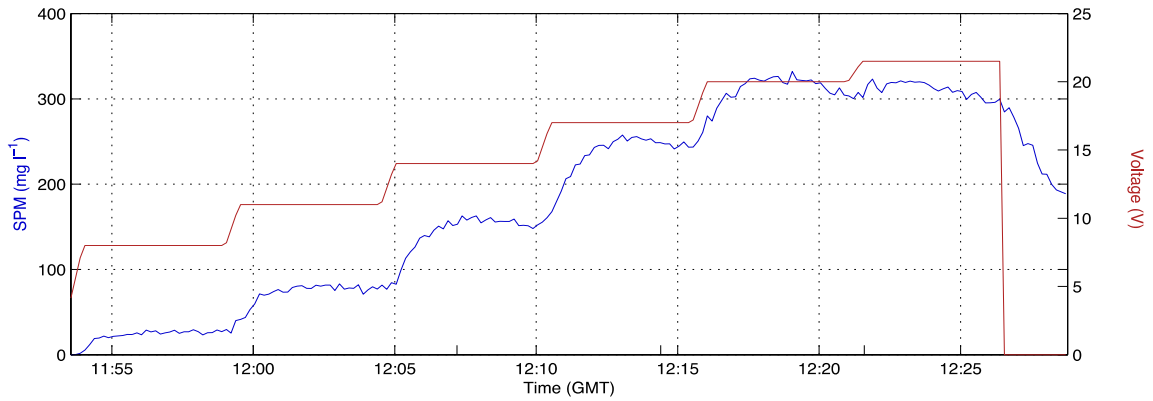


Figure 12. Applied voltage (solid red line) and total suspended solids concentration (mg l^{-1} , solid blue line) for Durmyon Bay 2.1 on 29/08/2013.

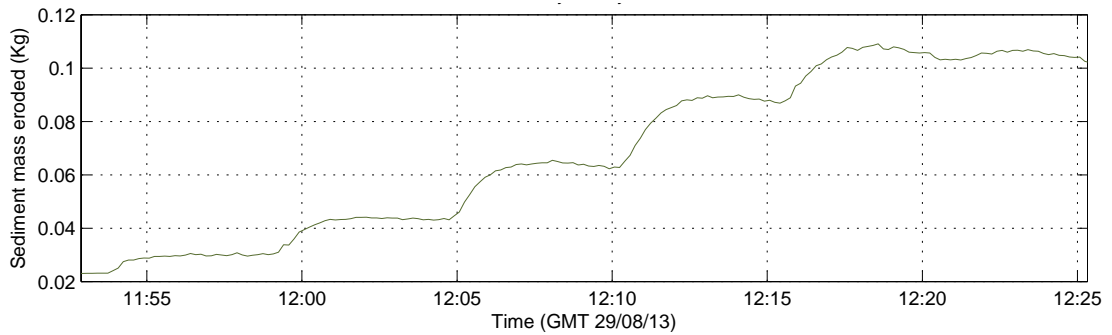


Figure 13. Mass of suspended sediment eroded (kg) for Durmyon Bay 2.1 on 29/08/2013.

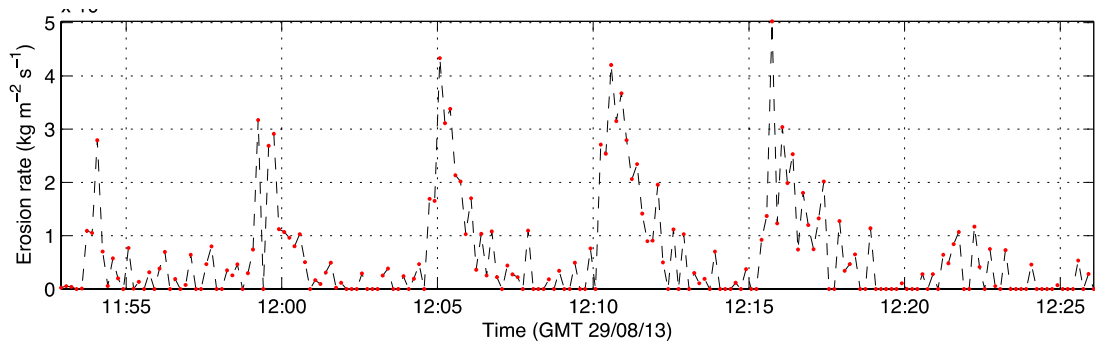


Figure 14. (Instantaneous) erosion rates ($\text{kg m}^{-2} \text{s}^{-1}$; computed every 20 s) for Durmyon Bay on 29/08/2013.

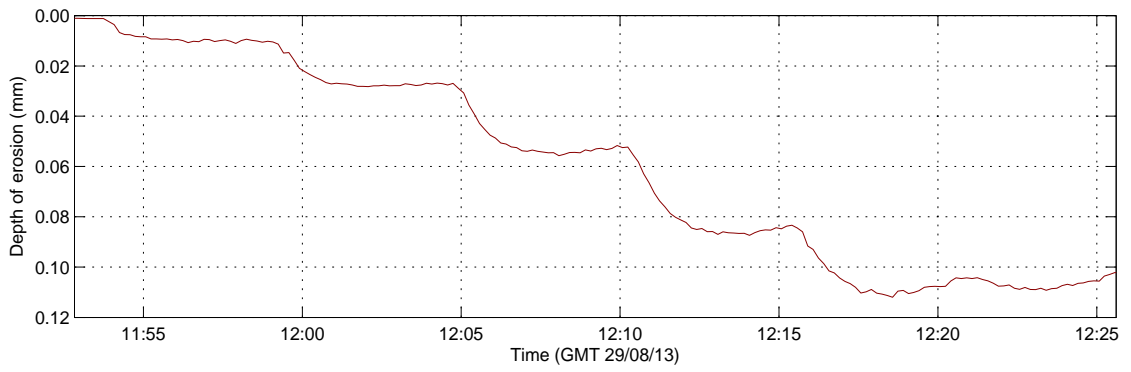


Figure 15. Depth of erosion (mm) for Durmyon Bay 2.1 on 29/08/2013.



Table 13. Maximum sediment concentration (S_{max}) at the end of each stress time-step. 'Saturated' indicates the OBS sensor is at the upper limit of measurement.

Site	Maximum Sediment Concentration S_{max} (kg m ⁻³) per Applied Voltage / Bed Stress Time-Step					
	8	11	14	17	20	21.5
Bloody Bay 1.1	0.0986	0.1343	0.2052	0.2137	Saturated	Saturated
Bloody Bay 1.2	0.0751	0.1644	0.1816	0.2137	Saturated	Saturated
Bloody Bay 2.1	0.0805	0.1375	0.2095	Saturated	Saturated	Saturated
Bloody Bay 2.2	0.0900	0.1803	0.2096	Saturated	Saturated	Saturated
Fiunary 1.1	0.1757	0.2549	0.4145	0.6078	0.8110	0.7874
Fiunary 1.2	0.1464	0.1551	0.1708	0.1957	0.2204	0.1956
Fiunary 2.1	0.1512	0.1569	0.1967	0.3063	0.4794	0.4878
Fiunary 2.2	0.1260	0.1270	0.1344	0.1485	0.1679	0.1568
Shuna Castle Bay 1.1	0.0934	0.2084	Saturated	Saturated	Saturated	Saturated
Shuna Castle Bay 1.2	0.0998	0.1681	0.2085	Saturated	Saturated	Saturated
Shuna Castle Bay 2.1	Data file corrupted					
Shuna Castle Bay 2.2	0.1726	0.4490	Saturated	Saturated	Saturated	Saturated
BDNC 1.1	0.0672	0.0987	0.1539	0.2022	0.2260	0.2135
BDNC 1.2	0.0569	0.0989	0.1624	0.2125	0.2272	Saturated
BDNC 2.1	0.0716	0.0901	0.1471	0.2523	Saturated	Saturated
BDNC 2.2	0.1011	0.1530	0.2727	0.3609	Saturated	Saturated
Ardfuir 1.1	0.1165	0.1919	0.3417	0.5681	0.6137	Saturated
Ardfuir 1.2	0.1304	0.2208	0.4085	0.6115	0.6140	Saturated
Ardfuir 2.1	0.0585	0.0630	0.0722	0.0909	0.1194	0.1254
Ardfuir 2.2	0.1061	0.1054	0.1069	0.1323	0.1735	0.1785
Port na Moine 1.1	0.0893	0.1402	0.1984	0.2238	0.2404	0.2101
Port na Moine 1.2	0.0734	0.1404	0.2094	0.2408	Saturated	Saturated
Port na Moine 2.1	Flume likely on a cobble/topographic high					
Port na Moine 2.2	0.1434	0.3380	Saturated	Saturated	Saturated	Saturated
Durmyon Bay 1.1	Time stamp issue					
Durmyon Bay 1.2	0.1092	0.1251	0.1719	0.2580	0.4322	0.4908
Durmyon Bay 2.1	0.1181	0.1692	0.2508	0.3448	0.4179	0.4097
Durmyon Bay 2.2	0.1075	0.1654	0.4278	0.4655	0.4908	0.4741



Table 14. Total eroded mass (EM_{max}) at the end of each stress time step. No data at discrete voltage / stress steps correspond to OBS sensor saturation.

Site	Total Eroded Mass (EM_{max} , kg) per Applied Voltage / Bed Stress Step					
	8	11	14	17	20	21.5
Bloody Bay 1.1	0.0257	0.0608	0.1144	0.1701	-	-
Bloody Bay 1.2	0.0196	0.0544	0.1018	0.1576	-	-
Bloody Bay 2.1	0.0210	0.0569	0.1116	-	-	-
Bloody Bay 2.2	0.0235	0.0706	0.1253	-	-	-
Fiunary 1.1	0.0459	0.1118	0.2200	0.3786	0.5903	0.7958
Fiunary 1.2	0.0389	0.0801	0.1250	0.1761	0.2340	0.2855
Fiunary 2.1	0.0395	0.0804	0.1318	0.2117	0.3369	0.4642
Fiunary 2.2	0.0370	0.0701	0.1052	0.1434	0.1878	0.2288
Shuna Castle Bay 1.1	0.0244	0.0788	-	-	-	-
Shuna Castle Bay 1.2	0.0261	0.0699	0.1243	-	-	-
Shuna Castle Bay 2.1	Data file corrupted					
Shuna Castle Bay 2.2	0.0451	0.1723	-	-	-	-
BDNC 1.1	0.0172	0.0429	0.0831	0.1359	0.1949	0.2506
BDNC 1.2	0.0148	0.0407	0.0831	0.1385	0.1978	-
BDNC 2.1	0.0187	0.0422	0.0806	0.1749	-	-
BDNC 2.2	0.0264	0.0663	0.1375	0.2317	-	-
Ardfuir 1.1	0.0304	0.0809	0.1700	0.3183	0.4785	-
Ardfuir 1.2	0.0279	0.0620	0.1196	0.2247	0.3845	-
Ardfuir 2.1	0.0152	0.0317	0.0505	0.0742	0.1054	0.1381
Ardfuir 2.2	0.0273	0.0548	0.0827	0.1172	0.1625	0.2091
Port na Moine 1.1	0.0233	0.0599	0.1117	0.1698	0.2326	0.2907
Port na Moine 1.2	0.0191	0.0558	0.1104	0.1734	-	-
Port na Moine 2.1	Flume likely on a cobble/topographic high					
Port na Moine 2.2	0.0378	0.1612	-	-	-	-
Durmyon Bay 1.1	Time stamp issue					
Durmyon Bay 1.2	0.0285	0.0612	0.1060	0.1734	0.2862	0.4143
Durmyon Bay 2.1	0.0308	0.0750	0.1405	0.2304	0.3395	0.4465
Durmyon Bay 2.2	0.0282	0.0714	0.1830	0.3028	0.4309	0.5547

Table 15. Maximum eroded depth (z_{max} mm) at the end of each stress time-step. No data at discrete voltage / stress steps correspond to OBS sensor saturation and thus no information on continued erosion depths.

Site	Total Eroded Depth (z_{max} , mm) per Applied Voltage / Bed Stress Step					
	8	11	14	17	20	21.5
Bloody Bay 1.1	0.0518	0.0712	0.1098	0.1144	-	-
Bloody Bay 1.2	0.0391	0.0708	0.0971	0.1146	-	-
Bloody Bay 2.1	0.0264	0.0613	0.1053	-	-	-
Bloody Bay 2.2	0.0519	0.1071	0.1251	-	-	-
Fiunary 1.1	0.0135	0.0365	0.0850	0.1429	0.2038	0.1968
Fiunary 1.2	0.0423	0.0451	0.0492	0.0563	0.0642	0.0568
Fiunary 2.1	0.0109	0.0128	0.0265	0.0643	0.1239	0.1268
Fiunary 2.2	0.0079	0.0027	0.0054	0.0095	0.0176	0.0131
Shuna Castle Bay 1.1	0.0664	0.1650	-	-	-	-
Shuna Castle Bay 1.2	0.0486	0.1071	0.1417	-	-	-
Shuna Castle Bay 2.1	Data file corrupted					
Shuna castle Bay 2.2	0.0445	0.1919	-	-	-	-
BDNC 1.1	0.0111	0.0250	0.0483	0.0687	0.0787	0.0735
BDNC 1.2	0.0079	0.0256	0.0524	0.0735	0.0797	-
BDNC 2.1	0.0292	0.0376	0.0635	0.1608	-	-
BDNC 2.2	0.0428	0.0663	0.1207	0.1608	-	-
Ardfuir 1.1	0.0340	0.0572	0.1021	0.1701	0.1845	-
Ardfuir 1.2	0.0312	0.0383	0.0657	0.1208	0.1842	-
Ardfuir 2.1	0.0016	0.0031	0.0061	0.0122	0.0215	0.0235
Ardfuir 2.2	0.0168	0.0171	0.0176	0.0259	0.0393	0.0409
Port na Moine 1.1	0.0374	0.0775	0.1235	0.1427	0.1566	0.1426
Port na Moine 1.2	0.0523	0.1052	0.1596	0.1847	-	-
Port na Moine 2.1	Flume likely on a cobble/topographic high					
Port na Moine 2.2	0.0819	0.2825	-	-	-	-
Durmyon Bay 1.1	Time stamp issue					
Durmyon Bay 1.2	0.0035	0.0076	0.0198	0.0423	0.0877	0.1029
Durmyon Bay 2.1	0.0106	0.0278	0.0553	0.0869	0.1115	0.1088
Durmyon Bay 2.2	0.0337	0.0531	0.1414	0.1519	0.1626	0.1570



Table 16. Critical surface erosion threshold stresses and associated regression coefficients. Some sites are classified as having no measurable, or very low critical entrainment stresses, where the regression line essentially goes through or very close to the origin.

Critical entrainment stress ($\tau_{crit.}$, N m ⁻²) and associated r ² value for each site		
Site	$\tau_{crit.}$ (N m ⁻²)	r ²
Bloody Bay 1.1	No $\tau_{crit.}$ / very low value	0.82
Bloody Bay 1.2	No $\tau_{crit.}$ / very low value	0.92
Bloody Bay 2.1	0.22	0.97
Bloody Bay 2.2	0.01	0.95
Fiunary 1.1	0.46	0.95
Fiunary 1.2	No $\tau_{crit.}$ / very low value	0.85
Fiunary 2.1	0.67	0.83
Fiunary 2.2	0.53	0.52
Shuna Castle Bay 1.1	0.15	1.00
Shuna Castle Bay 1.2	0.05	0.99
Shuna Castle Bay 2.1	Data file corrupted	
Shuna Castle Bay 2.2	0.30	1.00
BDNC 1.1	0.17	0.96
BDNC 1.2	0.25	0.97
BDNC 2.1	0.38	0.91
BDNC 2.2	0.01	0.95
Ardfuir 1.1	0.19	0.99
Ardfuir 1.2	0.4146	0.85
Ardfuir 2.1	0.61	0.87
Ardfuir 2.2	0.01	0.77
Port na Moine 1.1	No $\tau_{crit.}$ / very low value	0.89
Port na Moine 1.2	No $\tau_{crit.}$ / very low value	0.90
Port na Moine 2.1	Flume likely on a cobble/topographic high	
Port na Moine 2.2	0.25	1.00
Durmyon Bay 1.1	Time stamp issue	
Durmyon Bay 1.2	0.73	0.82
Durmyon Bay 2.1	0.33	0.97
Durmyon Bay 2.2	0.13	0.84



8.2.4 Results of Survey 2

Mini-flume (Voyager I) data are fundamentally the same in nature as those of the Voyager II instrument. Example results from DF002 (Dunstaffnage Bay 29/05/14) are presented in Figure 16. In this example, concentrations up to $\sim 550 \text{ mg l}^{-1}$ evolve in the annulus, instantaneous erosion rates are largely $10^{-4} \text{ kg m}^{-2} \text{ s}^{-1}$ and broadly increase with stress, and the maximum erosion depth is very small ($\sim 0.1 \text{ mm}$). Table 17 summarises the critical stress values derived from the time series using the 10 mg l^{-1} criterion established previously); the critical entrainment stress τ_{0crit} for Site DF002 is 0.221 N m^{-2} . Critical stress values range $0.057 \text{ (SB001)} - 0.221 \text{ N m}^{-2} \text{ (DF002)}$ which is generally lower than values for the outlying sites (Survey1; Table 17), but are largely in the region of 10^{-1} N m^{-2} . Well defined critical entrainment conditions are identified in all successful time series.

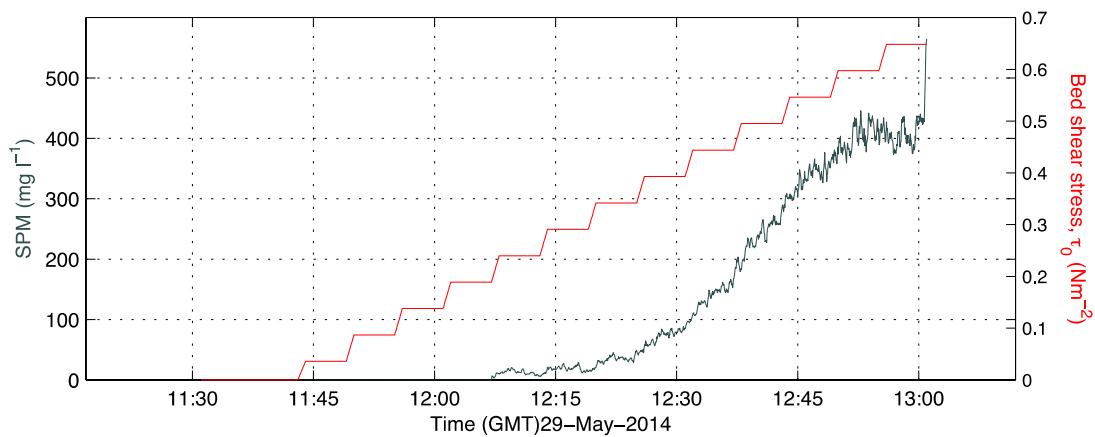


Figure 16. Suspended sediment concentration (mg l^{-1}) and bed shear stress time series for site DF002.

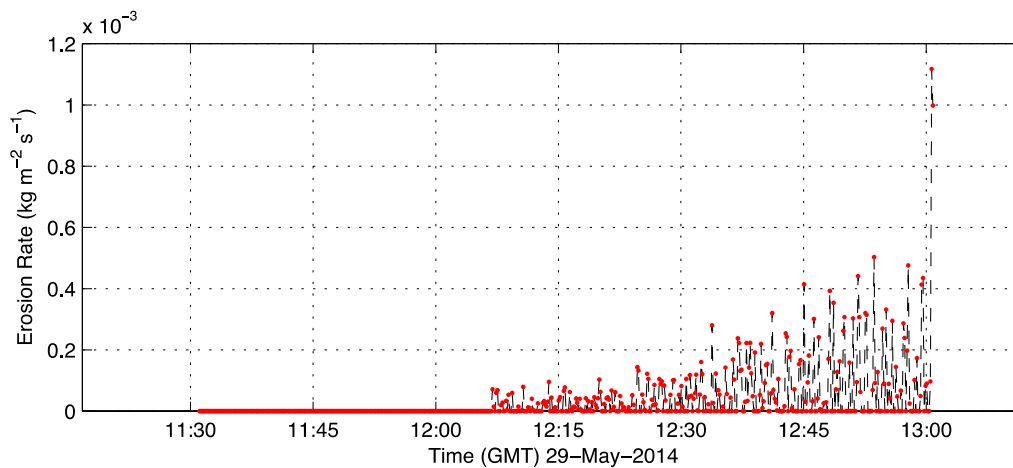


Figure 17. Instantaneous erosion rates ($\text{kg m}^{-2} \text{ s}^{-1}$); computed every 20 s for site DF002.

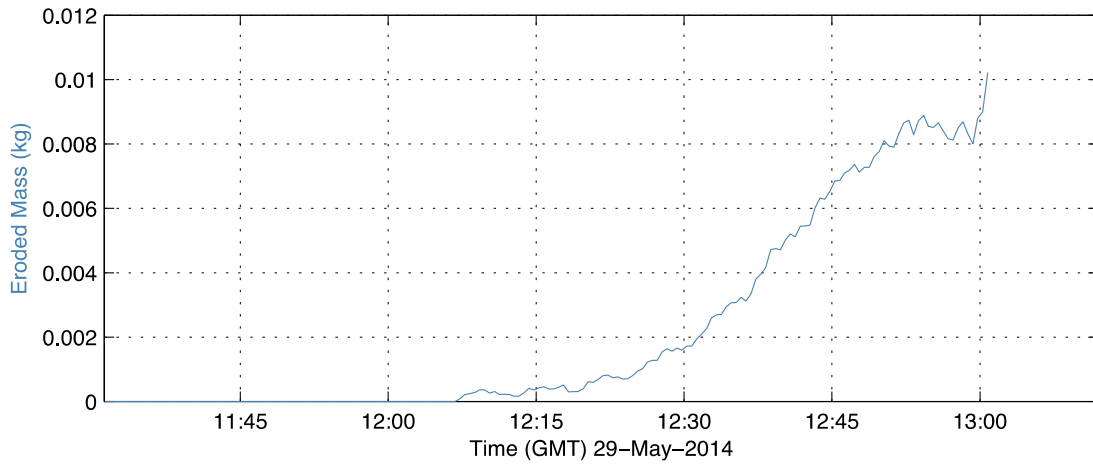


Figure 18. Time series of sediment mass eroded (kg) from site DF002.

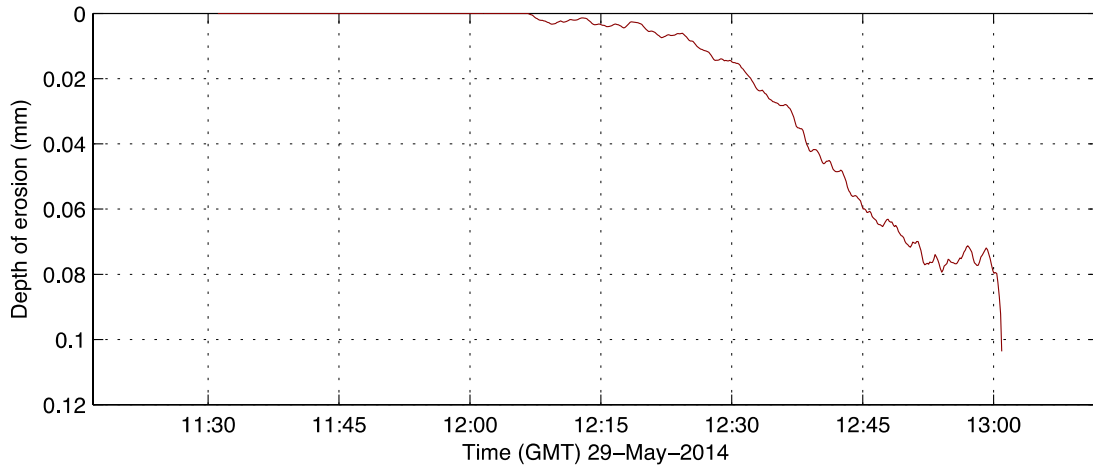


Figure 19. Depth of erosion time series for site DF002.



Table 17 Summary critical entrainment stress values ($N m^{-2}$) using a specified, over-background minimum concentration of $10 mg l^{-1}$.

Site	Critical shear stress ($N m^{-2}$)
BDNC001	0.04
BDNC002	Leakage
BDNC003	Leakage
DF001	0.02
DF002	0.04
DF003	0.02
PNG001	0.01
PNG002	0.02
PNM001	Leakage
PNM002	0.02
SB001	0.01
SB002	Leakage
SC001	0.02
SC002	0.02
SCB001B	0.02



8.3 Boundary Layer Flow Data

8.3.1 QC Summary

Table 18 summarises the general metadata associated with the deployment of the boundary layer rig. In terms of the outcomes of applied quality control procedures, Port na Moine 2, a deployment which lasted only 1.5 hours, shows no substantial change in tidal elevation unlike all other deployments, and the near bed velocity data for Durmyon Bay 2 was for unknown reasons highly irregular. Otherwise, the velocity obtained using all three instruments was considered of good quality.

8.3.2 Data

The data records were of variable length, and were well distributed over the tidal frame. Velocities were referenced to mean magnitudes at mid-depth; the maximum measured velocity was at the Fiunary 2 site (0.44 m s^{-1}), but more generally maximum velocities ranged $0.10 - 0.30 \text{ m s}^{-1}$. An exception was for BDNC1 where flow magnitudes did not exceed 0.03 m s^{-1} (likely low water period).

The initial assessment of the data was to establish whether the boundary layer occupied the whole of the water column, or just part of it. Boundary layers which occupy the entire water depth are frequently termed depth-limited (Soulsby, 1983). The importance of boundary layer thickness is fundamental to the assessment of boundary friction variables, as it provides some clue to the location in the vertical of the various sub-divisions of the boundary layer shown in Figure 7. In particular it is important to know a priori both the range of heights where a logarithmic velocity variation occurs, and where the zone known as the constant stress layer exists. In order to properly determine boundary friction parameters data within these layers should be used.

Two methods were used to indicate boundary layer thickness (δ), one which used measured velocity profiles and one a theoretical derivation (Table 19; Equation 14). Figure 20 shows an example of the velocity profile from the ADCP instrument for Fiunary Bay 1, where $\delta \sim 14 - 15 \text{ m}$. There was not a strong correlation with the theoretical estimate, however, both sources of information indicate typical values for δ of the order $10+$ m, excepting BDNC 1 which is $\sim 1 \text{ m}$ due to the extremely low flow magnitudes. A common assertion is that the logarithmic/constant stress layers occupies the lowermost 20-30% of the boundary layer thickness in shelf waters, 20 – 30 m deep (Soulsby, 1997). Excepting the BDNC site, there should be confidence in the data analysis if the velocity data are collected within 2-3 m of the seabed, which for the Profiler instrument they are.

An additional inspection of the Vector data using the ratio of mean flow velocity to shear velocity reveals a value of ~ 10 , indicating that the measurement volume of the instrument may be in the very lowest part of the boundary layer, perhaps in the viscous sub-layer (Figure 7) or the buffer layer immediately above.



Table 18. Metadata summary for the boundary layer rig deployments.

Site Name	QC Flags	Water Depth (h) During Rig Deployment (m)			Flow Velocity at h/2 (h) During Rig Deployment ($m\ s^{-1}$)			Rig	Tide State
		Min	Max	Average	Min	Max	Average	Deployment Duration	
Bloody Bay 1	x	31.83	32.51	32.29	0.081	0.117	0.099	01:50:00	Ebb
Bloody Bay 2	x	37.67	40.06	39.7	0.006	0.099	0.049	02:30:00	Flood
Fiunary 1	x	30.47	31.73	31.31	0.046	0.304	0.195	01:50:00	Ebb
Fiunary 2	x	32.31	33.36	32.38	0.117	0.446	0.266	03:00:00	Ebb-Low-Start of flood
Shuna Castle Bay 1	x	21.89	24.39	22.89	0.002	0.208	0.101	12:50:00	13 hours - ebb flood ebb
Shuna Castle Bay 2	x	35.48	36.01	35.67	0.063	0.145	0.102	01:20:00	Ebb
BDNC 1	x	34.06	34.25	34.23	0.005	0.031	0.016	01:30:00	Ebb
BDNC 2	x	20.16	21.11	20.98	0.009	0.114	0.067	02:20:00	Flood
Ardfuir 1	x	29.91	30.84	30.59	0.027	0.154	0.097	04:00:01	Ebb
Ardfuir 2	x	26.77	27.07	26.78	0.010	0.310	0.126	03:30:00	Flood
Ardfuir 3	x	33.82	34.49	34.36	0.008	0.337	0.061	12:10:04	12 hours. ebb-flood
Port Na Moine 1	x	25.42	26.12	26.11	0.019	0.120	0.068	04:00:00	Ebb
Port Na Moine 2	Unusual depth signal/no real tidal change	24.54	24.65	24.58	0.090	0.159	0.129	01:30:00	Flood
Durmyon Bay 1	x	30.64	30.85	30.84	0.071	0.219	0.135	02:10:00	Ebb
Durmyon Bay 2	Profile not exponential	19.44	19.59	19.59	0.081	0.119	0.102	01:30:00	Ebb

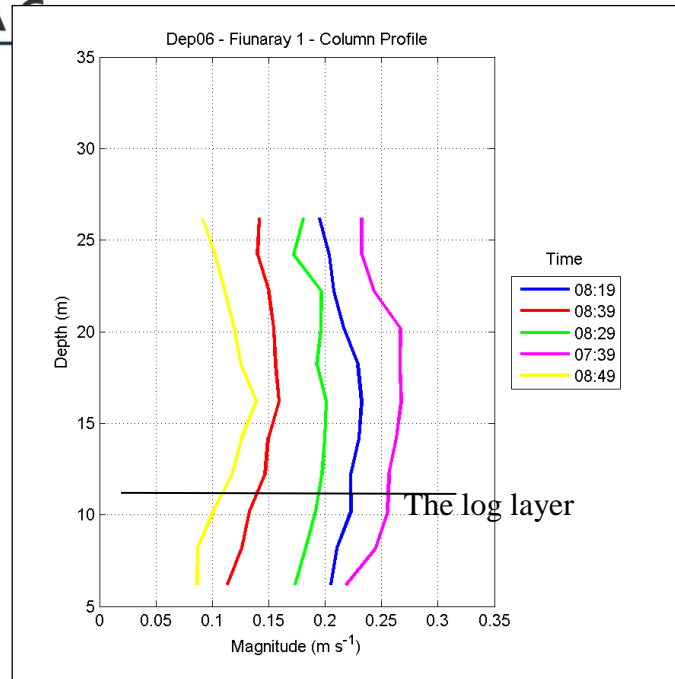


Figure 20. Water column profile (ADCP data only) of velocity magnitude at Fiunary 1 site to illustrate boundary layer character; ebb tide phase.

Table 19. Measured and computed (theoretical) values for boundary layer thickness.

Site	Boundary Layer Thickness δ (m)	
	From velocity profile	From Theory (Equation 14)
Bloody Bay 1	17	12
Bloody Bay 2	depth ltd	18
Fiunary 1	15	depth ltd
Fiunary 2	13	depth ltd
Shuna Castle Bay 1	x	15
Shuna Castle Bay 2	depth ltd	10
BDNC 1	1	10
BDNC 2	8	18
Ardfuir 1		18
Ardfuir 2	11	depth ltd
Ardfuir 3	x	11
Port Na Moine 1	13	13
Port Na Moine 2	x	depth ltd
Durmyon Bay 1	x	depth ltd
Durmyon Bay 2	x	depth ltd



PART B ABSTRACT

The seabed boundary was also classified in terms of whether it was hydraulically smooth, transitional or rough. These classifications seek to infer whether the topography of the seabed will influence negligibly or substantially the flow over it. A rough bed, which physically would correspond to a 'bumpy' bed, protrudes into the flow disrupting it and effecting the frictional drag (stress) and the velocity profile (as well as sediment transport and deposition); on the other hand a smooth bed offers no protrusions to the flow, and the interface sediments are notionally embedded within a stable and very thin flow sub-layer (see Figure 7). Typically, muds and fine silts are often turbulent smooth whereas coarse sands and gravels are often turbulent rough.

Table 20 shows calculations using the grain Reynolds number and the flow Reynolds number derived from the rig data. Two different shear velocity values are used in the calculation of the grain Reynolds number. Data relating to the flow Reynolds number show the maximum and minimum values related to the maximum and minimum flow velocities across the entire rig deployment period plus the value from the 10 minute data record. The two right-hand columns show the grain Reynolds number computed using $d_{50} = 10$ mm, which is indicative of a pelleted bed.

The data show that, regardless of the Reynolds number formulation used, the boundary is classified as largely turbulent smooth, with only two sites transitional-rough (according to which metric is used). It is only when the grain Reynolds number is computed assuming a much coarser bed (in this case, a notional pelleted bed with $d_{50} = 10$ mm) that the boundary classification changes (universally) to one of rough. These observations have implications on the parameterisation of the seabed in the DEPOMOD model, and influence how the roughness length (z_0) is calculated.



Table 20. Summary of boundary classification calculations. The table shows calculations using the grain and flow Reynolds numbers. Two different shear velocity values are used in the calculation of the grain Reynolds number. Data relating to the flow Reynolds number show the maximum and minimum values related to the maximum and minimum flow velocities across the entire rig deployment period plus the value from the 10 minute data record. The two right-hand columns show the grain Reynolds number computed using $d_{50} = 10$ mm, which is indicative of a pelleted bed.

Site	$Re = u_* k_s / \nu$ [$k_s = 1.1 d_{90}$]		$\bar{u}_{mid,z} \cdot Z / \nu$			Boundary Classif ⁿ	$Re = u_* k_s / \nu$ [$k_s = 2.5 d_{50}$ $d_{50} = 10$ mm]	
	Using u^* from TKE	Using U^* from LoW	Min	Max	Within 10 min Data Record		TKE	LoW
Bloody Bay 1	0.78	0.64	67183	96691	76936	smooth	73	60
Bloody Bay 2	5.44	3.73	4885	81368	58063	smooth	109	75
Fiunary 1	2.80	1.64	38246	250981	191567	smooth	225	132
Fiunary 2	85.79	17.82	96222	367595	331996	trans-rough	661	137
Shuna Castle Bay 1	4.95	7.69	1768	171692	95923	smooth	91	141
Shuna Castle Bay 2	3.07	4.97	52203	119646	73169	smooth	61	99
BDNC 1	0.63	1.07	3977	25168	14557	smooth	60	103
BDNC 2	6.27	3.77	7608	94362	62640	smooth	113	68
Ardfuir 1	3.01	2.06	14748	127261	86243	smooth	110	75
Ardfuir 2			8327	256065	256065	smooth	273	127
Ardfuir 3	0.00	0.00	2477	278213	20989	smooth	71	85
Port Na Moine 1	68.85	64.47	16069	98862	19196	trans-rough	83	77
Port Na Moine 2	20.56	9.57	74562	131005	114210	smooth	161	75
Durmyon Bay 1	3.51	1.99	58776	180787	180787	smooth	269	153
Durmyon Bay 2	0.68		67131	98545	79892	smooth	212.06	

Two methods were used to provide estimates of bed stress and thereby the roughness length: the Universal Law of the Wall and the Turbulent Kinetic Energy (TKE) method. An example of the velocity data used within the Universal Law of the Wall approach is given in Figure 21.

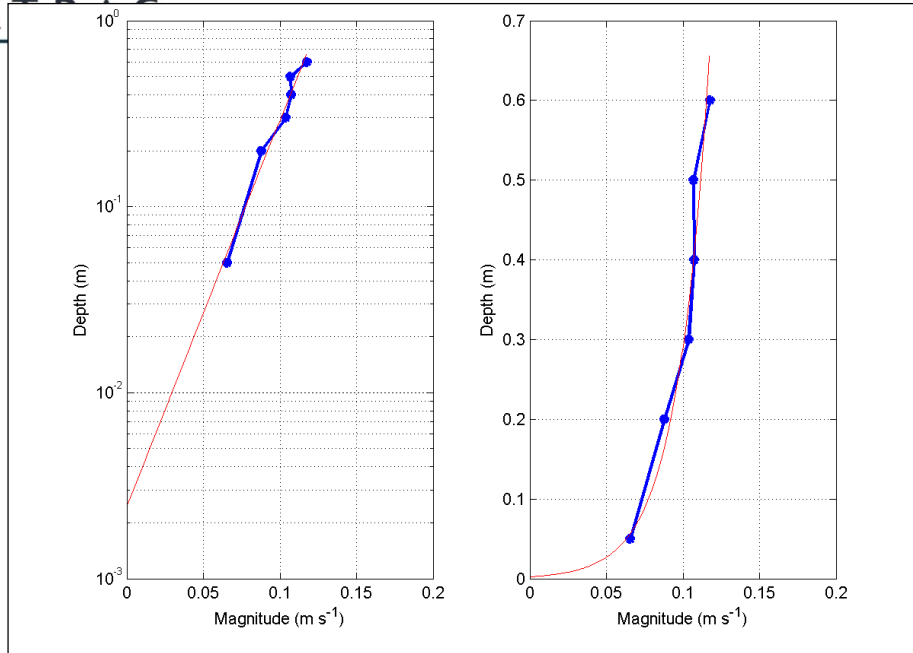


Figure 21. An example of the vertical variation of flow velocity on a linear and logarithmic scale ($r^2 = 0.97$) at the Ardfuir 1 site.

The results from the stress/roughness calculations are presented in Table 21.



Table 21. Bed stress and roughness length estimates from application of the Law of the Wall and TKE methodologies.

Site	Law of Wall Method					TKE Method		
	Shear velocity u^* ($m s^{-1}$)	Bed Stress ($N m^{-2}$)	Hydraulic roughness (z_o) (m)	No of Points used	Regression (r^2)	Shear velocity u^* ($m s^{-1}$)	Bed stress ($N m^{-2}$)	Hydraulic roughness z_o (m)
Bloody Bay 1	0.0029	0.0085	0.0028	6	0.84	0.0035	0.0127	0.00004
Bloody Bay 2	0.0036	0.0136	0.0207	6	0.84	0.0053	0.0289	0.00003
Fiunary 1	0.0064	0.0420	0.0046	6	0.80	0.0109	0.1216	0.00001
Fiunary 2	0.0067	0.0454	0.0145	6	0.92	0.0320	1.0522	0.07210
Shuna Castle Bay 1	0.0068	0.0480	0.0436	6	0.86	0.0044	0.0199	0.00003
Shuna Castle Bay 2	0.0048	0.0236	0.0648	6	0.74	0.0030	0.0090	0.00005
BDNC 1	0.0050	0.0253	0.0688	6	0.59	0.0029	0.0088	0.00005
BDNC 2	0.0033	0.0110	0.0376	6	0.69	0.0055	0.0305	0.00002
Ardfuir 1	0.0036	0.0136	0.0025	6	0.97	0.0053	0.0289	0.00003
Ardfuir 2	0.0061	0.0386	0.0032	6	0.98	0.0132	0.1792	0.00001
Ardfuir 3	0.0041	0.0172	0.0230	6	0.83	0.0035	0.0122	0.00004
Port Na Moine 1	0.0038	0.0145	0.0444	6	0.61	0.0040	0.0165	0.03570
Port Na Moine 2	0.0036	0.0135	0.0047	6	0.86	0.0078	0.0623	0.00002
Durmyon Bay 1	0.0074	0.0561	0.0253	6	0.72	0.0130	0.1739	0.00001
Durmyon Bay 2	No data available, profile irregular					0.0103	0.1083	0.0001

With (independent) knowledge of the roughness length, there is a means via Equation 15 of calculating the parameter k_s (Table 22); k_s is a metric related to roughness of the bed, and is more related to the roughness of grains rather than general bumpiness of the bed (macro-scale elements). Also shown are multipliers derived using actual site specific grain size data (Table 9) of common grain size metrics of use in providing grain Reynolds number inputs (i.e. $k_s=f(d_i)$).



Table 22. k_s values for each site determined from independent values for z_0 . Also shown are multipliers of common grain size metrics of use in providing grain Reynolds number inputs ($k_s = f(d_i)$)

Site	k_s (mm)	d_{10}	d_{50}	d_{90}
Bloody Bay 1	0.028	6080	800	115
Bloody Bay 2	0.022	5425	1122	19
Fiunary 1	0.013	754	78	46
Fiunary 2	0.226	73929	17398	77
Shuna Castle Bay 1	0.012	3034	580	10
Shuna Castle Bay 2	0.017	8817	1988	15
BDNC 1	0.016	3326	572	67
BDNC 2	0.025	8906	1894	20
Ardfuir 1	0.022	5897	202	35
Ardfuir 2	0.013	19	1	0
Ardfuir 3	0.020			
Port Na Moine 1	0.089	13538	1177	5
Port Na Moine 2	0.022	5641	365	8
Durmyon Bay 1	0.011	802	76	37
Durmyon Bay 2	0.028	5286	865	24



Table 23 summarises the data collected from the pellet mobility studies. These data indicate that for the smaller pellets (diameter=5 mm) there is a substantial difference in the stress required to move pellets on an otherwise smooth bed versus pellets on a bed of pellets, and this is the case for both hydraulic conditions. The same is true of the larger pellets (diameter=12 mm) for the incipient motion condition, but the stress required to general motion is the same for both conditions.

Table 23. Summary of pellet mobility studies.

Pellet Diameter (mm)	Hydraulic Condition	Critical shear stress (N m ⁻²)	Shear stress for 'weak, general movement' (N m ⁻²)
5	Pellets on smooth bed	0.004	0.008
5	Pellets on bed of glued pellets	Approx. 0.006	Approx. 0.008
12	Pellets on smooth bed	Approx. 0.008	Approx. 0.017
12	Pellets on bed of glued pellets	Approx. 0.012	Approx. 0.017



8.5 Settling Velocity

The deposition profile represents a mass deposition of sediments to the bed for which the following equation is valid:

$$\text{Mass deposition rate (kg m}^{-2}\text{s}^{-1}) = \text{settling velocity (m s}^{-1}) \times \text{concentration (kg m}^{-3}\text{)}$$

Representative values of mean settling velocity can be abstracted from the time series by placing a tangent to the curve at appropriate point[s] (Figure 22). For many natural fine sediments, the settling curve reveals the presence of a number of fractions, each with differing mean settling velocities; in Figure 22 three distinct fractions are evident. The mass deposition rate is given by the slope of the curve and the concentration used (in the right hand side) is that at the start of the selected period. Settling velocities are quoted in either m s⁻¹ or equivalent mm s⁻¹.

Results from the foregoing analysis are presented in Table 24. A range of values are observed, with some degree of variability. The mean, standard deviation, minimum and maximum are, respectively, 5.4 mm s⁻¹, 2.9 mm s⁻¹, 12.7 mm s⁻¹ and 5.4 mm s⁻¹ (a more accurate maximum value is 8.5 mm s⁻² as there is a single value only of 12.7 mm s⁻¹). These values are not dissimilar in magnitude to comparable data for estuarine flocs albeit at the upper end of observations, although it might be expected such an organically enriched sediment might have rather lower settling velocities. The higher values may reflect suspension of the native bottom sediment grains whereas mineral particles would have higher settling velocities. That said, other experience on the resuspension – settling of organic rich flocs shows them to have higher settling velocities than expected due to a high floc porosity which allows the passage of water during the process of settling.

A judicious choice for ω_s to be implemented within the model may be to select the lowest value reported (Table 24) for each erosion test, or some mean/median value thereof.

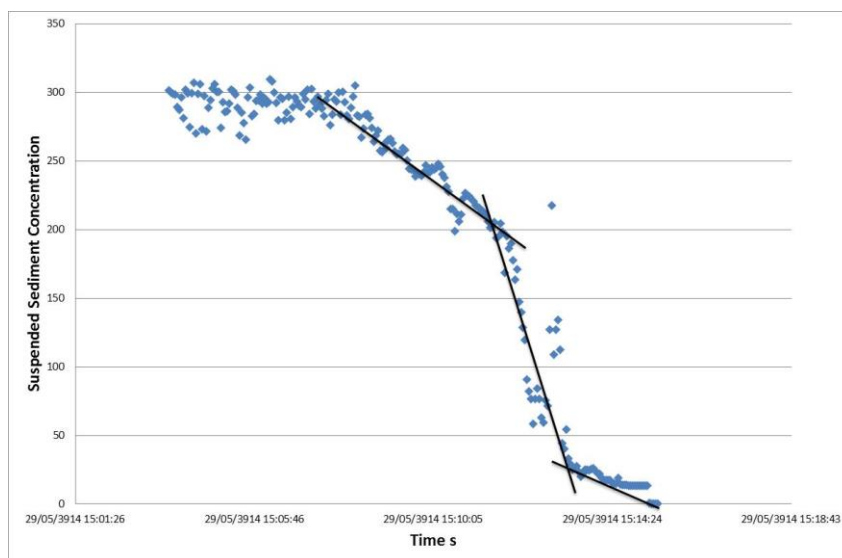


Figure 22. Example settling curve for site DF003; note the existence of three, discrete identifiable settling fractions within the sediment mass.



DF0001		PNG001	
1	3.2	1	3.1
2	6.2	2	8.5
BDNC001		PNG002	
1	7.6	1	3.4
2	2.8	SB001	
DF002		1	12.7
1	6.3	2	5.2
2	7.0	SBC001B	
DF003		1	6.6
1	1.4	2	3.1
2	7.7	3	5.7
		4	1.6



- Ali, A., and Lemckert, C.J., A traversing system to measure bottom boundary layer hydraulic properties. Open File Report. Griffith School of Engineering, Griffith University Gold Coast Campus. 30p.
- Amos, C.L., Bergamasco, A., Umgiesser, G., Cappucci, S., Cloutier, D., DeNat, L., Flindt, M., Bonardi, M., Cristante, S., 2004. The stability of tidal flats in Venice Lagoon: the results of in situ measurements using two benthic, annular flumes. *Journal of Marine Systems* 51, 211-241.
- Amos, C.L., Droppo, I.G., Gomez, E.A., Murphy, T.P., 2003. The stability of a remediated bed in Hamilton Harbour, Lake Ontario, Canada. *Sedimentology* 50, 149-168.
- Amos, C.L., Gaborn, G.R., Christian, H.A., Atkinson, A., Robertson, A., 1992a. In situ erosion measurements on fine-grained sediments from the Bay of Fundy. *Marine Geology* 108, 175-196.
- Amos, C.L., Grant, J., Daborn, G.R., Black, K., 1992b. Sea Carousel: a benthic, annular flume. *Estuarine, Coastal and Shelf Science* 34, 557-577.
- Amos, C.L., Sutherland, T.F., Zevenhuizen, J., 1996. The stability of sublittoral, fine-grained sediments in a subarctic estuary. *Sedimentology* 43, 1-19.
- Biron, P.M., Lane, S.N., Roy, A.G., Bradbrook, K.F., and Richards, K.S., 1998. Sensitivity of bed shear stress estimated from vertical velocity profiles: the problem of sampling. *Earth Surface Processes and Landforms* 23 (2), 133-139.
- Black, K.S., and Cramp, A., 1995; A device to examine the in situ response of intertidal cohesive sediment deposits to fluid shear. *Continental Shelf Research* 15(15), 1945-1954.
- Black, K.S., and Paterson, D.M., 1997 Measurement of the erosion potential of cohesive marine sediments: a review of current in situ technology. *Journal of Marine Environmental Engineering*. 4, 43-83.
- Cheng, R.T., Ling, C.H., Gartner, J.W. and Wang, P.F., 1999. Estimates of bottom roughness length and bottom shear stress in South San Francisco Bay, California. *Journal of Geophysical Research*, 104(C4), 7715-7728.
- Cromey, C.J., Nickell, T.D., Black, K.D., Provost, P., and Griffiths, C.R., 2002 Validation of a fish farm waste resuspension model by use of a particulate tracer discharged from a point source in a coastal environment. *Estuaries* 25(5), 916-926.
- Crowe, C.T., Elger, D.F. and Roberson, J.A., 2005. *Engineering Fluid Mechanics*, 8th Ed., John Wiley & Sons Inc., USA, 656p.
- Douglas, J.F. Gasiorek, J.M and Swaffield, J.A, 1986. *Fluid Mechanics*. Second Ed., Longman Singapore Publishers Pty Ltd, Singapore, 746p.
- Galperin, B., Kantha, L.H., Hassid, S. and Rosati, A., 1988. A quasi-equilibrium turbulent energy model for geophysical flows. *Journal of Atmospheric Sciences* 45(1), 55-62.
- Granger, R.A., 1985. *Fluid Mechanics*. Holt, Rinehart and Winston, Tokyo, Japan, 884p.
- Houwing, E.J., and van Rijn, L.C., 1992 In: (Sterr, H., Hofstede, J., and Plag, H-P., Eds) *Proc 1st Int. Coastal Congress*. Kiel, Germany, 223-239.
- Kabir, M.R. and Torfs, H., 1992. Comparison of different methods to calculate bed shear-stress. *Water Science and Technology*, 25(8), 131-140.
- Kim, S.C., Friedrichs, C.T., Maa, J.P. and Wright, L.D., Estimating bottom stress in a tidal boundary layer from ADV data. *Journal of Hydraulic Engineering*, 126, (6), pp399 - 406.



Nikora, V.I. and Goring, D.G., 1998. ADV measurements of turbulence: can we improve their interpretation? *Journal of Hydraulic Engineering, ASCE*, 124(6), 630-634.

Pope, N.D., Widdows, J. and Brinsley, M.D., 2006. Estimation of bed shear stress using the turbulent kinetic energy approach – A comparison of annular flume and field data. *Continental Shelf Research* 26, 959- 970.

Prandtl, L., 1926. *Über die Ausgebildete Turbulenz*. Proceedings of 2nd International Conference on Applied Mechanics, Zurich, 62-75.

Soulsby, R.L. and Dyer, K.R., 1981. The form of the near-bed velocity profile in a tidally accelerating flow. *Journal of Geophysical Research—Oceans and Atmospheres*, 86 (NC9), pages

Soulsby, R.L., 1983. The bottom boundary layer of shelf seas. *In*: Johns, B. (Ed.), *Physical Oceanography of Coastal and Shelf Seas*. Elsevier, Amsterdam, 189-266.

Stapleton, K.R. and Huntley, D.A., 1995. Seabed stress determinations using the inertial dissipation method and the turbulent kinetic energy method. *Earth Surface Processes and Landforms*, 20(9), 807–815.

Sutherland, T.F., Amos, C.L., Grant, J., 1998a. The erosion threshold of biotic sediments: a comparison of methods. *In*: Black, K.S., Paterson, D.M., Cramp, A., (Eds.), *Sedimentary Processes in the Intertidal Zone*. Geological Society of London, Special Publications, 139, 295-307.

Tennekes, H., and Lumley, J.L., 1972. *A First Course in Turbulence*. MIT Press, Cambridge, Massachusetts, USA. 300p.

Thompson, C.E.L., Couceiro, F., Fones, G.R., Helsby, R.H., Amos, C.L., Black, K.S., Parker, E.R., Greenwood, N., Statham, P.J., and Kelly-Gerryn, B., 2011 *In situ* flume measurements of resuspension in the North Sea. *Estuarine, Coastal and Shelf Science* 94, 77-88.

Widdows, J., Brinsley, M., Elliott, M., 1998. Use of an *in situ* flume to quantify particle flux (biodeposition rates and sediment erosion) for an intertidal mud flat in relation to changes in current velocity and benthic macrofauna. *In*: Geological Society of London, Special Publication, 139 85-97.

Widdows, J., Friends, P.L., Bale, A.J., Brinsley, M.D., Pope, N.D., Thompson, C.E.L., 2007. Inter-comparison between five devices for determining erodability of intertidal sediments. *Continental Shelf Research* 27, 1174-1189.

Wilkinson, R.H., 1986. Variation of roughness length of a mobile sand bed in a tidal flow. *Geo-marine Letters* 5, 231-239.



Survey 1

<p>Scallastle 2</p>	
<p>Bloody Bay 1</p>	
<p>Bloody Bay 2</p>	



Fiunary 2



Shuna Castle Bay 1





Shuna Castle Bay 2



Bagh Dail nan Ceann 1



Bagh Dail nan Ceann 2





Ardfuir 1



Ardfuir 2



Port na Moine 1





Port na Moine 2



Durmyon Bay 1



Durmyon Bay 2





Dunstaffnage DF002



Shuna Castle Bay SC001



Port na Moine PNM002





PARTRAC

Shuna Castle Bay SC002



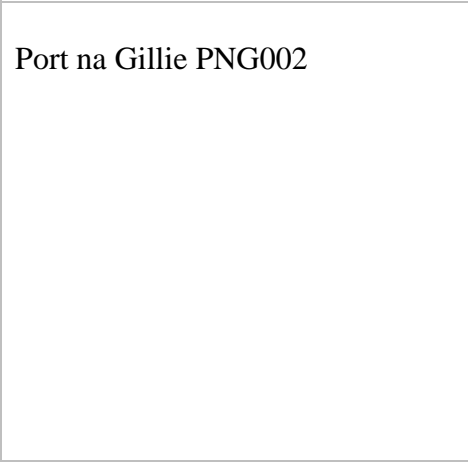
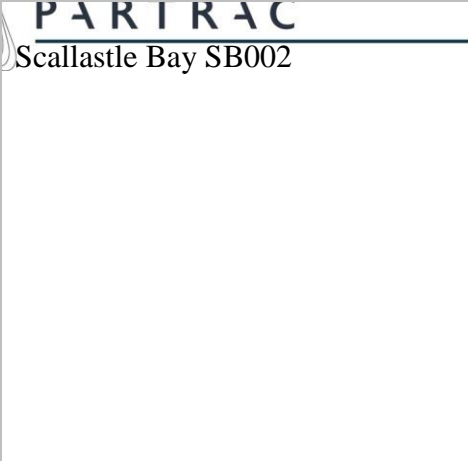
NTIAL

Shuna Castle Bay SCB001B

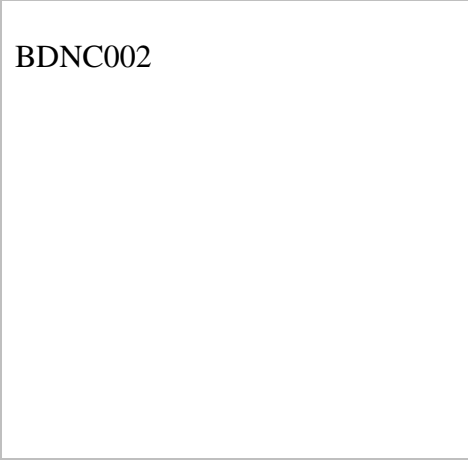


Scallastle Bay SB001





Port na Gillie PNG002



BDNC002





PARTRAC

Dunstaffnage D1

ENTIAL



Port na Gillie PNG001



Dunstaffnage D2





PARTRAC

Dunstaffnage DF001

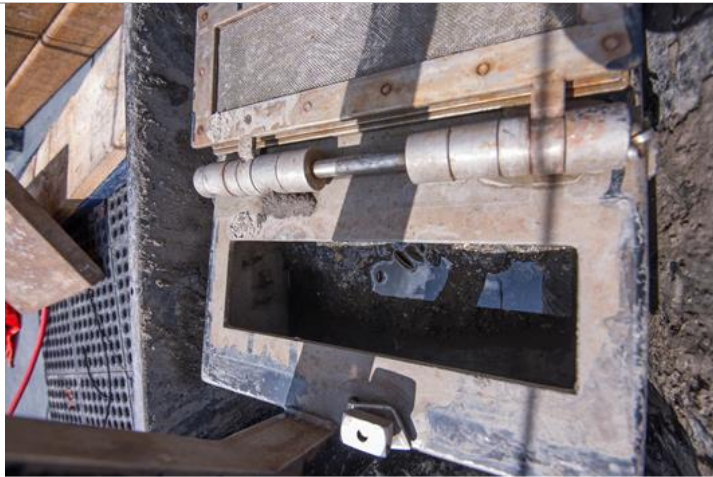
NTIAL



BDNC003



Port na Moine PNM001





PARTRAC

BDNC001

NTIAL



Dunstaffnage DF003



Annex 2. Recommendations from field and desk studies



Refining seabed process models for aquaculture: Recommendations from field and desk studies

(Partrac with Prof. C. Amos)

March 2015





DOCUMENT CONTROL

Version History					
Version	Date	Prepared by	Reviewed by	Approved by	Approved as
V03	31 st March 2015	C.L. Amos (Tuscan Consulting) & K. Black	C.L. Amos (Tuscan Consulting)	K Black	Final

Changes from the Previous Version	
v03	Various revisions to Section 4

Recipient	Distribution Method		
	Paper (copies)	PDF	Online
Kenny Black, SAMS		X	

Holders of controlled copies will automatically be provided with subsequent approved versions of this document when they become available.



CONTENTS

LIST OF FIGURES & TABLES	143
1. introduction	150
1.1 A summary of the recommended upgrades to DEPOMOD	150
2. Fundamental variables	153
2.1 Grain Density (ρ_s)	153
2.2 Water Temperature, Salinity, Density and Viscosity	154
2.3 Settling of Particles from the Fish Pen to the Seabed	155
2.4 Settling Velocity of Resuspended Faeces/Pellets	161
3. Sediment transport regime	163
3.1 Cohesive or Non-Cohesive Bed?	163
3.2 Critical Entrainment Stress of Impacted Faeces-Rich Sediments	164
3.3 Comparison with Far-Field Sediment Critical Entrainment Stresses	167
3.4 Resuspension Rates of Impacted (Cohesive) Bed Material & Erosion Through Eroded Depth	168
3.5 Onset of Motion of Intact Pellets on the Seabed	173
4. Flow (hydraulic) regime	182
4.1 Specification of Hydraulic Regime	182
4.2 Benthic Boundary Layer Parameterisation and Bed Roughness	184
5. eXternal concerns for the revised model	191
6. Recommendations for further upgrades in the future	193
7. References	194
8. Appendix BEd stress – erosion rate formulations	198



LIST OF FIGURES & TABLES

Figure 1. Compartments and processes within the DEPMOD/AUTODEPOMOD particle tracking model (from Cromey et al., 2002).....57

Figure 2. The Partrac 'Voyager II' benthic flume (top) and a schematic cross section.60

Figure 3. Photographs showing the paddle (left), the vertical OBS array (middle) and the Nortek Vectrino acoustic current sensor (right).....60

Figure 4. Example sediment concentration (turbidity) time series showing the various phases of an erosion experiment.....61

Figure 5. Partrac *Voyager I* benthic flume within a deployment frame. The red cable provides power to the flume; a horizontally mounted OBS turbidity meter is located on the flume outer channel wall on the right hand side. A sideways looking marine camera with integrated LED annulus is on the left (yellow).63

Figure 6. Voyager I benthic flume, communication/power cable and purpose-built control unit.63

Figure 7. Typical flow velocity and shear stress distributions within a turbulent bottom boundary layer (layer thickness is not to scale) (Souce Kim et al., 2000)..66

Figure 8. The boundary layer rig showing the Vector ADV (to the right), the Profiler (top left) and a marine altimeter, co-aligned with the Vector (but logger at the top). An TRDI ADCP is mounted on the top of the frame pointing upwards.72

Figure 9. Illustrative vector map (statistical temporal average) for a single velocity (paddle rotation rate) setting (what was the speed ?).....91

Figure 10. Example of echo intensity profile from the Profiler instrument; the red line indicates the seabed. X-axis is time, y-axis is height above bed in decimetres.....96

Figure 11. Streamwise current magnitude averaged every 5 seconds (solid red line). Dashed blue lines denote a change in applied voltage..... 105

Figure 12. Applied voltage (solid red line) and total suspended solids concentration (mg l^{-1} , solid blue line) for Durmyon Bay 2.1 on 29/08/2013..... 106

Figure 13. Mass of suspended sediment eroded (kg) for Durmyon Bay 2.1 on 29/08/2013..... 106

Figure 14. (Instantaneous) erosion rates ($\text{kg m}^{-2} \text{s}^{-1}$; computed every 20 s) for Durmyon Bay on 29/08/2013..... 106



Figure 15. Depth of erosion (mm) for Durmyon Bay 2.1 on 29/08/2013..... 107

Figure 16. Suspended sediment concentration (mg l^{-1}) and bed shear stress time series for site DF002..... 112

Figure 17. Instantaneous erosion rates ($\text{kg m}^{-2} \text{ s}^{-1}$); computed every 20 s for site DF002. 112

Figure 18. Time series of sediment mass eroded (kg) from site DF002..... 113

Figure 19. Depth of erosion time series for site DF002..... 113

Figure 20. Water column profile (ADCP data only) of velocity magnitude at Fiunary 1 site to illustrate boundary layer character; ebb tide phase. 118

Figure 21. An example of the vertical variation of flow velocity on a linear and logarithmic scale ($r^2 = 0.97$) at the Ardfuir 1 site. 121

Figure 22. Example settling curve for site DF003; note the existence of three, discrete identifiable settling fractions within the sediment mass. 125

Figure 1 Relationship between pellet diameter and settling velocity with each point representing the mean of a data set. The mean and standard deviation of all 16 data sets is 10.8 and 2.7 cm s^{-1} , respectively. Source Cromey et al., (2002a). 156

Figure 2 The relationship between drag coefficient of a particle and Reynolds number for particles of varying shape factors settling in still water (Mehta, 2014). 158

Figure 3 The threshold for suspension of particles sitting on the seabed (Bagnold, 1966)..... 160

Figure 4 Example settling curve for site DF003; note the existence of three, discrete identifiable settling fractions within the sediment mass. 162

Figure 5. Suspended sediment concentration (mg l^{-1}) and bed shear stress time series for site DF002..... 165

Figure 6 Covariance of the dry bulk density with critical entrainment stress. There is no significant trend in the relationship between these two parameters. 166

Figure 7 Excess bed stress ($\tau_0 - \tau_{0,crit.}$) versus erosion rate ε averaged over each velocity/stress time-step on a linear plot. 171

Figure 8 The threshold for suspension of particles sitting on the seabed (Bagnold, 1966)..... 173

Figure 9 The threshold Shields parameter for the onset of motion of particles sitting on the flat seabed of similar particles (adapted from Mantz, 1977). Note



that the Shields parameter encompasses both the lift and drag forces on the bed material. 175

Figure 10 The change in critical Shields parameter with change in relative protrusion (P/d) (after James, 1990). The red line shows the normally-accepted value (0.05) for granular material under turbulent rough flows..... 177

Figure 11 Field (time-averaged) velocity data plotted up on a Clauser plot. Note $u\tau$ in the axes labels is the friction velocity u^* 186

Figure 12 Photographs of surface sediment considered hydraulically transitional-rough from Fuinary 2 (left) and Port na Moine 1 (right). 188



Table 1. Operational parameters used in the Voyager I benthic flume deployments. Note that start and end lid rotation rates are not the induced current velocity at the bed.64

Table 2. Summary of flume deployments.74

Table 3. Summary of erosion run parameters for all flume deployments.76

Table 4. Settings and deployment details for instruments on the boundary layer rig.77

Table 5. Summary of flume deployments in Survey 2. 'Trial' denotes flume tests where deployment logistics, run testing etc., were done.83

Table 6. Summary of the predictive equations derived from least squares regression analysis of flow calibration data.91

Table 7. Summary of regression equations from the turbidity sensor calibrations (y=concentration, mg l⁻¹, x=instrument readout) for Survey 1.93

Table 8. Summary of regression equations from the turbidity sensor calibrations (y=concentration, mg l⁻¹, x = instrument readout) for Survey 2.93

Table 9. Summary dry bulk density (ρ_d), particle size (d), porosity (Φ), loss on ignition (LOI) and organic matter OM) from Survey 1 sediment samples.99

Table 10. Summary dry bulk density (ρ_d), particle size (d), porosity (Φ), loss on ignition (LOI) and organic matter (OM) from Survey 2 sediment samples. 101

Table 11. Shear velocity (u^*) and bed shear stress (τ_o) at a range of applied voltage settings for Survey 1. 102

Table 12. Bed shear stress values over the range of lid rotation rates (Ω) and channel depths (H) used in Survey 2. 104

Table 13. Maximum sediment concentration (S_{max}) at the end of each stress time-step. 'Saturated' indicates the OBS sensor is at the upper limit of measurement. 108

Table 14. Total eroded mass (EM_{max}) at the end of each stress time step. No data at discrete voltage / stress steps correspond to OBS sensor saturation. 109

Table 15. Maximum eroded depth (z_{max} mm) at the end of each stress time-step. No data at discrete voltage / stress steps correspond to OBS sensor saturation and thus no information on continued erosion depths. 110

Table 16. Critical surface erosion threshold stresses and associated regression coefficients. Some sites are classified as having no measureable, or very



low critical entrainment stresses, where the regression line essentially goes through or very close to the origin. 111

Table 17 Summary critical entrainment stress values ($N\ m^{-2}$) using a specified, over-background minimum concentration of $10\ mg\ l^{-1}$ 114

Table 18. Metadata summary for the boundary layer rig deployments. 117

Table 19. Measured and computed (theoretical) values for boundary layer thickness. 118

Table 20. Summary of boundary classification calculations. The table shows calculations using the grain and flow Reynolds numbers. Two different shear velocity values are used in the calculation of the grain Reynolds number. Data relating to the flow Reynolds number show the maximum and minimum values related to the maximum and minimum flow velocities across the entire rig deployment period plus the value from the 10 minute data record. The two right-hand columns show the grain Reynolds number computed using $d_{50} = 10\ mm$, which is indicative of a pelleted bed. 120

Table 21. Bed stress and roughness length estimates from application of the Law of the Wall and TKE methodologies. 122

Table 22. ks_s values for each site determined from independent values for z_o . Also shown are multipliers of common grain size metrics of use in providing grain Reynolds number inputs ($k_s=f(d_i)$) 123

Table 23. Summary of pellet mobility studies. 124

Table 24. Summary settling velocity data from deposition phase erosion runs. 126

Table 1 Summary settling velocity data from deposition phase erosion runs. 162

Table 2 Summary critical entrainment stress values ($N\ m^{-2}$) using a specified, over-background minimum concentration of $10\ mg\ l^{-1}$. Runs in which leakage occurred were not corrected for this anomaly. 165

Table 3 Nearfield (Survey 1) and farfield (Survey 2) values of surface critical erosion stress $\tau_{0,crit.}$ at 3 sites. 167

Table 4 Summary values for the friction coefficient ϕ in the surface layers (1) and sub-surface (2). 169

Table 5 Summary of pellet mobility studies. 180

Table 6 Summary of boundary classification calculations. The table shows calculations using the grain ($u * ks/\nu$) and flow ($umid, z.z/\nu$) Reynolds numbers. Two different shear velocity values are used in the calculation of the grain Reynolds number. Data relating to the flow Reynolds number show the



maximum and minimum values related to the maximum and minimum flow velocities across the entire rig deployment period plus the value from the 10 minute data record. The two right-hand columns show the grain Reynolds number computed using $d_{50} = 10$ mm, which is indicative of a pelleted bed..... 184

Table 7 Bed stress and roughness length estimates from application of the Wall Law and TKE methodologies to collected flow data..... 189

GLOSSARY OF TERMS

- Acceleration due to gravity (g) 9.81 m² s⁻¹.
- Angle of repose (ϕ) The steepest angle of descent or dip relative to the horizontal plane to which a granular material can be piled without slumping.
- Bed shear stress (τ_0) The shear stress on the seabed due to the motion of overlying water.
- Bed (hydraulic) roughness (z_0) A fictional height above the seabed where flow velocities diminish to zero.
- Bed slope (β) The angle of a seabed deviating from horizontal
- Critical entrainment stress ($\tau_{0, crit.}$) The bed shear stress which first generates sediment motion.
- Deposition rate (D) The mass flux of a particle(s) to the seabed; units of kg m⁻² s⁻¹
- Deposition threshold ($u_{*,dcrit}$) The bed shear stress beneath which a particle[s] of a given size will deposit to the seabed.
- Depth (into sediment) z Self-explanatory.



Drag coefficient (C_d)	A coefficient used in relating bed shear stress to a near-bed velocity.
Dry bulk density	The dry mass of sediment contained within a unit volume of sediment; units kg m^{-3} .
Effective stress (σ)	The average intergranular stress between solid particles within a sediment bed.
Erosion rate (ϵ)	The vertical mass flux of sediment due to an imposed bed shear stress; units $\text{kg m}^{-2} \text{s}^{-1}$.
Fluid density (ρ)	The mass per unit volume of a fluid, inclusive of salt (if seawater).
Friction (shear) velocity	A fictional parameter denoted u_* defined as $u_* = \sqrt{\tau_0/\rho}$, where τ_0 is the bed shear stress and ρ is the fluid density.
Friction angle (ϕ) with depth.	Expresses the rate of change in bed strength
Grain density (ρ_s)	The mass per unit volume of a solid body of sediment.
Grain diameter (d_p)	In general terms, the maximum diameter of a sediment particle.
Height above bed (z)	Self-explanatory.
Pivot angle	The angle of a sediment particle resting on a bed of sediment particles between the direction of easiest movement and the vertical
Settling velocity ($w_{s,o}$)	The vertical (downward) descent speed of a particle in a fluid.
Reynolds number (R_e)	A dimensionless quantity defined as the ratio of inertial forces to viscous forces within a fluid.
Rough turbulent flow	A turbulent flow over a solid boundary which is uneven, and in which the boundary roughness measurably affects the flow adjacent to the boundary.
Shields function (θ)	A dimensionless quantity that relates driving forces of particle motion (shear stress) to the resisting forces.
Smooth turbulent flow	A turbulent flow over a solid boundary which is essentially so smooth in character that it does not disturb the flow regime adjacent to the boundary.
Turbulent flow	A flow regime characterized by chaotic property changes; this includes low momentum diffusion, high momentum convection, and rapid variation of pressure and flow velocity in space and time.



On 20 February, 2014, a meeting was held at SEPA offices in Glasgow to examine and define possible upgrades to the software package (Auto) DEPOMOD. At that meeting Partrac Ltd (in association with Tuscan Consultancy Ltd.) presented recommendations for software upgrades, as well as the results of a joint marine survey to a number of key aquaculture sites off western Scotland and theoretical analyses. The presentation made is shown in Appendix 1 of this document. A considerable amount of discussion took place at the meeting and a number of recommendations were made. This report summarises those recommendations.

1.1 A summary of the recommended upgrades to DEPOMOD

DEPOMOD is a particle tracking model developed for the prediction of pellet and faecal matter dispersal from finfish pens in the marine environment (Cromeey *et al.*, 2002a, 2002b). The model was designed to forecast dispersal of fish pellets, fish wastage, and fish faeces. It is based upon unidirectional or tidal flows subject to a well-developed and constant benthic boundary layer. Wave motion is not considered to be important in this version due to the relatively sheltered nature of the fish farms¹². The model comprises four modules that are executed sequentially to solve for dispersal of particles. These are:

1. A set-up module to define grids, pens, input parameters and state variables;
2. A particle tracking module that advects, settles and disperses particles from the bottom of fish pens;
3. A resuspension module which tracks the erosion and advection of deposited particles ; and
4. A benthic impact module.

The model was developed in Scotland for application to Scottish fish farms which are largely situated in sheltered lochs and fjords of the western coastline. That is, the model works best for fine sands or muddy (cohesive) seabeds that are largely hydraulically flat at the model scale. In view of advances in our understanding of marine processes related to aquaculture impacts a series of recommendations are made for model upgrade. These are as follows (details of the

¹² Note that wave motion may be important in the rate settling rate of pellets in the near surface or under extreme cases, may influence the benthic boundary layer. Future versions should consider the addition of wave motion as a precaution in the event of such cases.



relevant equation, units, coefficients and constants to be used to implement these recommendations are provided later in this document):

1. To upgrade the model to input site specific measurements of temperature and salinity, from which seawater density and viscosity can be computed.
2. To upgrade the model to input grain density for both feed material and faecal material.
3. To upgrade the particle tracking module to account for settling through a flowing (turbulent) water column. At present particles are settled at the still water settling rate, whereas particle (pellet or fish faeces) settling rate in turbulent flows diminishes in proportion to the ratio of the flow shear stress to the critical (threshold) shear stress for particle resuspension.
4. To upgrade the particle tracking model via inclusion of field data in relation to the following parameters:
 - a. angle of repose (ϕ) for feed pellets
 - b. settling velocity of eroded aggregates
 - c. measured surface critical entrainment stress ($\tau_{0,crit.}$) for cohesive (faecal) sediments
 - d. (surface) critical entrainment stress ($\tau_{0,crit.}$) for feed pellets
 - e. friction angle (ϕ) for faecally impacted sediments
 - f. bed stress - erosion rate ($\tau_0 - \varepsilon$) relationship, including coefficients
 - g. bed roughness (z_0)
5. To upgrade the particle tracking model so it can decide, based upon the input of flow velocity data, whether the flow regime is hydraulically rough, transitional or smooth.
6. To upgrade the particle tracking model by providing a revised benthic boundary law nominally representative of marine aquaculture sites. This is a key area as it is from the lower part of the benthic boundary layer that bed stress, which drives sediment resuspension, is computed within the model.
7. To divide the resuspension module into two distinct pathways based upon the time (T_f) a settled particle has been deposited. If T_f is less than the breakdown threshold for fish feed pellet (or faeces), then particles are treated as discrete and non-cohesive in behaviour. If T_f is greater than the breakdown threshold for fish feed pellet (or faeces), then particles are treated as part of a deposited bed, and hence cohesive in behaviour.



-
8. Bed slope (β) should be included in the resuspension module as it may enhance (if transport is down slope) or reduce (if transport is upslope) dispersion.
 9. The threshold of motion of a non-cohesive particle transport should be estimated based upon the balance of forces acting on the particle while sitting on the bed. This should take into account bed slope (β), the angle of repose (ϕ) of the particle and relative protrusion (P).
 10. The transport rate of the particle in motion should be based upon accepted and calibrated algorithms for large-diameter particles (in particular the method of Bagnold [1956, 1966] is recommended which accounts for movement of particles as surface creep or saltation (bedload).



2. Fundamental variables

2.1 Grain Density (ρ_s)

The grain density, denoted ρ_s , and commonly also termed the grain specific gravity, is the density of the sediment grains, or this context the organic (faecal) material or feed pellets. It has units of kg m^{-3} . Grain density is akin to temperature or salinity and appears as a master variable in many sediment transport models.

Grain density for both feed pellets and faecal material can be measured directly using a helium pycnometric technique (BSI, BS 1377 1990), and we would recommend for all future users of the revised model that it is measured as a matter of good practise. However, whilst this test can be relatively easily made on feed pellet material, we recognise that no faecal material (in particular) may be available prior to site development for this to be possible.

Feed Pellets

In the absence of any measured data on grain density for feed pellets, our recommendation is to use of a value of $1,127 \text{ kg m}^{-3}$ for feed pellets which was presented by Cromey et al., (2002a), p. 918, and is based upon direct settling velocity experiments on density-adjusted tracer particles hydraulically matched to have the same properties as faecal material. In the absence of any new code via which to input grain density data, then this parameter will be a default parameter within the revised model for the feed.

Faecal Material

Samples of seabed, organically-enriched sediments were collected during the second survey at 9 sites. None of this material has been measured for ρ_s within this study; we would recommend that samples (which have been frozen) from a number of sites (3 minimum) is analysed to provide field data to the revised model on this parameter. As a minimum this data would thus form a default parameter within the revised model. Partrac can advise on this issue.

**2.2 Water Temperature, Salinity, Density and Viscosity**

For all analytical and numerical models the water temperature ($T^{\circ}\text{C}$) and salinity (S) are master variables which are important in themselves but also affect other variables, such a fluid viscosity. Data values for these parameters should preferably arise through direct measurement using oceanographic CTD sensors, but we note this may have financial consequences for the industry (they may not possess the equipment).

Our recommendation is that the model is revised to include code to accept input of both variables and to include cross referencing code for revised quantities such as fluid density and viscosity. If data are not available then the following default values are recommended:

- Temperature 10°
- Salinity 35 psu

The density of seawater (ρ) can be calculated using the Thermodynamic Equations of State (TEOS-10) (see Fofonoff and Millard Jr., 1983). TOES-10 is based upon measures of salinity (S , units of psu), temperature (T , units of $^{\circ}\text{C}$) and pressure (p , in units of km). For present purposes (shallow water) pressure is very small as it increases by only about 4 kg m^{-3} per 1000 m depth increase and so may be ignored; so temperature and salinity dominate. Density increases with salinity and decreases with temperature. The following is a summary of the main factors and values needed to estimate density:

$$\rho = \rho(T, S, p) \quad 2.2.1$$

$$\rho = C(p) + \beta(p)S - \alpha(T, p)T - \gamma(T, p)(35 - S)T \quad 2.2.2$$

where

$$C = 999.83 + 5.053p - 0.048p^2 \quad 2.2.3$$

$$\beta = 0.808 - 0.0085p \quad 2.2.4$$

$$\alpha = 0.0708(1 + 0.351p + 0.068(1 - 0.0683p)T) \quad 2.2.5$$



$$\gamma = 0.003(1 - 0.059p - 0.012(1 - 0.064p)T)$$

2.2.6

The **viscosity** of seawater (μ) is largely independent of salinity but strongly dependent on temperature. The following equation is suitable for the computation of viscosity for liquids:

$$\ln\left(\frac{\mu}{\mu_0}\right) = a + b\left(\frac{T_0}{T}\right) + c\left(\frac{T_0}{T}\right)^2$$

2.2.7

Where $T_0 = 273.16\text{K}$, $\mu_0 = 0.001792 \text{ kg/ms}$, $a = -1.94$, $b = -4.80$, and $c = 6.74$.

Our recommendation is that the model computes fluid density and viscosity using the above equations.

2.3 Settling of Particles from the Fish Pen to the Seabed

The existing settling module advects particles in the vertical (and horizontal) based on the still water settling rates ($W_{s,o}$). Settling rates are preferably measured using sea or fresh water at room temperature in a sedimentation tower, and we recommend that this is undertaken for new model runs (*some consideration as to the metric used e.g. the mean value, modal value etc., is required in the model code*). Preferably this testing should be performed using site seawater, as to maintain equivalence of temperature and salinity / density. An example of the appropriate equipment used is given by Rigler et al., (1981), but far simpler arrangement can, and has, been used (e.g. Cromey et al., 2002).

If measured data are not available, then literature values can be used. An example of settling tests done on feed material in water of ocean salinity (S~35 psu; temperature unknown) by Cromey et al., (2002a) is given in Figure 23. Statistics are provided within the Figure caption, but any user is directed towards the source reference¹³. It stands to reason that historic data should not be used where the particle characteristics of their particular feed material (size, shape, density) differ substantially from those relating to the literature material values.

¹³ Preferably Cromey's data should (if used) be corrected for the site specific ocean water salinity and temperature; methods are available to do this however Cromey does not provide his values for S and T.

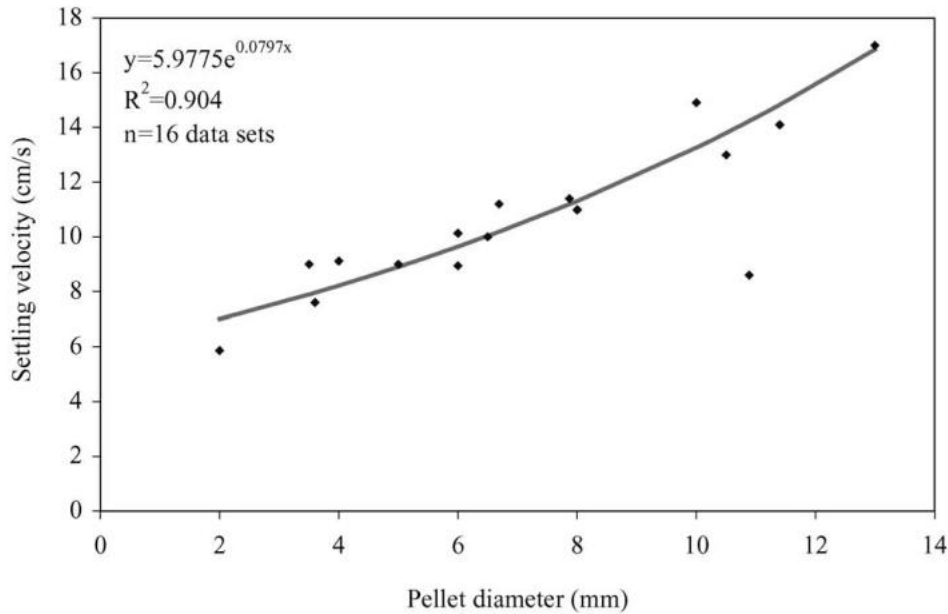


Figure 23 Relationship between pellet diameter and settling velocity with each point representing the mean of a data set. The mean and standard deviation of all 16 data sets is 10.8 and 2.7 cm s⁻¹, respectively. Source Cromey et al., (2002a).

Finally, in the absence of either new or literature / historic data then theoretical settling velocities can be computed given knowledge of the feed size (namely L_s short axis, L_m intermediate axis, and L_l long axis data), shape and density.

Pellet drag and hence settling through a water column of a particle of diameter (d_p) is strongly influenced by particle Reynolds number ($Re_p = \frac{w_s d_p}{\nu}$) and particle shape factor (SF), such that, for spherical particles:



$$\text{for } Re_p \leq 1, C_d = \frac{24}{Re_p}$$

2.3.1

$$\text{for } 1 > Re_p > 2300, C_d = \frac{24}{\sqrt{Re_p}}$$

2.3.2

$$\text{for } Re_p > 2300, C_d = 0.5$$

2.3.3

where:

$$\vartheta = \frac{\mu}{\rho}$$

2.3.4

$$SF = \frac{L_s}{\sqrt{L_l L_m}}$$

2.3.5

Where, L_s is the shortest axis, L_m is the intermediate axis, and L_l is the longest axis. The drag coefficient of settling particles of varying shape factors is shown in Figure 24.

Most particles settle in the turbulent range of Reynolds numbers and so Stokes Law is *not* appropriate. In this case, the Impact Law is to be used (based upon the same balance of forces as used to derive Stokes Law, but assuming a drag coefficient as defined in Figure 24).

$$W_s = \sqrt{\frac{2(\rho_s - \rho)gV}{C_d A \rho}}$$

2.3.6

Where V is the particle volume, ρ_s is particle density, and A is the area normal to settling direction. The appropriate drag coefficient (C_d) can be extracted from Figure 24. The settling rate so derived will be the still water settling rate, and it is this value which can be used.

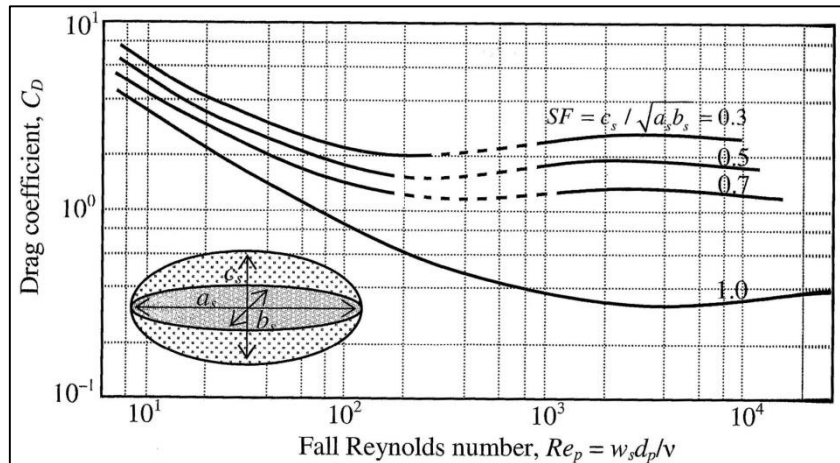


Figure 24 The relationship between drag coefficient of a particle and Reynolds number for particles of varying shape factors settling in still water (Mehta, 2014).

For the still-water settling velocity parameter our recommendation is for the revised model to include code to accept externally inputted data (either measured, from literature sources, or derived theoretically), but should also have a facility for a default value. We are not in a position to recommend the value for a default value.

2.3.1 Modification of Settling Velocity for Moving Flow Situations

When dealing with fish feed pellets or fish faeces, the volume concentration is low enough that free settling can be assumed (that is, no interaction of particles). The **true settling rate** of feed particles will be less than the still water value in proportion to the friction velocity of the flow (U_*). The best approximation of friction velocity at height z in the water column is to assume a constant stress layer to the surface and to equate the bed friction velocity ($U_{*,b}$) with $U_{*,z}$. The friction velocity is a function of the bed shear stress as follows:

$$\tau_b = C_{b,z} \rho \overline{U_z^2} \tag{2.3.7}$$

$$U_* = \sqrt{\frac{\tau}{\rho}} \tag{2.3.8}$$

A reasonable first approximation of the bed drag coefficient ($C_{b,z}$) is to use results from the Aquadopp instrument deployed in this project to define the near bed velocity gradient as follows:



$$\frac{U_z}{U_*} = \frac{1}{k} \ln \frac{z}{z_0}$$

2.3.9

Where z_0 is the roughness length (see Section 4.2), or the height above the bed that the mean velocity goes to zero. $C_{b,z}$ is defined as:

$$C_{b,z} = \left(\frac{U_*}{U_z}\right)^2$$

2.3.10

The true (flow adjusted) settling velocity $W_{s,t}$ to be used in a revised model is defined as a function of the Krone (1962) relationship:

$$W_{s,t} = W_{s,0} \left(1 - \left(\frac{U_*}{U_{*,dcrit}}\right)^2\right)$$

2.3.11

Where $U_{*,dcrit}$ is the threshold value for the onset of deposition. It is equated with the suspension threshold of Bagnold (1966, see Figure 25, Equation 2.3.12).

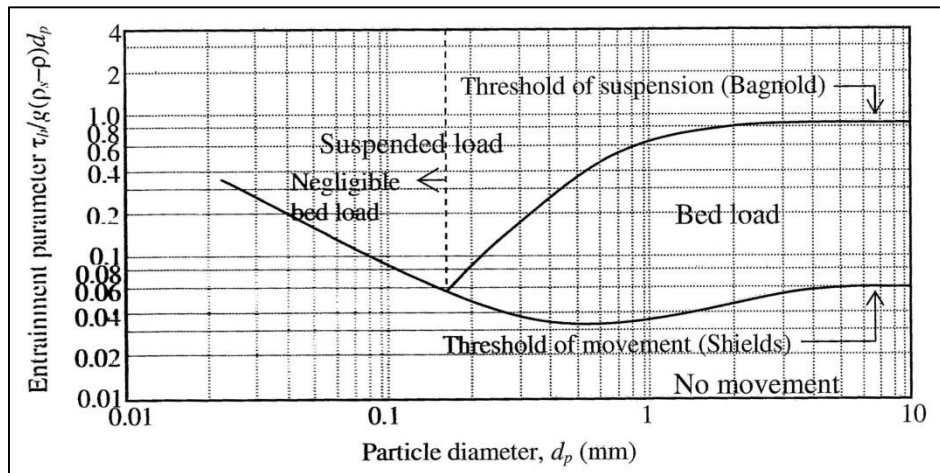


Figure 25 The threshold for suspension of particles sitting on the seabed (Bagnold, 1966).

The threshold for suspension is defined by Bagnold (1966) as:

$$\frac{\tau_b}{(\rho_s - \rho)gd_p} = \theta_s = \frac{0.64w_{s,0}^2}{\left(\frac{\rho_s}{\rho} - 1\right)gd_p} \quad 2.3.12$$

where

$$\tau_b = C_b \rho \bar{u}_z^2 \quad 2.3.13$$

C_b is the relevant bed drag coefficient, g is the acceleration due to gravity, d_p is mean grain diameter, ρ is the fluid density, ρ_s is the sediment grain density, and \bar{u}_z is the near-bed mean flow velocity (measured at the height relevant, z , to the estimated drag coefficient).

Our recommendation is for the revised model to use equations 2.3.11 to parameterise the influence of a moving flow on settling rates for feed material.



2.4 Settling Velocity of Resuspended Faeces/Pellets

The revised model needs to specify the hydraulic properties of eroded bed material in order that subsequent time-steps advect and treat the particles appropriately. Most commonly this is difficult to know. In this project, however, the use of the in situ mini-flume can provide some data into this area. Following each erosion run, the flume is stopped and unhindered, still-water sedimentation occurs. The deposition profile represents a mass deposition of sediments to the bed for which the following equation is valid:

$$\text{Mass deposition rate (kg m}^{-2}\text{s}^{-1}) = \text{settling velocity (ms}^{-1}) \times \text{concentration (kgm}^{-3}) \quad 2.4.1$$

Representative values of mean settling velocity can be abstracted from the time series by placing a tangent to the curve at appropriate point[s] (Figure 22). For many natural fine sediments, the settling curve reveals the presence of a number of fractions, each with differing mean settling velocities; in Figure 22, for example, three distinct fractions are evident. The mass deposition rate is given by the slope of the curve and the concentration used (in the right hand side) is that at the start of the selected period. Settling velocities are quoted in either m s^{-1} or equivalent mm s^{-1} .

Results from the foregoing analysis are presented in Table 24. A range of values are observed, with some degree of variability. The mean, standard deviation, minimum and maximum are, respectively, 5.4 mm s^{-1} , 2.9 mm s^{-1} , 12.7 mm s^{-1} and 5.4 mm s^{-1} (a more accurate maximum value is 8.5 mm s^{-1} as there is a single value only of 12.7 mm s^{-1}). These values are not dissimilar in magnitude to comparable data for estuarine flocs albeit at the upper end of observations, although it might be expected such an organically enriched sediment might have rather lower settling velocities. The higher values may reflect suspension of the native bottom sediment grains in addition, which as mineral particles would have higher settling velocities. That said, other experience on the resuspension – settling of organic rich flocs shows them to have higher settling velocities than expected due to a high floc porosity which allows the passage of water during the process of settling.

Our recommendation for the revised model is to use the lowest value reported (see Table 1) for each erosion test, or a mean/median value for the dataset as a whole.

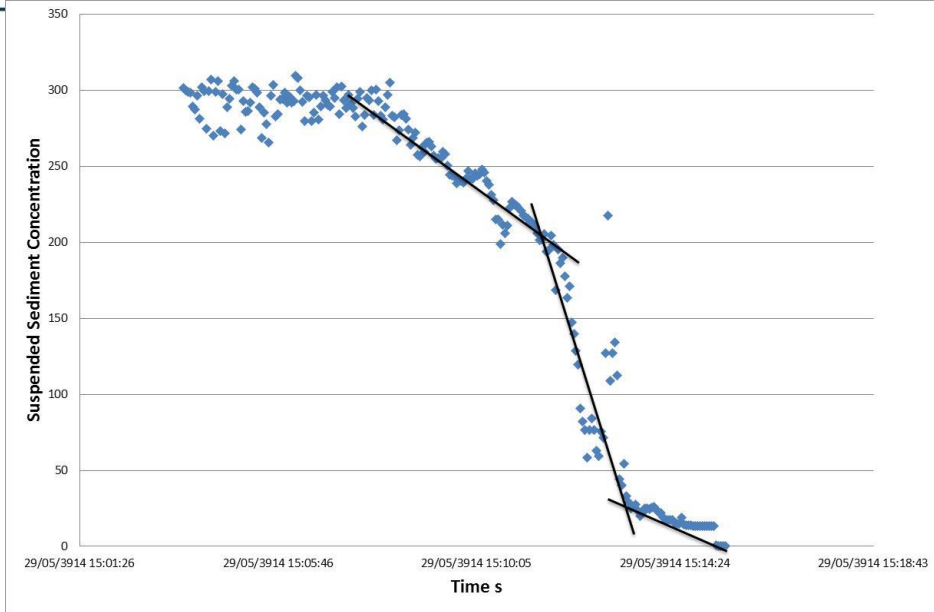


Figure 26 Example settling curve for site DF003; note the existence of three, discrete identifiable settling fractions within the sediment mass.

Table 25 Summary settling velocity data from deposition phase erosion runs.

Sample	Settling Velocity ω_s (mm s ⁻¹)	Sample	Settling Velocity ω_s (mm s ⁻¹)
DF0001		PNG001	
1	3.2	1	3.1
2	6.2	2	8.5
BDNC001		PNG002	
1	7.6	1	3.4
2	2.8	SB001	
DF002		1	12.7
1	6.3	2	5.2
2	7.0	SBC001B	
DF003		1	6.6
1	1.4	2	3.1
2	7.7	3	5.7
		4	1.6



3. Sediment transport regime

3.1 Cohesive or Non-Cohesive Bed?

The resuspension and redeposition of material on the seabed is modelled in DEPOMOD as if it were cohesive and semi-consolidated. That is, it requires an erosion threshold, erosion rate, deposition threshold and a deposition rate (Cromeey *et al.* 2002a and 2002b). The rates of deposition and erosion are classical formulae derived from fine-grained material that cannot be simulated as single particles but are considered from a perspective of mass per unit volume (i.e. a turbid cloud of fine particles where only the behaviour of the cloud is known). T.F. Sutherland (pers.comm. 2013) has indicated that pellets and fish faeces remain largely intact during settling and remain so for up to 4 days after immersion. The time-scale (T_p) for pellet/faeces breakdown can be determined by simple laboratory experimentation. The time scale (T_f) for erosion if dominated by tides is the semi-diurnal constituent that has a period of 12.4 hours. The peak currents that disperse settled pellets peak at mid-flood and mid-ebb, thus the appropriate time scale (T_f) of forcing is 6.2 hours. The ratio $\frac{T_p}{T_f}$ defines whether the particles form part of the bed or should be considered as individual particles moving over a bed. If $\frac{T_p}{T_f} < 1$ then a cohesive bed simulation such as that in DEPOMOD is appropriate as the particles are able to consolidate with the bed within the time period of forcing. However, if $\frac{T_p}{T_f} > 1$ then the forcing takes place on intact pellets, and the existing version of DEPOMOD is inappropriate for use. In the Canadian case (tide dominated, 4-day pellet disintegration time), $\frac{T_p}{T_f} = 16$ which suggests the latter statement is true. If the forcing is shorter than tidal periods (steady flows) then the greater is the likelihood that the fish pen waste needs to be treated as particles; if the forcing is storms, then the greater is the likelihood that fish pen waste needs to be treated as a cohesive bed.

Our recommendation is that the model acknowledges these timeframes in the computational code.



3.2 Critical Entrainment Stress of Impacted Faeces-Rich Sediments

Mini-flume (Voyager I) data were collected directly upon organic rich, faecally-impacted sediments at numerous sites. This was confirmed by the measurements of organic content of surficial sediments. The flume runs enabled direct measurement of the critical entrainment stress, and erosion through depth, of surficial sediments. The critical shear stress is operationally defined as the stress at which the concentration of sediment within the flume waters is $\geq 10 \text{ mg l}^{-1}$. Well defined critical entrainment conditions are identified in all successful time series.

Example results from DF002 (Dunstaffnage Bay 29/05/14) are presented in Figure 27. Table 17 summarises the critical stress values derived from the time series. These range $0.01 - 0.04 \text{ N m}^{-2}$, which is generally lower than values for the outlying sites. The mean \pm stdev is $0.02 \pm 0.01 \text{ N m}^{-2}$ across all sites, which is very close to the existing model $\tau_{0,crit.}$ value (0.018 N m^{-2}). Although the relationship is sensitive to the choice of bed roughness, these critical erosion stress values can be transformed into equivalent critical mean current velocities at **2 m** above the bed ($\bar{u}_{crit.}$) (the reference velocity height within the present model) using $u_{(z)} = u_* / \kappa (z/z_0)$ with a value for z_0 of 0.00162 m (i.e. a smooth boundary, see Section 4.2.1). This gives values for $\bar{u}_{crit.}$ at 2 m above bed ranging from $0.06 - 0.11 \text{ m s}^{-1}$ (mean velocity is 0.08 m s^{-1} , σ is 0.02 m s^{-1}). These data are very close to the present value within the model for $\bar{u}_{crit.}$ at 2 m, which is 0.095 m s^{-1} . The data collected within this project confirm and reaffirm Cromey et al.,'s (2002a) comment that critical erosion thresholds of recently deposited fishfarm sediments are much lower than thresholds typically used for modelling (minerogenic) suspended sediment in coastal models.

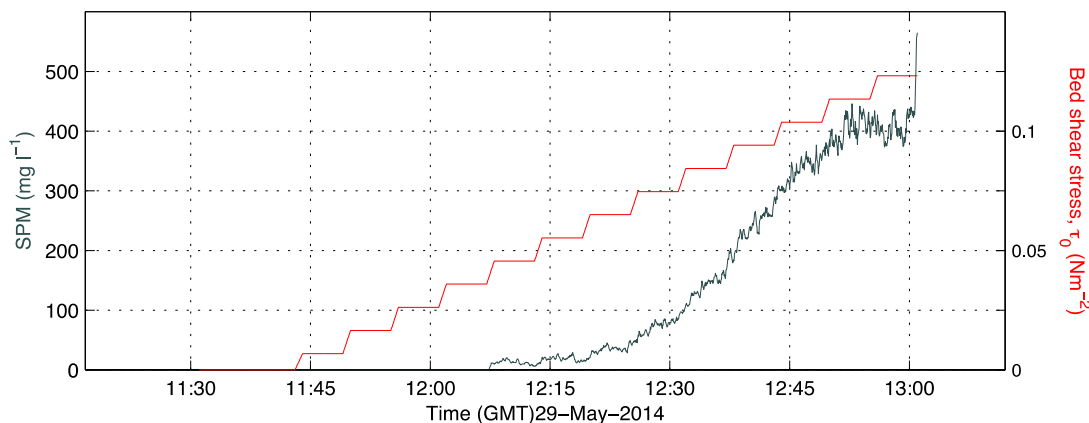




Table 26 Summary critical entrainment stress values (N m⁻²) using a specified, over-background minimum concentration of 10 mg l⁻¹. Runs in which leakage occurred were not corrected for this anomaly.

Site	Critical shear stress (N m ⁻²)
BDNC001	0.04
BDNC002	Leakage
BDNC003	Leakage
DF001	0.02
DF002	0.04
DF003	0.02
PNG001	0.01
PNG002	0.02
PNM001	Leakage
PNM002	0.02
SB001	0.01
SB002	Leakage
SC001	0.02
SC002	0.02
SCB001B	0.02

It is unlikely that future users of the revised model would use, or have access to, the mini-flume technology used here to measure the critical erosion stress. In any case, for an undeveloped site there would be no faecal material on the seabed.

Our recommendation is that the model uses the mean value of 0.02 N m⁻² for the value of the critical entrainment stress for faecally-impacted sediments.



3.2.1 Relationship with Dry Bulk Density Parameter (ρ_d)

A common drive amongst sediment transport researchers, especially for those involved in cohesive sediment research, is to correlate the critical entrainment stress parameter with more commonly measured bed compositional parameters, such as grain size, organic content and bulk density. Trevor Carpenter requested a correlation be undertaken between $\tau_{0,crit.}$ and the dry bulk density (ρ_d). Figure 28 shows this for the dataset for Survey 2 (nearfield); a single QC edit has removed sample BDNC001 as this gives $\rho_d = 400 \text{ kg m}^{-3}$, whereas 2 additional samples from the BDNC site both show 780 and 770 kg m^{-3} (possibly an analytical error), and all other sites have $700 < \rho_d < 820 \text{ kg m}^{-3}$. The data analysis indicates no significance, with $\tau_{0,crit.}$ ranging between 0.01 and $\sim 0.04 \text{ N m}^{-2}$ over the density range 750 – 820 kg m^{-3} . The sites visited displays a particularly narrow range of dry density, and it might be expected that a stronger trend would reveal itself (a positive co-variation) with a broader range of densities. Further, mono-parameter correlations such as this usually have limited predictive power, since the erosion resistance is a multi-parametric issue, in which no single variable accounts for the surface cohesive strength; this is particularly true for organically enriched sediments where highly cohesive/adhesive bacteria, which can bind sediments together, thrive.

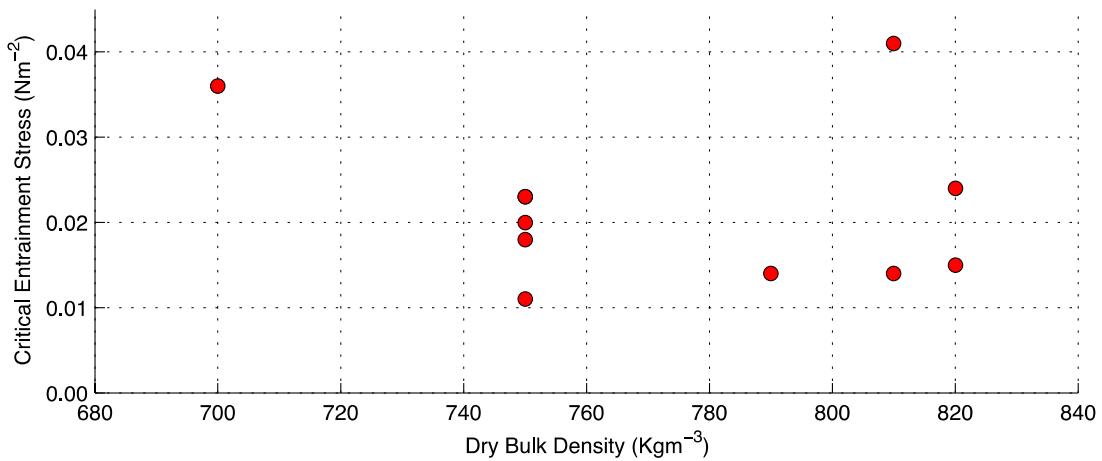


Figure 28 Covariance of the dry bulk density with critical entrainment stress. There is no significant trend in the relationship between these two parameters.



3.3 Comparison with Far-Field Sediment Critical Entrainment Stresses

Within the model there is a necessity to specify values for the critical entrainment stress $\tau_{0,crit}$ for outlying (i.e. semi-, or largely non-impacted sediments) in order that billions of particles are not entrained within the resuspension module unnecessarily. There is a limited, but useful, data set of measured $\tau_{0,crit}$ for 3 sites; at each of these sites flume measurements were collected at both the far-field and near-field, and this affords a comparison (Table 27). Generally it is found that far-field sediments, which are measurably less impacted by organics, are more resistant to erosion than the more organically enriched near-field sites by an order of magnitude. Mean critical stress value \pm stdev for the sites is $0.19\pm 0.10 \text{ N m}^{-2}$ (far-field) and $0.02\pm 0.009 \text{ N m}^{-2}$ (nearfield). As a guide, equivalent mean flow velocity at 2 m above the bed for $\tau_0=0.19 \text{ N m}^{-2}$ is approximately 24 cm s^{-1} .

Table 27 Nearfield (Survey 1) and farfield (Survey 2) values of surface critical erosion stress $\tau_{0,crit}$ at 3 sites.

	Farfield (Survey 1)	Nearfield (Survey 2)
Site	$\tau_{0,crit} \text{ (N m}^{-2}\text{)}$	
Shuna Castle Bay 1.1	0.15	0.02
Shuna Castle Bay 1.2	0.05	0.02
Shuna Castle Bay 2.2	0.30	0.02
BDNC 1.1	0.18	0.04
Port na Moine 2.2	0.25	0.02

Our recommendation is that the revised model uses wherever possible real data within its updated versions. As such, we recommend that the model uses the $\tau_{0,crit}$ data for the Survey 2 outlying sites collected here ($0.19\pm 0.10 \text{ N m}^{-2}$).

That assumes, however, the all future sites have outlying sediments of similar nature to those found in this project, which may not necessarily be the case. Nonetheless it will serve functionally to limit the amount of resuspension in the outlying regions



3.4 Resuspension Rates of Impacted (Cohesive) Bed Material & Erosion Through Eroded Depth

3.4.1 Erosion With Eroded Depth (Friction Coefficient)

The erosion threshold is the surface threshold ($\tau_{0,crit.}$) only, and does not express an increase in strength with eroded depth. The implication is that bed strength is constant with eroded depth, and, in reality, this is rarely the case due to processes such as consolidation and compaction. Although the erosion depths for the Survey 2 (nearfield) sites are relatively shallow (at most 1 mm), sequential Type I erosion is observed which indicates an increase in $\tau_{0,crit.}$ with eroded depth (denoted $\tau_{0,crit,z}$); the chief consequence of the down-core increase in $\tau_{0,crit,z}$ is that erosion, when it occurs, becomes at some point limiting as the flow induced bed stress τ_o approaches the datum where $\tau_o = \tau_{0,crit.}$. This increase with depth can be parameterised in one of two ways, via the friction angle (ϕ) which essentially represents the rate of change in bed strength ($\tau_{0,crit.}$) with depth, or in a functional form which is given by the best-fit of $\tau_{0,crit.}$ versus z datasets. Herein we present data on the friction coefficient only.

Friction Coefficient ϕ

The increase in bed strength with eroded depth is estimated through the internal friction coefficient (ϕ). A mean value of around 14° is reported for normally consolidated sediment (Amos et al., 2010). The critical erosion threshold with depth is thus defined as:

$$\tau_{crit,z} = \tau_{0crit.} + \sigma \tan(\phi)$$

3.4.1

Where σ is the effective stress (or overburden weight) to the depth (in the sediment mass) z in consideration:

$$\sigma = (\rho_s - \rho)gz$$

3.4.2

Summary values for the friction coefficient ϕ are presented in Table 28. Whilst some variability is observed, especially at DF002 where the gradient in the surface sediment layers is very steep



(but not unknown elsewhere e.g. Amos et al., 2010), mean friction coefficients for the surface and sub-surface zones are 26° and 20°, respectively, with an arithmetic mean of 23°.

For comparison Amos et al., (2010) report friction coefficients 40±29° for central Venice Lagoon fine sediments, and (as found here) generally larger values in the surface sediments. The difference between these two mean values is not considered significant and would consider that 23° is a value representative of deposited organic-rich faecal / feed deposits.

Our recommendation is that the model uses the mean value of 23° for the value of the friction coefficient ϕ for faecally-impacted sediments.

Table 28 Summary values for the friction coefficient ϕ in the surface layers (1) and sub-surface (2).

Site	Friction coefficient	Friction coefficient
	1 (°)	2 (°)
DF001	16	6
DF002	72	20
DF003	10	22
PNG001	10	**
PNG002	11	**
SC001	17	**
SB001	48	33

3.4.2 Resuspension Rates of Impacted (Cohesive) Bed Material

The bottom boundary layer module of the DEPOMOD model requires a relationship between bed erosion rate ϵ ($\text{kg m}^{-2} \text{s}^{-1}$) and ambient (or applied) bed stress, τ_0 , in order to resuspend bed material into the flow. The actual form of this relationship has been found by others to vary according to, amongst other things, geographic location, sediment stratification, density and sediment type (composition). Proposed forms for the relationship ((Thorn and Parsons, 1980; Ariathurai and Arulanadan, 1978; Mehta and Parthenaides, 1979; Kusuda *et al*, 1982; Lavelle and Mofjeld, 1987; Villaret and Paulic, 1986; Houwing, 1999) include:

1. A direct simplistic dependence on $\tau_{0,crit}$ either linearly or to some power;
2. A linear relationship between ϵ and $\tau_{0,crit}$;
3. A power law relationship between ϵ and $\tau_{0,crit}$;
4. A linear relationship between ϵ and the excess bed stress ($\tau_0 - \tau_{0,crit}$);



5. A power law relationship between ε and the excess bed stress ($\tau_0 - \tau_{0,crit}$);
6. A linear relationship between ε and the excess bed stress incorporating depth dependency ($\tau_0 - \tau_{0,crit,z}$); and
7. A power law relationship between ε and the excess bed stress incorporating depth dependency ($\tau_0 - \tau_{0,crit,z}$).

The present representation of the $\varepsilon - \tau_0$ relationship within the AUTODEPOMOD model is via [4] above.

The mini-flume erosion data collected during Survey 2 has been processed to examine which of the foregoing parameterisations provides the minimum variance in the data sets. The data have been plotted up in various ways (See Appendix I). A similar process was undertaken by Amos et al., (2010) for sediment erosion studies using a benthic flume in Venice Lagoon, Italy. He found the best solution was represented by [7] above, and reported differences in the coefficient between summer and winter.



Appendix I presents the data plotted up in a number of ways (linear/non-linear), which include erosion rate ϵ versus:

- Bed stress, τ_0
- Excess bed stress, $(\tau_0 - \tau_{0,crit.})$
- Excess bed stress with depth dependency $(\tau_0 - \tau_{0,crit,z})$.

A simple assessment of the magnitude of the correlation via the r^2 statistic is used to judge which of the relationships is preferred in the revised model (this mimics the approach used by Amos et al., 2010, for Venice Lagoon). The lowest observed value for r^2 is 0.29 ($\log \epsilon$ vs τ_0); The largest r^2 value (0.68) is given by equation 3.4.3 below and the data are reproduced in Figure 29. This reflects a linear dependence of ϵ on the excess bed stress:

$$\epsilon \text{ (kg m}^{-2} \text{ s}^{-1}\text{)} = 0.031(\tau_0 - \tau_{0,crit.}) \quad r^2=0.68 \quad 3.4.3$$

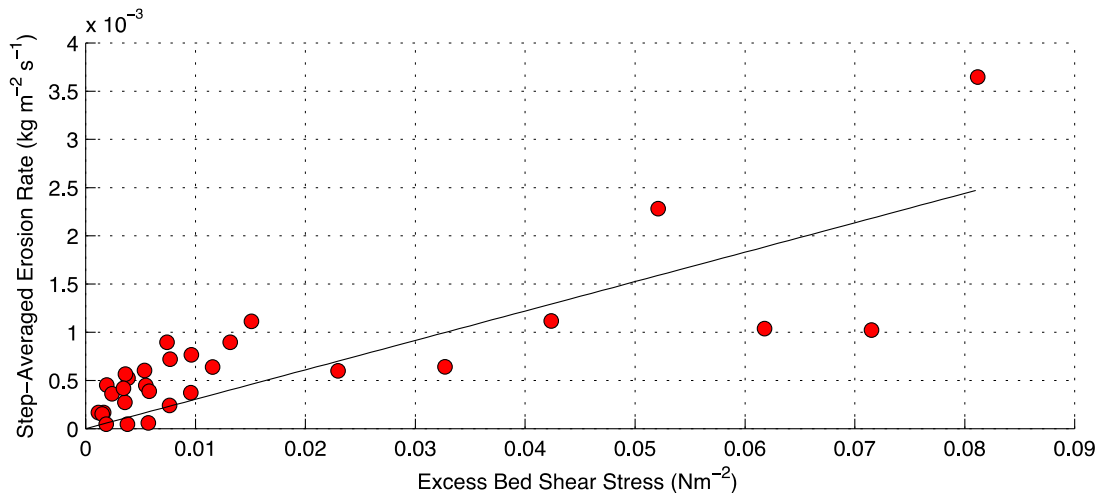


Figure 29 Excess bed stress ($\tau_0 - \tau_{0,crit.}$) versus erosion rate ϵ averaged over each velocity/stress time-step on a linear plot.

Mehta (2014) commented upon the number of different formulations that have been published relating steady or quasi steady flow magnitude to surface erosion flux, and Amos et al., (2010) show that scatter in the data is a pre-eminent characteristic of these types of erosion experiments, and that commonly r^2 values for various formulations do not exceed 0.5. A depth dependent excess stress formulation could also be selected here ($r^2=0.45$), however the spread of data points (due to the manner in which the miniflume steps us the velocity increments; see



Appendix I), is a discounting factor. Simple dependence on bed stress τ_0 , rather than excess bed stress, gives lower r^2 values centred on 0.3.

Equation 3.4.3 has been found by various previous workers to adequately parameterise benthic flux for fine-grained, cohesive sediments; Delo (1988) found the coefficient $[m_e] = 0.002$ although his erosion rate is in g rather than kg. Ariathurai and Arulanandan (1978), Kandiah (1974) and Lee et al., (2004) all report a similar linear dependence of erosion flux on excess bed stress, as do Mitchener et al., (1996), who quote the coefficient m_e as between $2 - 6 \times 10^{-4}$ ($\text{kg m}^{-2} \text{s}^{-1}$). Finally, Owen (1975) report linearity and give $m_e = 2.63 \times 10^{-3}$. However, it is worth stating the equation relating to the second highest r^2 value:

$$\varepsilon (\text{kg m}^{-2} \text{s}^{-1}) = 0.009(\tau_0 - \tau_{0,crit.})^{0.36} \quad r^2=0.52 \quad 3.4.4$$

Again, various other workers have found this parameterisation (e.g. Amos et al., 2010, found $m_e = 0.006$ and $n=1.23$ with a reported r^2 value of 0.4). It may be that during the model testing / validation phase, then the above equation may be a better parameterisation of benthic flux than equation 3.4.3, but this cannot be known at this stage.

It should be noted that erosion (and hence also the coefficients in the foregoing equations) is frequently found to be temporally variable, with time-variation attributable to processes such as temperature-linked seasonal changes, seasonal wave action, biological activity, and consolidation and compaction processes (Black et al., 2002). Inclusion of a new benthic flux representation within the model based upon studies at real, faecally impacted sites will hopefully improve parameterisation but it goes no further relative to the current model in providing the model with a time-varying facility.

Our recommendation is that the model uses Equation 3.4.3 to parameterise benthic flux at the seabed for faecally impacted seabed areas. The formulation requires input (or a default value) for the critical entrainment stress, $\tau_{0,crit.}$



3.5 Onset of Motion of Intact Pellets on the Seabed

3.5.1 Theoretical Approach

Bagnold (1956) has shown that bed slope β and friction angle φ are important parameters that influence the onset of motion of grains sitting on the seabed under a moving fluid. Friction angle (or the angle of repose of granular material) has been studied in the marine sediment transport context, under the concept of the pivotal angle by Li and Komar (1986) and Komar and Li (1988). It is a function of the diameters of the entrainment particle (pellet or faeces, d) size relative to the supporting bed grain diameter (or roughness, Ks) as well as to the degree of exposure of the entrainment particle to the moving flow (Figure 30). The balance of forces at threshold of a particle sitting on a rough bed is defined to first order as:

Fd + Fl = W(tan(φ) - tan(β))

3.5.1

where Fd is the fluid drag force and Fl is the lift force applied to the pellet, W is the immersed weight of the pellet, φ is the pivotal (friction) angle (also called the angle of repose), and β is the bed slope. This equation directly allows for inclusion of local bed slope effects on grain mobility.

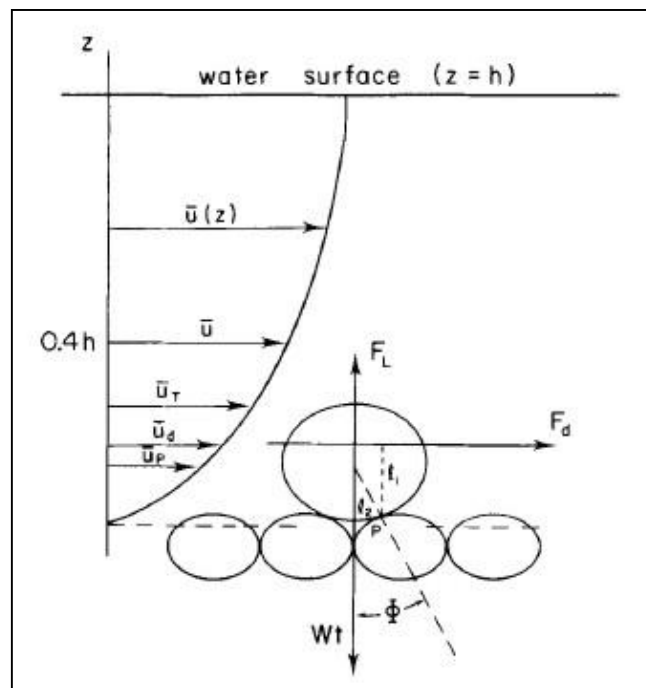


Figure 30 The threshold for suspension of particles sitting on the seabed (Bagnold, 1966).



$$F_d = A \cdot C_{d,z} \rho U_z^2 = A \rho U_*^2$$

3.5.2

where $A (= \frac{\pi}{4} d^2)$ is the exposed area of the (spherical) particle, and $C_{d,z}$ is the appropriate drag coefficient for a flow (U_z) at height z (note that this coefficient will vary depending on the height of the input steady flow measurement, and is assumed to be within the logarithmic part of the benthic boundary layer).

$$F_l = \frac{C_{d,z}}{b} A \cdot \rho U_z^2$$

3.5.3

where b is a coefficient that varies between -5 and 2 (depending on the flow Reynolds number (James, 1990). Bagnold (1956) undertook experiments on the ratio of lift (dispersive, P) to drag (tangential, T) stresses and found that for fully turbulent rough flows.

$$\frac{T}{P} = \tan(\phi)$$

3.5.4

Where ϕ is the pivot angle (see Figure 30), which essentially is the angle between the direction of easiest movement and the vertical. The Shields function (Figure 31) expresses the critical entrainment condition as a function of the drag and lift forces (Equations 3.5.2 and 3.5.3) on a particle sitting on a flat bed of similar particles, with a constant friction (pivot) angle (about 30°) and no bed slope.

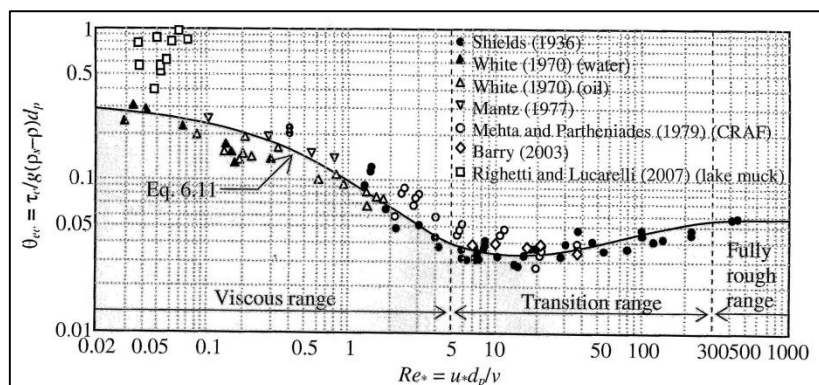




Figure 31 The threshold Shields parameter for the onset of motion of particles sitting on the flat seabed of similar particles (adapted from Mantz, 1977). Note that the Shields parameter encompasses both the lift and drag forces on the bed material.

Soulsby and Whitehouse (1997) offer the following algebraic equation for the curve in Figure 31:

$$\theta_{cr} = \frac{0.30}{1+1.2D_*} + 0.055[1 - \exp[-0.020D_*]]$$

3.5.5

Where

$$D_* = \frac{g(s-1)/\nu^2}{\rho} d$$

3.5.6

And ν is the kinematic viscosity and $s = \rho_s/\rho$.

For natural seabed environments the Shields function is an oversimplification of the real world and some accounting is required for a) the effects of relative protrusion of pellets on a bed of pellets and B) accumulation of pellets in shallow seabed depressions ('divots').

Relative Protrusion

The pivotal angle (ϕ) is a function of the nominal diameter (d_n) of the moving particle to the diameter of the substrate grains (K) on which the particle sits and takes the form:

$$\phi = n \frac{d_n}{K}^{-0.75}$$

3.5.7

where n varies between 20 (grain-top rotation) and 35 (saddle rotation). The exponent -0.75 is valid for spheres, but also varies with particle shape and is -0.36 for ellipses.

James (1990) investigated the effects of relative protrusion on grain mobility. Figure 32 shows the variation in the Shield's parameter (expressed in this instance as u_*^2 rather than τ_0 ; see



Equation 2.3.8 for the inter-conversion) against relative protrusion P/d . P/d can be equated with $\tan(\phi)$, where ϕ is the friction (pivot) angle. Thus, for a given pellet nominal diameter d , P can be derived by assuming (or specifying) ϕ .

$$P = d \tan \phi$$

3.5.8

Measurement of ϕ for feed pellets recommended for use in the revised model (see Section 3.5.3) give $\phi = 33^\circ$. Using this value in conjunction with Figure 10 enables the critical entrainment stress to be calculated¹⁴. Figure 32 (from James, *op cit.*) shows that if the protrusion is 0.8 or larger, then the particle will move under essentially all flows, and when P/d approaches zero for all intents the pellets will no longer move. The nominal protrusion (i.e. for Shields' case of a level, flat bed of similar size sediment where the Shields function θ 0.05) is 0.2. As an example, for a friction (pivotal) angle of 30° and $P/d = 0.58$, which yields a threshold (Shields) parameter of 0.03.

Divot Effects (Sheltering)

Figure 30 shows a relatively larger particle resting on a bed of particles ~half the diameter. On a relative level this particle would be easily moved by the nearbed flow; an inverse to this is the situation where the top particle is much smaller than the underlying grain, or where a particle of a given size is in a seabed depression whose depth exceeds that of the grain diameter by as a minimum $2 - 3d$. The approach to mobility assessment is the same for the relative protrusion influence above, providing some estimate is available of the divot depth (e.g. from diver observations). However, in this case P/d needs to be redefined, and D may be thought of as a bed roughness length scale rather than grain diameter.

One practical approach is to define the bed in a look-up table for divers (or from bottom photographs, or, for example, using sediment profile imagery camera systems¹⁵) such that one can classify beds into types which reflect values of P/d . For example, a planar level bed might be given a value of 0.2 whereas a bedrock roughened bed, or where divots are on the scale of cm, would be a maximum of 1. A bed roughness scale, and perhaps a Guidance Note containing

¹⁴ Our understanding is that Trevor Carpenter is to digitise the curve in Figure 10 to achieve this.

¹⁵ See www.remots.com, for information on this technique. Useful on *soft sediment beds only*, not rock.



representative photographs for model Users, could be setup as gradations from smooth to divots from 1 – 10.

A second approach would be to conduct mini-flume experiments on beds of controlled micro topography (in fact, some experiments of this nature were discussed early in the project timeframe). The approach would be to configure a series of artificial beds with differing scales of microtopography (e.g. mm to cm). A bed of pellets, perhaps of two differing sizes (e.g. 5mm and 12 mm) would then be spread over the topographies. Simple visual observations in conjunction with flow velocity data would indicate limiting length scales for semi- or permanent entrapment of pellet; this information could be translated into the model coding. These studies are comparatively simple to setup and run.

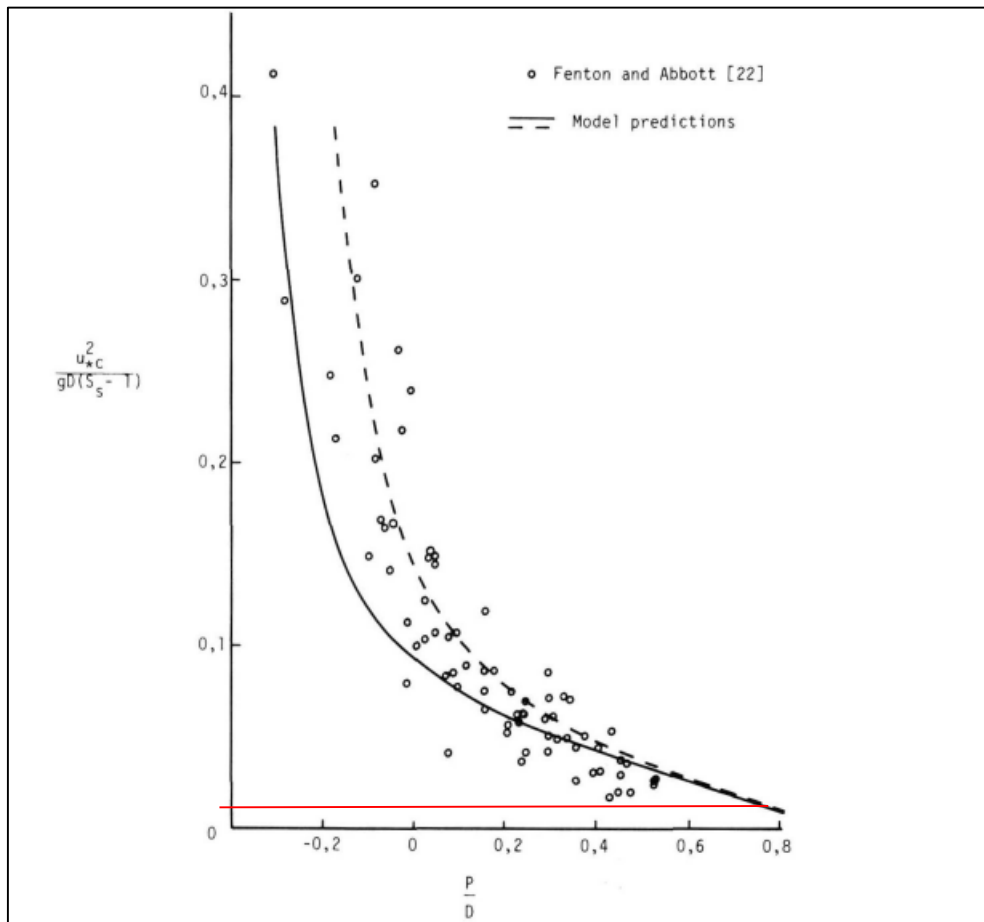


Figure 32 The change in critical Shields parameter with change in relative protrusion (P/d) (after James, 1990). The red line shows the normally-accepted value (0.05) for granular material under turbulent rough flows.

Pellet Velocity Once in Motion



If the flow exceeds the threshold condition, Bagnold (1966) has shown that the velocity of a particle moving as bedload (U_g) is approximately 10% of the near-bed flow. As the approximate relationship $\frac{U_g}{U_*} \approx 0.1$, then we can say that above the traction threshold $U_g \sim U_*$. Thus the distance (L) travelled by a particle is defined as:

$$L = \int_{t, \text{bedload}} \Delta t U_*$$

3.5.9

The direction of pellet motion is in the direction of the steady flow.

3.5.2 Project Data on Pellet Mobility

Within this project a series of laboratory mini-flume studies were undertaken to directly measure the onset of motion of real feed pellets of two sizes: 5 mm and 12 mm nominal diameter. Two different motion criteria were explored and two pellet configurations used; the fluid stress was measured at:

- i. the true initiation of motion of 1 or more pellets as determined visually, and
- ii. the moment defined visually as 'weak general transport' (WGT), in which there is a weak, general movement of all pellets in the downstream direction

The two pellet configurations were as follows:

- i. where a free, monolayer of pellets was arranged spanning the mid-channel axis, and
- ii. where a layer of pellets were glued into a recession in the flume floor as to generate no roughness step, and a free, monolayer of pellets emplaced on top of this layer.

Table 29 summarises the data collected from the pellet mobility studies. These data indicate that a monolayer of otherwise freely mobile pellets on the smooth mini-flume base are more easily eroded (less stable) than the same pellets atop a bed of pellets. This is not surprising given the foregoing theoretical points about particles and their relation to the sheltering due to the natural asperity of the bed. The observation of higher fluid stress required to generate



'weak, general transport' is self-evident, but it is interesting to note that the stress is the same (within experimental error) for 12 mm diameter pellets regardless of the pellet arrangement. Overall, very low flow velocities are required to bring the pellets of either size into motion. For example, the flow velocity at 2 m required to initiate motion of 5 mm diameter pellets on a bed of pellets is $2 - 4 \text{ cm s}^{-1}$, according to the boundary roughness. It should be noted that these experiments are controlled and use only pellets; in the sea the pellets will be admixed with other material including native sediments, microbes, faecal material etc., and the miniflume studies on the natural seabed (Section 3.2) provide more pertinent information of the seabed mobility than here.

Table 29 Summary of pellet mobility studies.

Pellet Diameter (mm)	Configuration	Critical shear stress (N m ⁻²)	Shear stress for 'weak, general movement' (N m ⁻²)
5	Pellets on smooth bed	0.004	0.008
5	Pellets on bed of glued pellets	Approx. 0.006	Approx. 0.008
12	Pellets on smooth bed	Approx. 0.008	Approx. 0.017
12	Pellets on bed of glued pellets	Approx. 0.012	Approx. 0.017

3.5.3 Direct Measurements of ϕ

The friction angle (ϕ) was measured directly in air for pellets of 5 mm and 12 mm, using the tilting plate method of Li and Komar (1986). This was achieved by gluing a monolayer of pellets onto a small board (0.3 x 0.3 m) on top of which a mobile monolayer (non-glued) of pellets was arranged. The board was then gradually tilted to the point of avalanche; this is the friction angle. At this point the adjacent (a) and opposite (o) sides of the triangle so created was measured, from which ϕ can be computed as:

$$\phi = \tan^{-1}(o/a) \quad 3.5.10$$

For 5 mm pellets ϕ is 33°, and for 12 mm diameter pellets ϕ is 33°.



Equation 3.5.5 can be used to determine the critical entrainment stress for a pellet on a planar bed.

Equation 3.5.1, in conjunction with the Shields function, can be used to parameterise bed slope effects on pellet mobility within the revised model.

Equation 3.5.7 can be used to parameterise pellet transport rate once pellets are in motion.

We recommend that a value of $\phi=33^\circ$ is taken for pellets within the revised model regardless of size.

Equation 3.5.6, using $\phi=33^\circ$, can be used to parameterise protrusion effects and the consequent changes to pellet mobility.

The ratio P/d can be redefined in terms of the depth of microtopography ('divots') to assess divot effects on pellet mobility. This will work if data is available on the distribution of divot depths at a site; we recommend that a method be developed to guide new model users based upon diver observations/marine photography, or that specific miniflume studies are conducted to development limiting pellet entrapment criteria.



4. Flow (hydraulic) regime

4.1 Specification of Hydraulic Regime

The seabed boundary can be classified in terms of whether it was hydraulically smooth, transitional or rough, and the model needs to know which regime it is within in order to function correctly in terms of the parameterisation of nearbed processes. These classifications seek to infer whether the topography of the seabed will influence negligibly or substantially the flow over it. A rough bed, which physically would correspond to a ‘bumpy’ bed, protrudes into the flow disrupting it and effecting the frictional drag (stress) and the velocity profile (as well as sediment transport and deposition); on the other hand, a smooth bed offers no protrusions to the flow, and the interface sediments are notionally embedded within a stable and very thin flow sub-layer. Typically, muds and fine silts are found under hydrodynamically smooth flows whereas coarse sands and gravels are found under hydrodynamically rough flows.

Two different versions of the Reynolds number are used to perform this classification: a ‘grain’ Reynolds number = $u_* k_s / \nu$ where k_s was taken as equal to $1.1d_{90}$ (after Soulsby, 2007, d_{90} is the 90th percentile grain diameter and values from size analysis of bottom sediments were used; see Section 5.1), and ν is the kinematic viscosity @10°C = $1.212 \times 10^{-6} \text{ m}^2 \text{ s}^{-1}$; and a ‘flow’ Reynolds number ($\bar{u}_{mid,z} z / \nu$ where z is a mid-depth datum). u_* values from both the TKE and LP methods were used within these formulae to provide some redundancy. The following classifications are given:

- vi. $u_* k_s / \nu > 70$ rough turbulent
- vii. $u_* k_s / \nu < 5$ smooth turbulent
- viii. $5 < u_* k_s / \nu < 70$ transitional
- ix. $\bar{u}_{mid,z} z / \nu > 500,000$ rough turbulent
- x. $\bar{u}_{mid,z} z / \nu < 500$ smooth turbulent

Table 20 shows calculations based upon data collected using the grain and flow Reynolds numbers. Two different shear velocity values are used in the calculation of the grain Reynolds number. Data relating to the flow Reynolds number show the maximum and minimum values related to the maximum and minimum flow velocities across the entire rig deployment period



plus the value from the 10 minute data record. The two right-hand columns show the grain Reynolds number computed using $d_{50} = 10$ mm, which is indicative of a highly pelleted bed.

The data show that, regardless of the specific Reynolds number formulation used, the boundary is classified as largely turbulent smooth, with only two sites as transitional-rough (according to which metric is used). It is only when the grain Reynolds number is computed assuming a much coarser bed (in this case, a notional pelleted bed with $d_{50} = 10$ mm) that the boundary flow classification changes (universally) to one of rough. These observations have implications on the parameterisation of the seabed boundary zone in the DEPOMOD model, and influence how the roughness length (z_o) is calculated.

Several different approaches within the model are possible. The simplest would be to use (iv) and (v) to define the flow regime; these can be calculated in the model if it is provided with a velocity profile e.g. from an ADCP (currently the norm for the model and industry). The value used for u_{mid} should be the maximum (peak) Spring tide velocity. Alternatively the grain Reynolds number could be implemented within the model; if this were done then u_* and k_s need to be provided or known to the model. k_s is traditionally computed from grain size data, and thus in order to run the model samples of the local seabed would need to be analysed for grain size distribution. We recommend k_s is taken as equal to $1.1d_{90}$ (after Soulsby, 2007, d_{90} is the 90th percentile grain diameter). Industry would need to be informed of the requirement to collect bottom sediment samples to run the model.

u_* is usually computed from velocity profile data, and this is problematic from e.g. ADCP data as velocity profile data in the nearbed region is not collected due to nearfield acoustic blanking. In this study, u_* was derived using a different method which involved measuring velocity ~ 5 cm above the bed and using the TKE methodology to derive u_* . This approach is preferred and involves no assumptions. Should the grain Reynolds number be used to define the hydraulic regime within the revised model, then industry would need to change the way in which site velocity data is collected (i.e. they would need to measure u_* using the velocity profile or TKE methods). This may be important in terms of the practical implementation of the model.



Table 30 Summary of boundary classification calculations. The table shows calculations using the grain (u_*k_s/v) and flow ($\bar{u}_{mid,z}z/v$) Reynolds numbers. Two different shear velocity values are used in the calculation of the grain Reynolds number. Data relating to the flow Reynolds number show the maximum and minimum values related to the maximum and minimum flow velocities across the entire rig deployment period plus the value from the 10 minute data record. The two right-hand columns show the grain Reynolds number computed using $d_{50} = 10$ mm, which is indicative of a pelleted bed.

Site	Re = u_*k_s/v [$k_s=1.1d_{90}$]		$\bar{u}_{mid,z}z/v$			Boundary Classif ⁿ	Re = u_*k_s/v [$k_s=2.5d_{50}$ $d_{50}=10$ mm]	
	Using u^* from TKE	Using U^* from LoW	Min	Max	Within 10 min Data Record		TKE	LoW
Bloody Bay 1	0.8	0.6	67183	96691	76936	smooth	73	60
Bloody Bay 2	5	4	4885	81368	58063	smooth	109	75
Fiunary 1	3	2	38246	250981	191567	smooth	225	132
Fiunary 2	86	18	96222	367595	331996	trans-rough	661	137
Shuna Castle Bay 1	5	8	1768	171692	95923	smooth	91	141
Shuna Castle Bay 2	3	5	52203	119646	73169	smooth	61	99
BDNC 1	0.6	1	3977	25168	14557	smooth	60	103
BDNC 2	6	4	7608	94362	62640	smooth	113	68
Ardfuir 1	3	2	14748	127261	86243	smooth	110	75
Ardfuir 2	No data		8327	256065	256065	smooth	273	127
Ardfuir 3			2477	278213	20989	smooth	71	85
Port Na Moine 1	69	64	16069	98862	19196	trans-rough	83	77
Port Na Moine 2	21	10	74562	131005	114210	smooth	161	75
Durmyon Bay 1	4	2	58776	180787	180787	smooth	269	153
Durmyon Bay 2	0.6	No data	67131	98545	79892	smooth	212	

Our recommendation is to use the flow Reynold’s number ($\bar{u}_z z/v$) to test for the type of hydraulic regime within the revised model, where \bar{u}_z is the peak Spring tide current velocity at mid-depth. This is possibly the simplest approach and which can be achieved using an ADCP, and it does not require information on other parameters, nor place any onerous additional data collection obligations on Users.

4.2 Benthic Boundary Layer Parameterisation and Bed Roughness

Once the model has established the hydraulic regime for the site, it can then parameterise the gradient in velocity vertically from the bed into the nearbed flow. It is though this parameterisation that the bed stress, which drives sediment resuspension, is computed, and the name often given to the graphical presentation of nearbed velocity data is the ‘*Clouser plot*’ (Figure 33) (Topea al., 2007). The advantage of the method is that it does not require



measurements in the viscous sub-layer, which is the lowermost layer of water closest to the sediment surface. The plot provides a pragmatic approach to discriminating between turbulent smooth and turbulent rough cases. The approach uses the following notation:

1. u^+ (given by $\frac{u_z}{u_*}$) (dimensionless current speed)
2. y^+ (given by $\frac{yu_*}{\nu}$) (dimensionless height above the seabed)

Where u_z is the time averaged velocity at height z above the bed, u_* is the friction (or shear) velocity, y is height above the bed and ν is the kinematic viscosity. For smooth boundaries u^+ is related *linearly* to y^+ whereas for rough boundaries u^+ is related to the *logarithm* of y^+ i.e. $u^+ = m(y^+) + b$ in the smooth case, and $u^+ = m.\log(y^+) + b$ in the rough case

Nearbed (time-averaged) velocity data collected across all sites visited during the first survey using the Partrac velocity rig is plotted up in Figure 33. An iterative process was used to develop analogous (Clauser) wall laws from this data for smooth, transitional and rough boundaries. These are:

i. Smooth $\frac{u_z}{u_*} = 0.65\left(\frac{z}{5z_0}\right)$ 4.2.1

ii. Transitional $\frac{u_z}{u_*} = 8.18\log\left(\frac{z}{5z_0}\right)$ 4.2.2

iii. Rough $\frac{u_z}{u_*} = 5.6\log\left(\frac{z}{5z_0}\right)$
4.2.3

Figure 33 shows a good fit of the field data to the Clauser format, which provides some confidence that the data are of good quality. The following expression should be used to provide an estimate of bed stress, τ_0 , from u_* values:

$$\tau_0 = \rho u_*^2$$

4.2.4

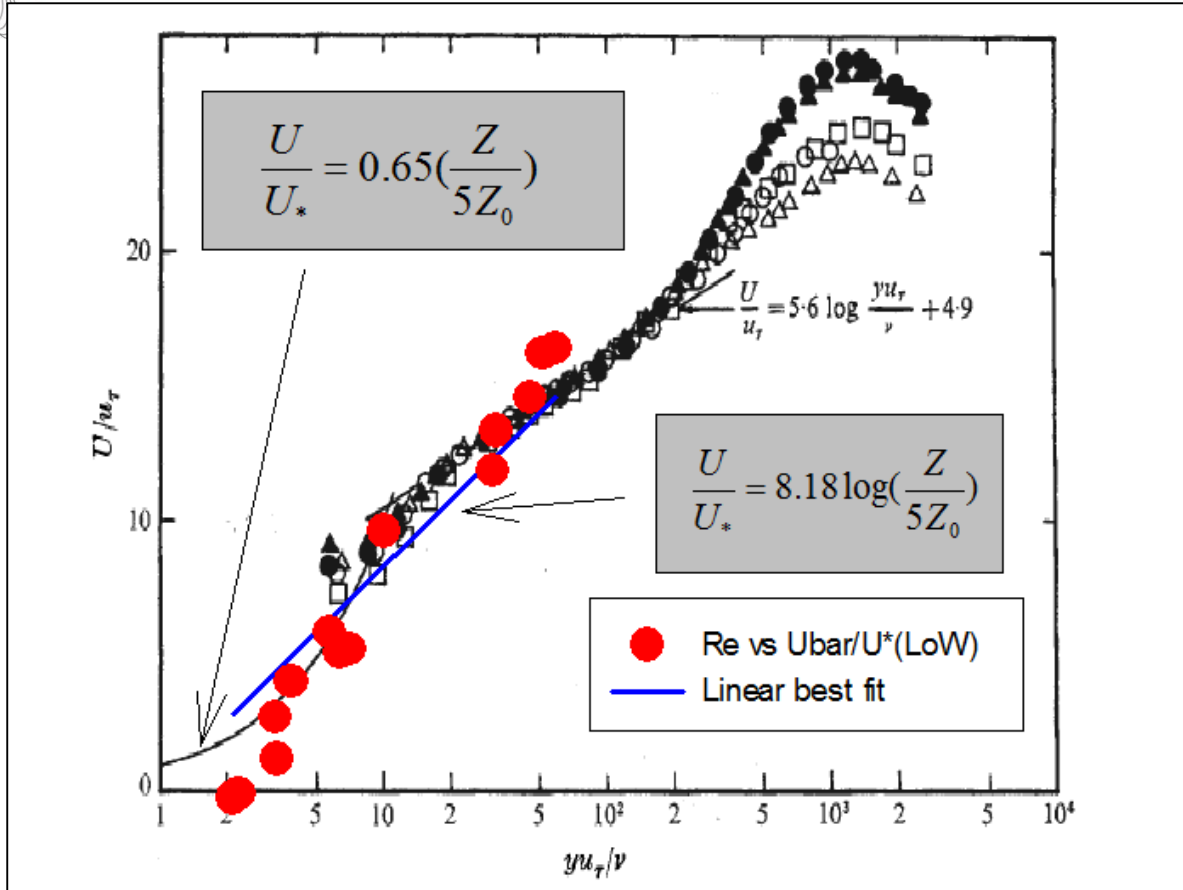


Figure 33 Field (time-averaged) velocity data plotted up on a Clauser plot. Note u_τ in the axes labels is the friction velocity u_* .

Our recommendation is that once the revised model has determined the relevant flow regime (smooth, transitional or rough) then the wall region is parameterised, appropriately, through use of Equations 4.2.1, 4.2.2 and 4.2.3.

4.2.1 Bed Roughness Parameterisation

In order to derive τ_0 a value for z_0 is required; at present the DEPOMOD model assumes a default value for z_0 of 2×10^{-4} m. This has been used in the present model on the assumption that the flow boundary is hydraulically smooth and the site is nominally and largely muddy (i.e. fine-grained). In this project values for z_0 were derived from field measurements using two different methods, the Law of the Wall and the TKE methods. Using the Law of the Wall method z_0 can be directly estimated from recorded velocity profiles. The velocities and corresponding elevations measured from a water column are plotted on a logarithmic graph, and roughness height and shear velocity u_* are obtained from curve fitting. The TKE method provides a better estimate of bed stress (Kim et al., 1999) but only indirectly computes z_0 according to whether the boundary is judged to be rough, transitional or smooth



Table 21 summarises the results from these measurements. These data need some filtering prior to use, and values within the Law of the Wall method with r^2 values <0.8 are disregarded on the basis of the sensitivity of the method to the strength of the regression (e.g. Kim et al., 2000). The range in z_0 found here is from 0.0007 m (0.7 mm) in Durmyon Bay to 0.044 m (44 mm) in Shuna Castle Bay 1, and there is a trend wherein Wall Law-derived values are generally higher than those derived from the TKE methodology. The TKE methodology is generally considered to be a better predictor of bed stress (e.g. Thompson et al., 2003; Dyer et al., 2004; Kim et al., 2000), which gives greater credence to the z_0 values derived using this approach. Further, the model is mimicking a situation of accumulation of organically enriched fish faeces/pellets onto a virgin seabed, and intuitively this is expected to give rise to smaller than larger z_0 values since the faecal material is fine-grained (see e.g. Pope et al, 2006). The present model selects (uses) a value for z_0 on the basis that the seabed beneath pens is expected to be a ‘muddy bottom’ (Cromeey et al., 2002a).

Excluding those sites found to be transitional – rough in nature (i.e. for smooth sites only), the mean z_0 value from the TKE method is $3/100$ mm ($=3 \times 10^{-5}$ m). This is a single order of magnitude smaller than that currently used within the model as a default (2×10^{-4} m). z_0 for the two sites found to be transitional – rough is 54 mm ($=5.4 \times 10^{-2}$ m). Figure 34 shows photographs of surface sediments for these two sites, which reveal quite heterogeneous, shelly, topographically roughened sediments.

We would advance these values as default values in the revised model for smooth and rough flow regimes, although some caution is advocated for the rough value since there were only 2 sites found in this hydraulic regime. However, insofar as the project is designed to provide improvements to the model and z_0 is invariably a site specific parameter, we would strongly recommend that site specific values for z_0 are obtained *via measurement*. The TKE / Law of the Wall approaches are both appropriate¹⁶. Whilst this will place additional data collection obligations on Users of the revised model, at present the industry is required to collect velocity (profile) data and for this they commonly use ADCP instruments. This would form a natural extension of this pre-consent work; with the principal difference that additional instruments

¹⁶ If measurements are made at precisely 1 m above the bed then a third method known as the ‘quadratic stress method’ can also be applied here.



(hireable from common marine instrument leasing agencies) and a different methodology would be needed for the determination of roughness. The methodology for the collection of the roughness data is the same as used within this project, and we would be happy to generate a Method Statement in order that new Users understand the technical details of this requirement. This would be available in the new model Manual.



Figure 34 Photographs of surface sediment considered hydraulically transitional-rough from Fuinary 2 (left) and Port na Moine 1 (right).

Table 31 Bed stress and roughness length estimates from application of the Wall Law and TKE methodologies to collected flow data.

Site	Roughness Length (z_0) (m)	
	From Law of Wall Method	From TKE Method
Fiunary 1	0.005	0.00001
Fiunary 2	0.015	0.07200
Shuna Castle Bay 1	0.044	0.00003
Shuna Castle Bay 2	0.065	0.00005
BDNC 1	0.070	0.00005
BDNC 2	0.040	0.00002
Ardfuir 1	0.003	0.00003
Ardfuir 2	0.003	0.00001
Ardfuir 3	0.023	0.00004
Port Na Moine 1	0.044	0.03570
Port Na Moine 2	0.005	0.00002
Durmyon Bay 1	0.025	0.00001

4.2.2 Revision of z_0 during model testing

In terms of testing (validating) the revised model against an existing dataset for a well documented site, the roughness length can operate as a tuneable parameter. That is, the revised model can be run to generate a dataset on dispersion, impact footprint etc, from which it may appear that erosion and transport has been over- or under-prescribed. One approach is to then adjust the model so that the variance between the model prediction and the observations is minimised (this approach is routinely performed in many advection-dispersion models). Therefore, whilst the default values can be used in revised model runs, these can be updated during the model testing. Note, in addition, that our recommendation (see below) advocates *measurement* of z_0 at new and future sites, and equally we would recommend measurement of z_0 at any site at which the revised model is validated if possible.



Our recommendation is that new Users of the revised model are encouraged to collect velocity data which can be analysed to derive z_0 . The model will need a facility to input this z_0 value into the model. The Manual for the model will need a section written describing the data acquisition methodology.

In the absence of any new, site specific data then we recommend the following z_0 values:

- **For smooth boundaries – $z_0 = 3.0 \times 10^{-5}$ m**
- **For rough boundaries – $z_0 = 5.4 \times 10^{-2}$ m**



5. eXternal concerns for the revised model

There are a number of external concerns relevant to publication of the model and to how it is used, and which data are required, for its operation. This project has highlighted improvements to the model which in some areas may give rise to additional incumbencies on the industry as it uses the model. These incumbencies may have financial consequences, as well as a need to become familiar with additional measurement procedures.

The areas of concern include:

1. Temperature and salinity – we recommend that temperature and salinity are provided to the model as input parameters. This means that the industry, if not already equipped (we envisage that fish farms would be equipped), would need to buy an oceanographic conductivity-temperature-depth (CTD) sensor.
2. Grain density (ρ_s) – this parameter is used within various sediment transport formulae; we recommend that grain density for faecal material is measured, and this can be achieved through a British Standard methodology (helium pycnometry). However, we recognise that for new sites no material will be available upon which to do such analyses. The DEPOMOD Manual may wish to navigate through this issue, and/or direct the reader to the relevant methodology. Alternatively, a sub-set of the samples from Survey 2 can be sent now for ρ_s determination. The fee per sample analysis is around £200. If data from this analysis are forthcoming then this could be included within the revised model as a default parameter.
3. Settling velocity of feed material – our recommendation is to provide the model with measured data (especially if different users use differing feed with varying hydraulic characteristics), which may be achieved through use of a sedimentation tower, or similar, using site specific water to maintain parity of temperature and salinity. The DEPOMOD Manual may wish to navigate through this issue, and/or direct the reader to the relevant methodology. It may be a concern that industry may not have such facilities, although they are commercially available in the UK and are also quite simple to build in-house. If this is not done then a default value must be used as described.
4. Bed roughness (z_0) – upon consideration of the data obtained in this study, our recommendation is that for the model to be optimised in terms of better physics and coding then the hydraulic roughness, which is always a site specific parameter, should be measured rather than assumed. There is already an onus on the community to measure the mean flow profile as an input to the model, and therefore we would anticipate collection of additional



flow data might be received well by the User community, and not overly more expensive (e.g. vessel costs and staff costs would already be paid for). The DEPOMOD Manual may wish to provide a Method Statement on how this can be achieved on a practical level (i.e. Law of the Wall or TKE method), and Partrac would be happy to contribute to this Section as required.

5. Pellet entrapment – an approach to pellet entrapment within divots has been summarised; in order to advance this we have recommended that a photographic guide be developed for a site based upon diver photography/direct measurement of divot depth and distribution. However, this issue would also be usefully informed by controlled mini-flume studies which would be able to derive quantitative data on limiting divot depths for permanent entrapment of pellets. Such studies would be relatively simple to configure and to complete, but if performed would not obviate the need for diver observations. We would anticipate that one or both these recommendations are up-taken, as this issue is not especially easy to deal with from a fundamental point of view.



6. Recommendations for further upgrades in the future

The following areas have been identified as potentially advantageous improvements to future versions of the model.

1. Stratification (either thermal or haline) can often take place in sheltered sites where aquaculture sites are located. Stratification influences the flow structure of the water column as well as the turbulence structure and may well be important in dispersal from pens. Estimation of the Richardson number would provide a first approximation of the relative importance of stratification in water column structure.
2. Laboratory tests are preferred to define the behaviour of fish faeces and fish pellets as a function of flow speed, and with time, in order to provide more accurate input to the model.
3. Wave motion should preferably be included in the calculations of DEPOMOD. Surface wave can influence settling from fish pens, internal waves (when stratification occurs) can influence dispersal patterns, and long period waves may in extreme cases influence the bed shear stresses.



7. References

- Amos, C.L. and Mosher, D.C. 1985. Erosion and deposition of fine-grained sediments from the Bay of Fundy. *Sedimentology*, 32: 815-832.
- Amos, C.L., Grant, J., Daborn, G.R. and Black, K. 1992a. Sea Carousel – a benthic annular flume. *Estuarine, Coastal and Shelf Science*, 34: 557-577.
- Amos, C.L., Daborn, G.R., Christian, H.A., Atkinson, A. and Robertson, A. 1992b. In situ erosion measurements on fine-grained sediments from the Bay of Fundy. *Marine Geology*, 108(2): 175-196.
- Amos, C.L., Feeney, T., Sutherland, T.F. and Luternauer, J.L. 1997. The stability and erodibility of fine-grained sediments from the Fraser river delta foreshore and upper foreslope. *Estuarine, Coastal and Shelf Science*, 45: 507-524.
- Amos, C.L., Brylinsky, M., Sutherland, T.F., O'Brien, D., Lee, S. and Cramp, A. 1998. The stability of a mudflat in the Humber estuary, south Yorkshire, UK. In Black, K.S., Paterson, D.M. and Cramp, A (eds). *Sedimentary Processes in the Intertidal Zone* Geological Society, London Special Publications 139: 25-43.
- Amos, C.L., Sutherland, T.F., Cloutier, D. and Patterson, S. 2000. Corrasion of a remoulded cohesive bed by saltating littorinid shells. *Continental Shelf Research*, 20: 1291-1315.
- Amos, C.L. Bergamasco, A., Umgiesser, G., Cappucci, S., Cloutier, D., Flindt, M., Denat, L. and Cristante, S. 2004. The stability of tidal flats in Venice lagoon – the results of in situ measurements using two benthic flumes. *Journal Marine Systems*, 51: 211-242.
- Amos, C.L., Umgiesser, G., Ferrarin, C., Thompson, C.E.L., Whitehouse, R., Sutherland, T.F. and Bergamasco, A. 2010. The erosion rates of cohesive sediments in Venice lagoon. *Continental Shelf Research*, 30(8): 859-870.
- Ariathurai, R. and Arulanadan, K., 1978. Erosion rates of cohesive soils. *Journal Hydraulics Division* 104 (2), 279–283.
- Bagnold, R.A. 1956. The flow of cohesionless grains in fluids. *Philosophical Transactions of the Royal Society of London*, Series A. 249(964): 235-297.
- Bagnold, R.A. 1966. *An approach to the sediment transport problem from general physics*. US Geological Survey Professional Paper 422-I, 37p.
- Black, K., Tolhurst, T., Paterson, D., and Hagerthey, S. (2002). Working with Natural Cohesive Sediments. *J. Hydraul. Eng.*, 128(1), 2–8.
- Bowden, K.F. 1978. Physical problems of the benthic boundary layer. *Geophysical Surveys*, 3: 255-296.
- British Standards Institution. (1990) *BS 1377 - 2. Standard Test Methods for Specific Gravity of Soil Solids by Water Pycnometer*. *Soil*. London: BSI.



Chamberlain, J. and Stucchi, D. 2007. Simulating the effects of parameter uncertainty on waste model predictions of marine finfish aquaculture. *Aquaculture*, 272: 296-311.

Cromey, C.J., Nickell, T.D. and Black, K.D. 2002a. DEPOMOD – modelling the deposition and biological effects of waste solids from marine cage farms. *Aquaculture*, 214: 211-239.

Cromey, C.J., Nickell, T.D., Black, K.D., Provost, P.G. and Griffiths, C.R. 2002b. Validation of a fish farm waste resuspension model by use of a particle tracer discharged from a point source in a coastal environment. *Estuaries*, 25(5): 916-929.

Cromey, C.J., Thetmeyer, H., Lamadariou, N., Black, K.D., Kogeler, J. and Karakassis, I. 2012. MERAMOD: predicting the deposition and benthic impact of aquaculture in the eastern Mediterranean Sea. *Aquaculture Environment Interactions*, 2: 157-176.

Dudley, R.W., Panchang, V.G. and Newell, C.R. 2000. Application of a comprehensive modeling strategy for management of net-pen aquaculture waste transport. *Aquaculture*, 187: 319-349.

Fofonoff, P. and R. C. Millard Jr 1983. Algorithms for computation of fundamental properties of seawater. *Unesco Technical Papers in Marine Sciences*. 44, 53 pp.

Houwing, E.J., 1999. Determination of the critical erosion threshold of cohesive sediments on intertidal mudflats along the Dutch Wadden Sea Coast. *Estuarine, Coastal and Shelf Science* 49 (4), 545–555.

James, C.S. 1990. Prediction of entrainment conditions for non-uniform, non-cohesive sediments. *Journal of Hydraulic Research*, 28(1): 25-41.

Julien, P.Y. 1998. *Erosion and Sedimentation*. Publ. Cambridge University Press: 280p.

Kandiah, A., 1974 Fundamental aspects of surface erosion of cohesive soils. PhD thesis, Univ. California, Davis.

Komar, P.D. and Li, Z. 1988. Applications of grain-pivoting and sliding analyses to delective entrainment of gravel and to flow-competence evaluations. *Sedimentology*, 35: 681-695.

Krone, R.B. 1962. Flume studies of the transport of sediment in estuarial shoaling processes. *Final Report Hydraulic Engineering Laboratory and Sanitary Engineering Research Laboratory*, University of California.

Kusuda, T., Umita, T., Koga, K., Yorozu, H. and Awaya, Y., 1982. Depositional processes of fine sediments. *Water Science and Technology* 14 (4–5), 17–184.

Lavelle, J.W., Mofjeld, H.O., 1987. Do critical stresses for incipient motion and erosion really exist. *Journal Hydraulic Engineering* 113 (3), 370.

Lee, C., Wu, C.H., Hoopes, J.A., 2004 Automated sediment erosion testing system using digital imaging. *J. Hydraul. Eng.*, 130(8), 771-782.



Lefebvre, A. 2009. *Bed roughness over vegetated beds: sonar techniques and effects on unidirectional currents*. University of Southampton, unpublished PhD thesis: 187p.

Lefebvre, A., Lyons, A.P., Thompson, C.E.L. and Amos, C.L. 2009. A new system for seafloor characterization: BRAD, the Benthic Roughness Acoustic Device. In: *Underwater Acoustic Measurements: Technology and Results* (Greece), 8p.

Li, Z. and Komar, P.D. 1986. Laboratory measurements of pivoting angles for application to selective entrainment of gravel in a current. *Sedimentology*, 33: 413-423.

Lyons, A.P., Fox, W.L.J., Hasiotis, T. and Pouliquen, E. 2002. Characterisation of the two-dimensional roughness of wave-rippled sea floors using digital photogrammetry, *J. Oceanic Engineering*, 27: 515-524.

Mehta, A. J. 2014. *An Introduction to Hydraulics of Fine Sediment Transport*. Publ. World Scientific, 1039pp.

Mehta, A.J. and Parthenaides, E., 1979. Kaolinite resuspension properties. *Journal Hydraulics Division* 105 (4), 111–116.

Penchang, V., Cheng, G. and Newell, C. 1997. Modeling hydrodynamics and aquaculture waste transport in coastal Maine. *Estuaries*, 20(1): 14-41.

Postma, H. 1967. Sediment transport and sedimentation in an estuarine environment. In Lauf, G.H. (ed) *Estuaries*. Publ. Am. Ass. Advancement Science: 158-179.

Rigler, J.K., Collins, M.B., and Williams, S.J., 1981, A high-precision digital-recording sedimentation tower for sands: *Journal of Sedimentary Petrology*, v. 51, p. 642-644.

SEPA. 2006. Investigation into impact of marine fish farm deposition on maerl beds. *Scottish Natural Heritage Report*. 213: 64p.

Sternberg, R. W. 1972. Predicting initial motion and bedload transport of sediment particles in the shallow marine environment. *In* Swift, D.J.P., Duane, D.B., and Pilkey, O.H. (eds) *Shelf Sediment Transport: Process and pattern*. Publ. Dowden, Hutchinson & Ross: 61-82.

Sutherland, T.F., Amos, C.L., Ridley, C., Droppo, I.G. and Petersen, S.A. 2006. The settling behaviour and benthic transport of fish pellets under steady flows. *Estuaries and Coasts*, 29(5): 810-819.

Sutherland, T.F. 2013. Quantifying benthic transport of aquaculture waste material for inclusion in predictive models. Unpublished presentation to CEPA.

Sutherland, T.F., Amos, C.L. and Grant, J. 1998a. The effect of buoyant biofilms on the erodibility of sublittoral sediments of a temperate microtidal estuary. *Limnol. Oceanogr.* 43(2): 225-235.

Thompson, C.E.L. and Amos, C.L. 2002. The impact of mobile disarticulated shells of *Cerastoderma edulis* on the abrasion of a cohesive bed. *Estuaries*, 25(2): 204-214.



Thompson, C.E.L., Amos, C.L., Jones, T.E.R. and Chaplin, J. 2003. The manifestation of fluid-transmitted bed shear stress in a smooth annular flume – a comparison of methods. *Journal Coastal Research*, 19(4): 1094-1103.

Thompson, C.E.L., Amos, C.L. Lecouturier, M. and Jones, T.E.R. 2004a. Flow deceleration as a method of determining drag coefficients over roughened flat beds. *Journal Geophysical Research*, 109(C03001): 1-12.

Thompson, C.E.L., Amos, C.L. and Umgiesser, G. 2004b. A comparison between fluid shear stress reduction by halophytic plants in Venice lagoon, Italy and Rustico Bay, Canada – an analysis of in situ measurements. *Journal Marine Systems*, 51: 293-308.

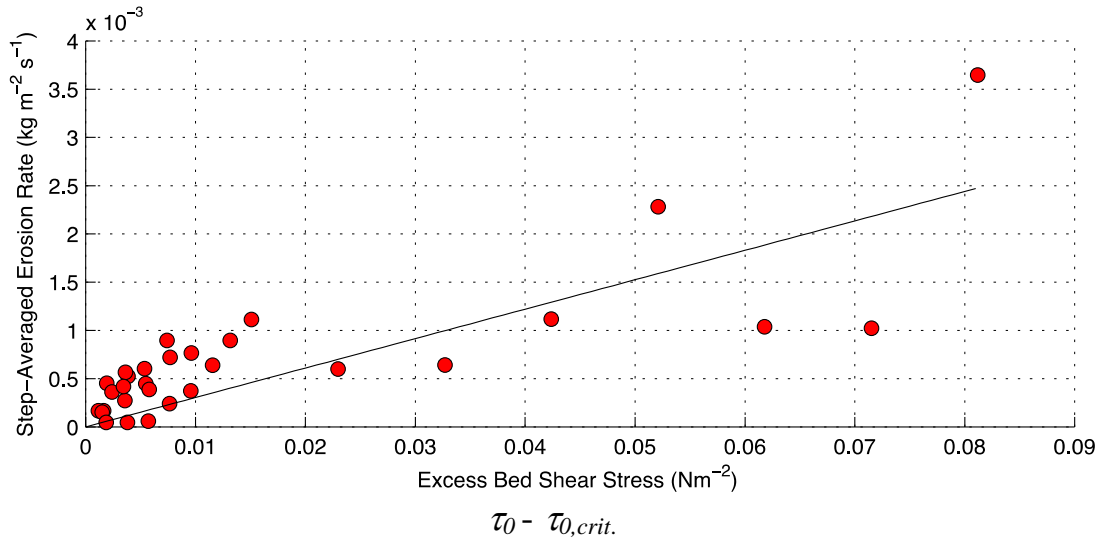
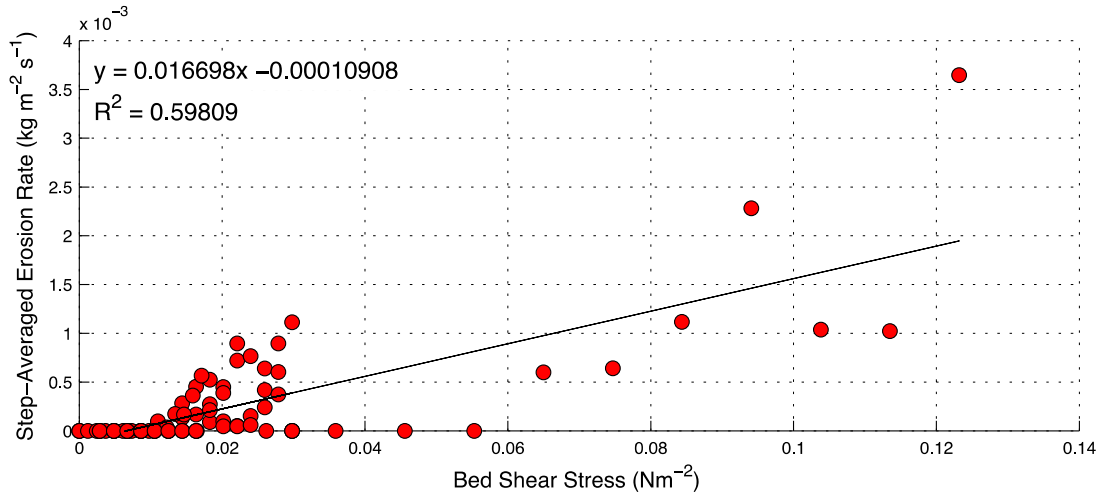
Thorn, M.F.C. and Parsons, J.G., 1980. Erosion of cohesive sediments in estuaries: an engineering guide. In: Third International Symposium on Dredging Technology, Bordeaux, pp. 349–358.

Van Rijn, L.C. 1993. *Principles of Sediment Transport in Rivers, Estuaries and Coastal Seas*. Publ. Aqua Publications, Zwolle, the Netherlands.

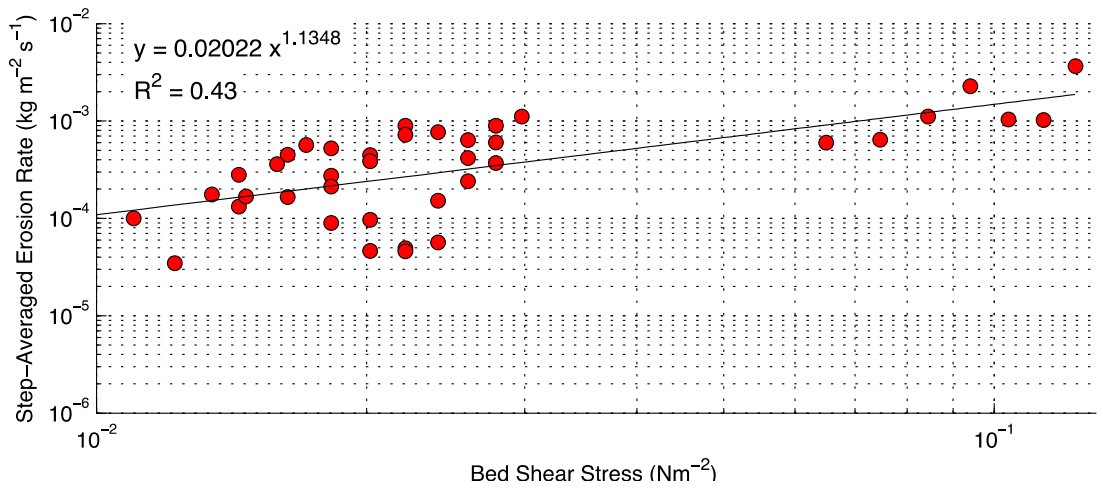
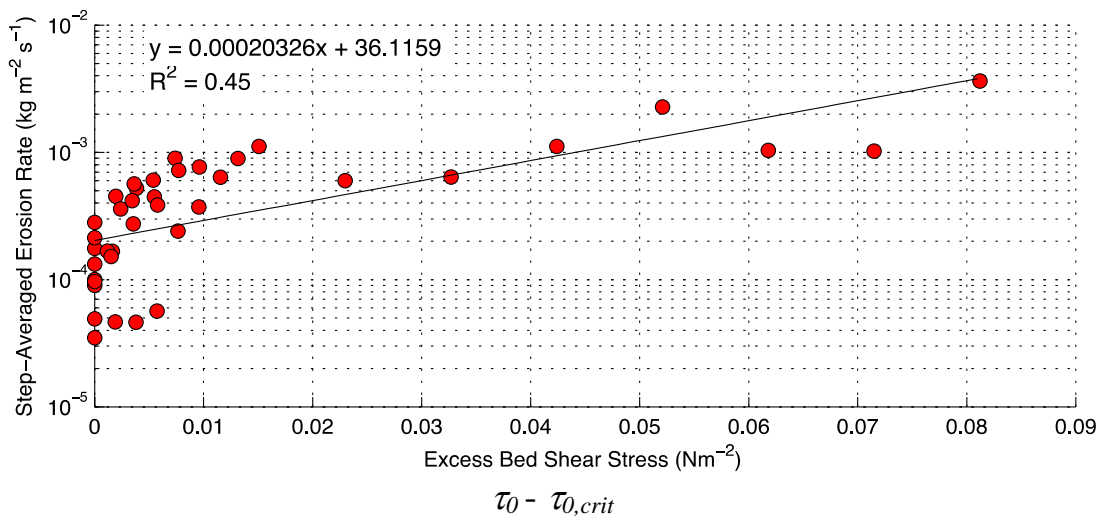
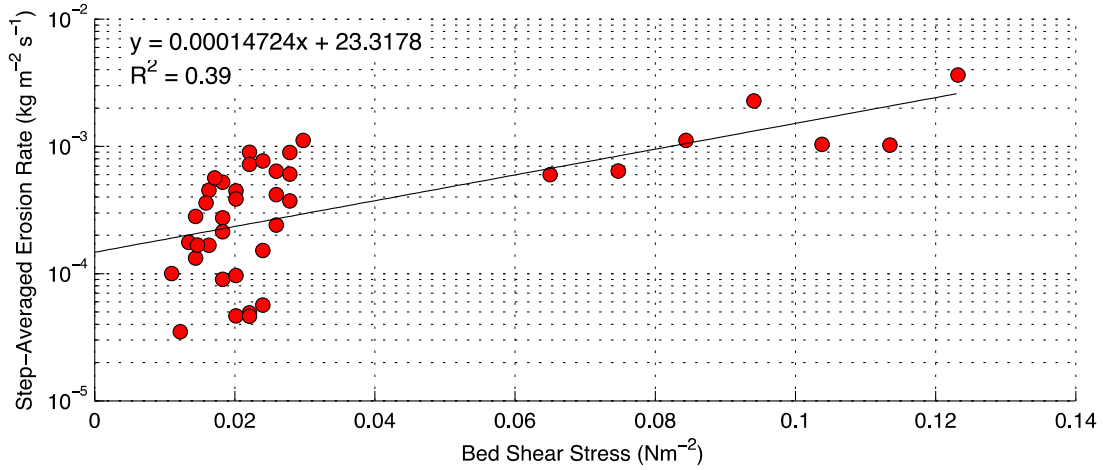
Villaret, C. and Paulic, M., 1986. Experiments on the erosion of deposited and placed cohesive sediments in an annular flume. Report to Coastal and Oceanographic Engineering Department, University of Florida, Gainesville.

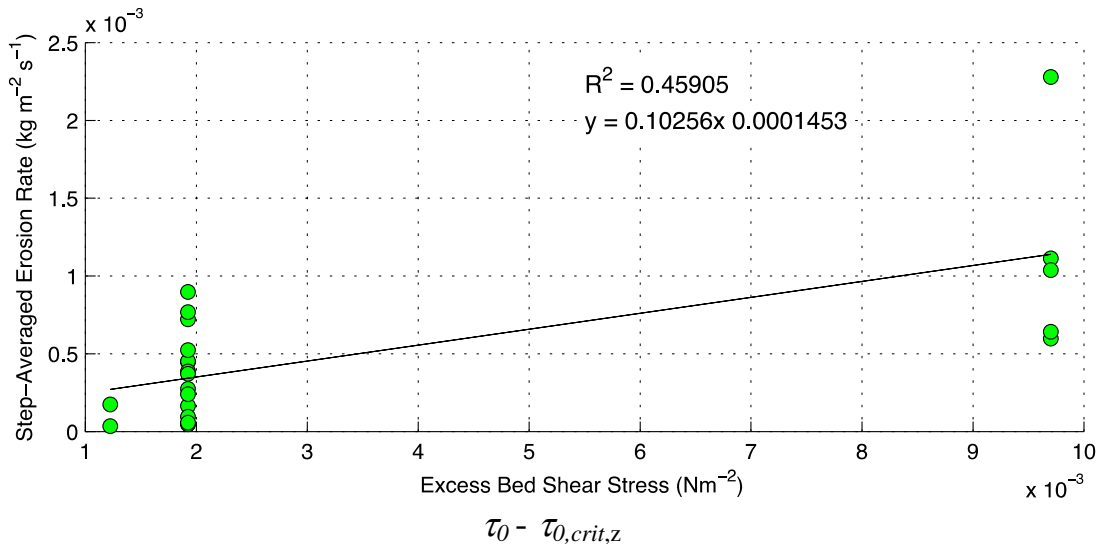


8. Appendix BEd stress – erosion rate formulations



[Function recommended in the report]





- Black, K.D., Cromey, C.J., Dale, A. and Nickell, T.D., 2010 Modelling benthic effects of salmon cage farms in Scotland: driving autoDEPOMOD with hydrodynamical model outputs. 143 pp.
- Chamberlain, J. and Stucchi, D. 2007. Simulating the effects of parameter uncertainty on waste model predictions of marine finfish aquaculture. *Aquaculture*. 272. 296-311.
- Cromey, C.J., Nickell, T.D. and Black, K.D. 2002a. DEPOMOD - modelling the deposition and biological effects of waste solids from marine cage farms. *Aquaculture*. 214. 211-239.
- Cromey, C.J., Nickell, T.D., Black, K.D., Provost, P.G. and Griffiths, C.R. 2002b. Validation of a fish farm waste resuspension model by use of a particulate tracer discharged from a point source in a coastal environment. *Estuaries*. 25. 916-929.
- Mayor, D.J., Zuur, A.F., Solan, M., Paton, G.I. and Killham, K. 2010. Factors Affecting Benthic Impacts at Scottish Fish Farms. *Environmental Science & Technology*. 44. 2079-2084.
- Sanford. 2006. Modelling a dynamically varying mixed sediment bed with erosion, deposition, bioturbation, consolidation, and armoring. *Computers & Geosciences*. 1263-1283.
- Wells, A., 2007 Marine fish farm data review. SEPA. 67 pp.